Geological Survey of Israel
Ministry of National Infrastructures
Energy and Water Resources

Paleo-hydrology and paleo-limnology of Lake Kinneret during the late Quaternary from lake sediments and carbonate shells

Lilach Lev

This thesis was submitted for the degree "Doctor of Philosophy" to the senate of Tel-Aviv University.

The study was carried out under the supervision of:

Prof. Zvi Ben-Avraham, The Department of Geophysics and Planetary Sciences, Tel Aviv University.
Prof. Mordechai Stein, Geological Survey of Israel.
Dr. Ahuva Almogi – Labin, Geological Survey of Israel.

Report GSI/14/2016 Jerusalem, April 2016

Acknowledgment

I would fist like to express my special appreciation and thanks to my supervisors, Prof. Zvi Ben Avraham, Prof. Moti Stein, and my "non-official" supervisor, Dr. Ahuva Almogi-Labin. Moti and Ahuva, I would like to thank you for sharing your enormous knowledge with me, for patiently leading and teaching me, for encouraging my research and allowing me to grow as a research scientist. You have been tremendous mentors for me and it has been an honor to be your student. I would like to thank you Zvi for all the support and advices you have given me during this long journey.

I would like to thank Michael Kitin from the Geological Survey of Israel for his assistance, both in field and in the laboratory, especially with sieving the soil samples. Special thanks to Nataliya Teplyakov from the Department of Geochemistry for her guidance through a variety of laboratory procedures which were the basis of my work. Many thanks to Avner Ayalon and Tami Zilberman for guidance and for their generous help with the stable isotope analyses. Thanks to Amir Sandler for guiding me with XRD analyses and Raanan Bodzin for helping with SEM analyses. Special thanks to Irena Segal, Olga Yoffe, Ruth Beinstock and Nadya Teutsch and all the other wonderful people from the Department of Geochemistry for all their assistance. Thanks to Channa Netzer-Cohen, Bat-Sheva Cohen, and Nili Almog for help with graphics and publications, to Ira Peer, Anna Feigin, Masha Kahalani, and to other people of Geological Survey of Israel that offered help whenever needed during many years.

Many thanks to Aminadav Nishri from the Kinneret Limnological Laboratory and to Emi Ito from the University of Minnesota for fruitful discussions.

Special thank to the technical and administrative stuff of the geophysics department, in the past and at present, especially to Zehava Eliezer, Yafit Cohen-Dahari, Shoshi Barak, Zipi Rozen and Gilad Hadasy.

Many thanks to the No Glory Roof Top students from all times.

And last but not least - many thanks to my dear parents and family for their love and endless support.

I thank and apologize to all people that extended a helping hand and offered an attentive ear and support during my research, that I may have inadvertently omitted from these acknowledgements.

Table of Content

List of Figures

List of Tables

Abstract

This work attempts to shed light on the limnological history of Lake Kinneret (LK) during the last 40 ka. This time-period includes the last glacial, the Heinrich (H) 2 and Younger Drays (YD) events and a partial Holocene record. The different periods are characterized by distinct regional climate conditions that are reflected by the limnological and hydrological indicators. The main changes that were examined and discussed in this study were water level, water sources to the lake and sources of dust material to the lake: The water that fills Lake Kinneret is comprised a mixture of Ca-chloride brines and freshwater. The brines originated in the late Neogene Sedom lagoon and have recharged into the lake in response to hydrological conditions that reflects regional climate. Climate changes during the Pleistocene and Holocene have influenced on desert dust transport and they are recorded in the sedimentary sections that were deposited in Lake Kinneret.

The lithology, mineralogy and grain size of the sediments and the chemistry (Sr/Ca) and isotope ratio ($^{87}Sr/^{86}Sr$ and $\delta^{18}O$) of ostracod shells are the main tools used in this study. Also used are the calcareous microfauna (ostracods and foraminifera) assemblages. The results are compared to contemporaneous Lake Lisan and Dead Sea and changes in Lake Kinneret were examined as part of a regional and extended inland aquatic system.

Water and surface sediment samples containing living ostracods were collected from four sites around Lake Kinneret (Ginosar, Ma'agan, Shitim and Tabgha). Fossil ostracods, foraminifera and bulk sediments were recovered from four cores and a trench: Ohalo trench and KIN2 borehole at the southwest shore of the lake, SOG2 borehole at the south part of the lake at surface elevation of 224.0 m bsl and SOG3 at the northwest part of the lake at surface elevation of 229.0 m bsl.
The cores and the trench comprise mainly alternating massive and laminated layers of primary calcite and detrital calcite, quartz and clays. The primary calcite was deposited from the lake, whereas the detrital material was transported into the lake by rivers, runoff and direct settled dust.

Organic debris (branches and wood remains), calcite ostracod shells and aragonite *Melanopsis* shells were dated by radiocarbon and aragonite stem casts were dated by

U-Th to reconstruct depth-age models for the Ohalo trench and the other 3 boreholes drilled in Lake Kinneret. The Ohalo trench covers the period from 27 to 20 ka cal BP while the adjacent KIN2 core covers the time-period between ~40 and 21 ka cal BP. The SOG2 covers the time interval from 25 to 12 ka cal BP and SOG3 between 25 and 2 ka cal BP.

The glacial period between 27 and 25 ka BP was wet in the surrounding of Lake Kinnert. Lake level was high (~170 m bsl) and the lake merged with Lake Lisan. Based on chemistry and isotope values of bulk carbonates, it is concluded that brine contribution to the lake was enhanced during the high lake stand. On the contrary to the wet conditions that prevailed in the Levant, extreme arid conditions characterized the Sahara desert. Based on grain size analysis it is likely that the detrital component have traveled long distances, all the way from the Sahara to Lake Kinneret.

The decrease in lake level between 24 and 20 ka BP is related to the increasing aridity in the region, during and after the H2 cold event at the northern Atlantic. The 2‰ decrease in the $\delta^{18}O$ values at the end of this event is consistent with the change in the composition of east Mediterranean waters – the source of the regional precipitation at the same period, indicating that the Ohalo-shore environment was dominated at that period by regional run-off. Analysis of Fe_2O_3 vs. Al_2O_3 from sediments from H2 event also indicates that dust was carried into the lake from less distance source resulting in less leaching. High numbers of ostracods, mainly of *Cyprideis torosa* and of the brackish benthic foraminifera *Ammonia tepida*, at the base of Ohalo trench (~ 23 ka BP) indicate higher salinity during the H2 event than modern Lake Kinneret. The youngest sediment at Ohalo is ~20 ka old, indicating that sediment accumulation at this site ceased apparently because equilibrium between sediment supply and removal was reached in this region.

The Younger Drays event is known as a return to sub-glacial conditions, expressed in the lake by an increase in water level. $^{87}Sr/^{86}Sr$ ratios reflect decreased in runoff compared with H2 event and higher contribution of the brines, similar to conditions during high stand period. Climate conditions during YD event were not as extreme as during the high lake level period. In accordance, high contribution of desert dust from intermediate distance is probably the source for detritus during the YD event.

The study emphasized the connection between arid/wet periods, lake level and contribution of the brines as major water source during wet periods. This finding is in agreement with the Goldschmidt model, according to which brines are pushed by the meteoric groundwater so that higher precipitation results in higher saline discharge.

Chapter 1: Introduction

1.1: Overview

Lake Kinneret (the Sea of Galilee) is the major source of fresh water in Israel. The length of Lake Kinneret is ~20 km, its width is ~12 km and its max depth is ~ 46 m (in accordance with lake level of ~210 m bsl). Lake Kinneret (Figure 1.1) currently fills the northern part of the Kinnarot basin, which extends from the Bethsaida Valley in the north to the outlet of the Yarmouk River in the south comprising one of the morphotectonic depressions along the Dead Sea Transform (DST), along with the Hula Lake and the Dead Sea (Figure 1.1). While Lake Kinneret evolved as a flow-through lake which is fed and drained by the Jordan River, the other lacustrine water bodies that existed in the Dead Sea basin (i.e. lakes Amora, Lisan and the Holocene Dead Sea) were terminal and hypersaline. The lakes that existed in the DST are located between the Mediterranean and the arid (desert) climatic zones (Bartov et al., 2002a; Begin et al., 1974; Neev and Emery, 1967; Neev and Emery, 1995). The water compositions and limnological configurations of the lakes (e.g. surface water and water column structure) reflect the hydrological conditions in the watershed, which in turn reflect the regional climatic conditions that prevailed in the region (Neev and Emery, 1995b; Stein, 2001).

The Dead Sea and the former saline and hyper-saline lakes in the Dead Sea basin have been studied extensively for their paleo-limnological and paleo-hydrological histories (Enzel et al., 2006 and references within there; Neev and Emery, 1967; Neev and Emery, 1995a; Niemi et al., 1997), yet significantly fewer efforts were devoted to the reconstruction of the paleo-hydrology of LK. Several paleo-limnological works carried out at LK included pollen analysis (Baruch, 1986); geochemical–limnological studies (Stiller and Kaufman, 1985); biogeochemistry studies (e.g. primary productivity, Dubowski et al., 2003); sedimentology and limnological reconstruction (e.g. lake level, Hazan et al., 2005); and geochemistry and chronology of *Melanopsis* shells (Lev, 2008).

This work attempts to shed light on the limnological history of LK, to understand the evolution of the lake in the transition from high to low water level and to compare the limnological and geochemical parameters that characterized the lake during these periods to the Holocene lake. In particular I am interested in the water sources and contribution of the brines to the lake during the high stand period (~27-25 ka BP), the post-high stand (~24-21 ka PB), and during low stand periods of the Deglaciation and short periods during the Holocene. Lake Kinneret supported fauna such as ostracods (Hazan et al., 2005; Lev, 2006; Martens and Ortal, 1999; Tchernov, 1975). I use shell assemblages and various geochemical indicators (e.g., Sr/Ca, $^{87}Sr/^{86}Sr$ and $\delta^{18}O$) in ostracod valves (*Cyprideis torosa*) as tracers of the sources and relative contributions of the brines in the late Quaternary Lake Kinneret. The results are compared to the values that were measured in modern LK and Dead Sea and in aragonites from contemporaneous Lake Lisan. Other tools used are lithology and mineralogy of the sediments, and chemistry of bulk carbonates.

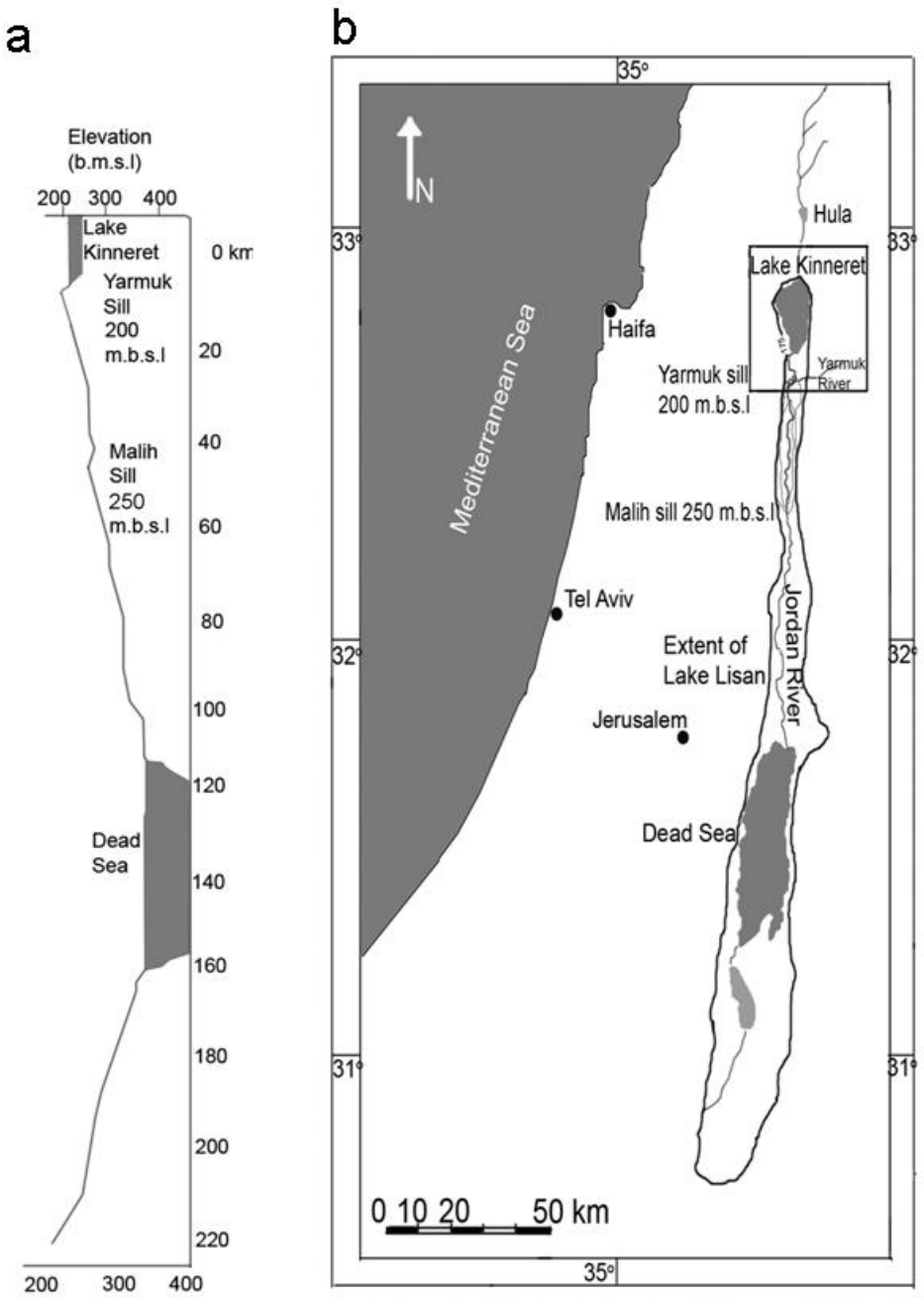

Figure 1.1 (a) Cross section along the Jordan Valley showing the Yarmouk and Wadi el Malih thresholds (after Begin et al., 1974). **(b)** Location map. The Hula and Lake Kinneret are fresh water bodies located in the northern part of the Dead Sea Transform, and the Dead Sea is a hypersaline water body in the south of the transform. The contour line that describes the highest water level, when LK merged with Lake Lisan is shown. Also shown are the Yarmouk and the Malih sills (200 and 250 m b.s.l, respectively).

1.2 Geological background

Lake Kinneret is situated in the northern part of the Kinnarot basin, one of the deepest sedimentary basins along the DST (Figure 1.1). The DST extending from the Gulf of Aqaba to the Taurus Mts. comprises a plate boundary between the Sinai and Arabian sub-plates (Freund, 1965; Garfunkel, 1981). Lake Kinneret shows features of a pull-apart structure, which is complicated by several intersecting fault systems (Ben-Avraham et al., 1981; Ben-Avraham et al., 1986; Ben-Avraham et al., 1996; Hurwitz et al., 2002; Reznikov et al., 2004). The N-S oriented fault system is part of the DST, which has been active since the Miocene (Bartov et al., 1980). Another fault system is located west to Lake Kinneret, having a main NW striking and a secondary ENE oriented faults. The Kinnarot – Kinneret basin is surrounded by Pliocene-Pleistocene basalts, Eocene limestones and chalks and Neogene sandstones (Figure1.2, Heimann and Braun, 2000).

The information on the early sedimentary and magmatic history of the Kinnarot basin comes from the Zemah-1 borehole (Heimann et al., 1996; Marcus and Slager, 1985). The basin comprises a very deep sedimentary structure with more than 4 km of Neogene - Quaternary sediments and magmatic-basaltic sequences recovered at the Zemah drill hole (Marcus and Slager, 1985). The late Pleistocene-Holocene sedimentary section in the Kinnarot basin comprises the Kinneret Formation (Hazan et al., 2005). The formation consists of laminated lacustrine sediments (mainly primary calcite and fine detritus material) intercalated with clastic sequences of sand and pebbles (Figure 1.3, Hazan, 2003). During the last glacial period, when Lake Lisan arrived to its maximum extent and elevation (~ 170 m below mean sea level), filled the entire Dead Sea-Jordan basin and converged with Lake Kinneret, mainly calcitic marls (up to 90% calcite) were deposited in LK forming laminated intervals (Hazan et al., 2005). During the late Holocene (past 5 ka) the sediments compose homogeneous light grey to light brown silty to clayey marls (Thompson et al., 1985). At present, in the center of the lake sedimentation rates are estimated to be 2-7 mm/yr, (Stiller, 1974) and the sediments consist mostly of primary calcites and fine-detritus of dust origin (Ganor et al., 2000; Stiller and Kaufman, 1985). Based on the composition of sediment cores drilled in the central part of the lake, Stiller and Kaufman (1985) estimated the content of "endogenic" carbonate as 70-85% of the total carbonate.

1.3 Limnological and hydrological background

1.3.1 Paleo-limnology and hydrology

During the late Pleistocene and Holocene the paleo-Lake Kinneret co-existed with the saline and hyper-saline Lake Lisan and Dead Sea, whereas the water level and geographical dimensions of the lakes reflected the regional hydrological and climate regime (Hazan et al., 2005). During the past 40 kyr, the water level of Lake Kinneret fluctuated between < 220 m and ~170 m below mean sea level (bsl). The highest level was reached at the maximum of the Last Glacial Period, between ~27-25 ka BP (modified after Hazan et al., 2005, according to Oxcal 4.1) when Lake Lisan arrived to its maximum elevation (Figure 1.1) and extended all the way to Lake Kinneret (Bartov et al., 2003; Hazan et al., 2005). Then, at ~ 24 ka BP Lake Lisan and Lake Kinneret retreated and separated to a hypersaline and fresh flow-through water bodies, respectively. This lake drop and retreat coincided with the timing of Heinrich event 2 (H2) in the north Atlantic (Bartov et al., 2003). After the lake retreat the southernmost part of the modern Lake Kinneret basin became exposed and accumulated fluvial sediments (Hazan et al., 2005). Another high stand of ~200 m bsl occurred at the mid-Holocene (~5200 ka BP, Hazan et al., 2005; Neev and Emery, 1995a) contemporaneously with a Dead Sea high stand (e.g. Migowski et al., 2006). Several low stands occurred: (1) before 41 ka BP, (2) between ~40 and 36 ka BP, (3) between 33 and 27 ka BP and, (4) between 14 and 10 ka years BP (Hazan et al., 2005). The timing of these low stands coincide with Lake Lisan and Dead Sea low levels (Bartov et al., 2003) indicating a similar response of both lakes to the regional hydrological-climatic conditions (Hazan et al., 2005).

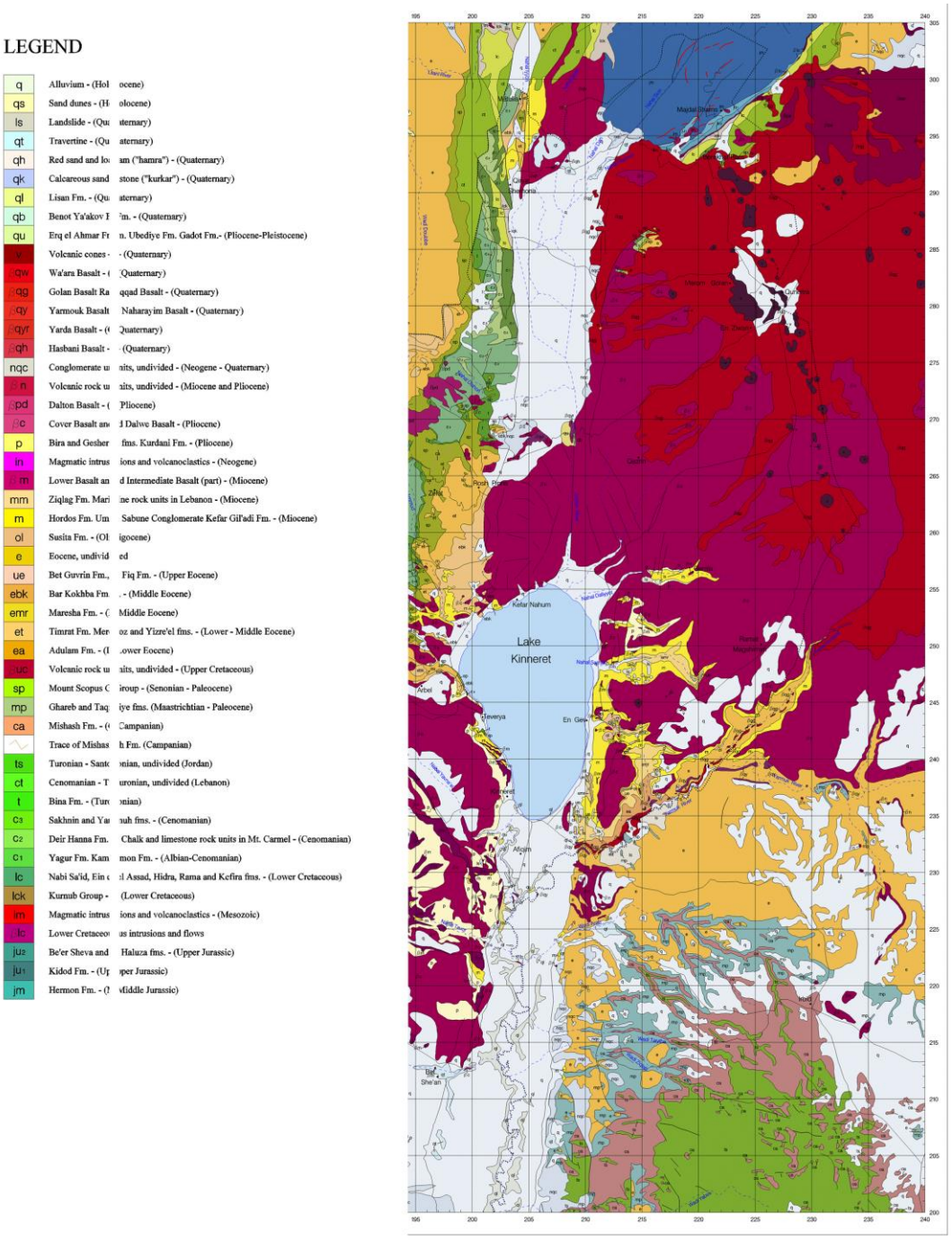

Figure 1.2 Geological map of the Kinnarot basin and the upper catchments of the Jordan River (Geological Survey of Israel). The Kinnarot – Kinneret basin is surrounded by Pliocene-Pleistocene basalts, Eocene limestones and chalks and Neogene sandstones.

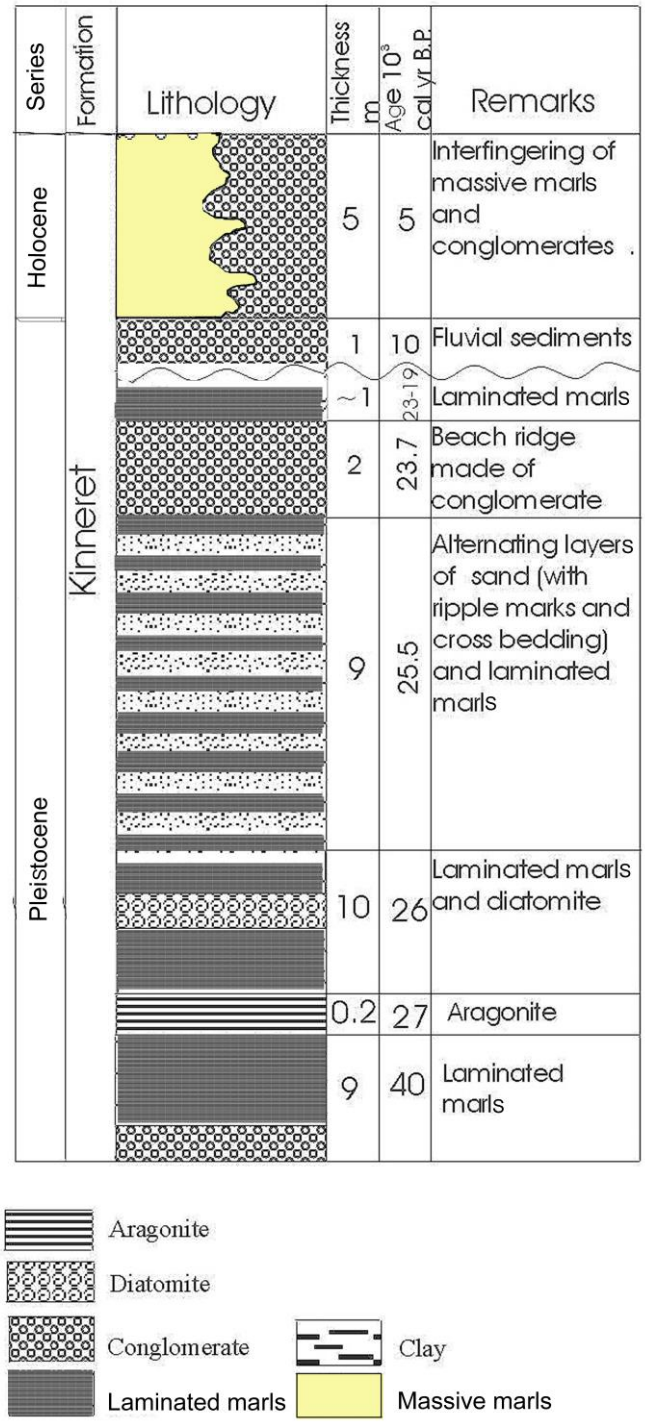

Figure 1.3 A composite stratigraphic section of the Kinneret formation. After Hazan et al., (2005). The Kinneret formation consists of laminated lacustrine sediments (mainly primary calcite and fine detritus material) intercalated with clastic sequences of sand and pebbles.

1.3.2 Modern hydrology

Lake Kinneret is currently a monomictic lake with winter water temperature of ~15°C. In spring and summer, the depth of the epilimnion is 15-25 meters, its maximum temperature is 29 °C and the temperature of the hypolimnion is ~15 °C (Serruya, 1977). The Jordan River contributes about 70% of the fresh water inflow to the Lake Kinneret (Flexer et al., 2000). The tributaries of the Jordan River (Figure 1.4) are the Dan, Banias and Hazbani (confluence at Yoseph Bridge), which discharge the Jurassic carbonate aquifers of Mt. Hermon and rivers draining the basaltic terrains of the Golan Heights in the east (e.g., Yarmouk River). Additional freshwater comes from rivers flowing to the Beitecha valley and rivers from the Galilee Mountains draining mainly carbonatic terrains (e.g. Zalmon and Amod rivers flowing to the Ginosar valley) in the west and from runoff from the surrounding hills and from the surrounding carbonatic and basaltic aquifers of the Galilee and Golan Height.
The pH of the Kinneret water fluctuates from 8.0 to 9.1 and the major dissolved ions in the lake water are Na^{+}, Ca^{+2}, Mg^{+2}, K^{+} and Cl^{-}. The salinity of Lake Kinneret, ~400 mg/l before 1967, is much higher than its freshwater sources (Katz, 2003). It reflects the mixtures of onshore and underwater saline springs (i.e., Tabgha, Fuliya and Tiberia Spa, 300-18,000 mg/l, Goldstein, 2004; Klein-BenDavid et al., 2005) and of meteoric waters (e.g., Gat et al., 1969; Goldshmidt et al., 1967; Starinsky, 1974). Also, the composition of the dissolved salts in Lake Kinneret and in the Jordan River is different (Kolodny et al., 1999). The main reason is onshore and marine saline springs (i.e., Tabgha, Fulya and Tiberias Spa, 300-18,000 mg/l) (Goldstein, 2004; Klein-BenDavid et al., 2005). The wide range of salinities in the springs along the Dead Sea basin-Jordan valley reflects the mixtures of ancient brines and of meteoric waters (Goldshmidt et al., 1967; Starinsky, 1974). It was suggested that the brines originated in the Sedom lagoon that invaded into the Jordan Valley-Dead Sea basin possibly in the Pliocene and precipitated evaporitic halite and gypsum (Zak, 1967).

Hurwitz et al. (1999) used time domain electromagnetic model and argued that brines with salinities of 11,000-22,000 mgCl/l underline the subsurface of Lake Kinneret. The discharge mechanism of the saline water to the lake is still under debate. Several mechanisms were proposed to explain the discharge of the saline springs into the lake: 1. location along deep faults that enable the upwelling of saline groundwater (Golani, 1962); 2. hydrological head driven by tectonic pressure or a geothermal energy mechanism (Mero and Mandel, 1963; Mero and Zaltzman, 1967); and 3. the hydrological head due to the presence of freshwater aquifers in the Galilee Mountains west to Lake Kinneret (Goldshmidt et al., 1967). Whatever the mechanism, it is agreed that the chemical evolution of the lake is affected from the contribution of the brines, which in turn are attributed to parameters such as water level and regional climate. Following this model, Rimmer et al., (1999) proposed to drill into the freshwater aquifers at the Galilee Mt. to relax the hydrological head and relax the flow of the saline springs into Lake Kinneret.

The main questions that are addressed in this thesis are:

1. *What were the water sources to the lake during the high stand period, the post-high stand period and during the Younger Dryas and Holocene?* The answer to this question lies in the chemistry and isotopes data that were recovered from ostracods shells and bulk sediments.
2. *What were the sources of detrital material that entered the lake and how they change through time?* The tools used in this study are the grain size analysis and the comparison to contemporaneous Lake Lisan and Dead Sea.
3. *How do changes in water sources and sources of detrital material express changes in regional climate?* Chronology, sedimentology and geochemistry data were combined to understand changes in regional climate.

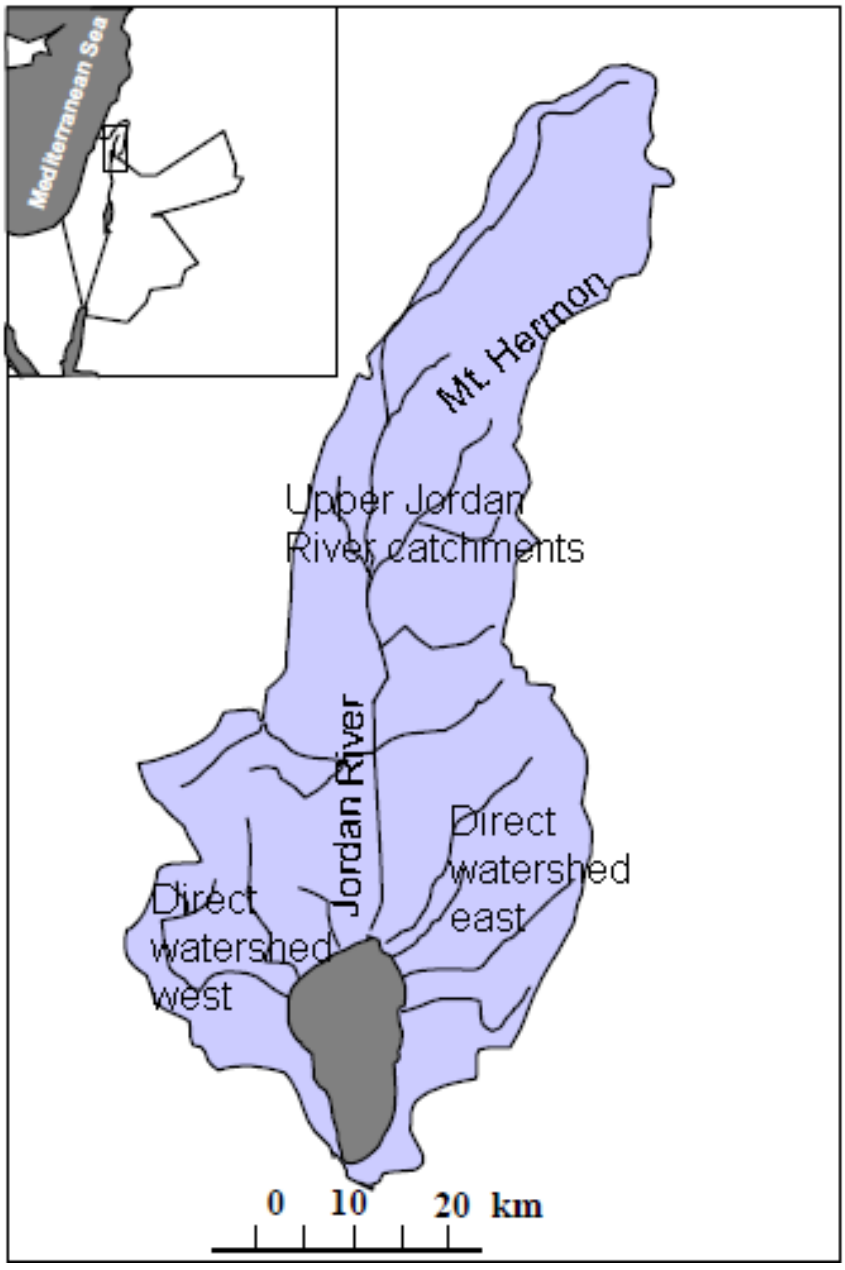

Figure 1.4 Lake Kinneret watershed, including the upper catchments of the Jordan River and the direct watersheds (east and west). The Jordan River contributes about 70% of the fresh water inflow to the Lake Kinneret. Additional freshwater comes from rivers flowing to the Beitecha valley and rivers from the Galilee Mountains draining mainly carbonatic terrains in the west and from runoff from the surrounding hills and from the surrounding carbonatic and basaltic aquifers of the Galilee and Golan Height.

1.4 Late Pleistocene global climate

The Late Pleistocene period extended from ~132ka BP to ~11.7ka BP (e.g., Gibbard and van Kolfschoten, 2004, Walker et al., 2009). It is characterized by rapid changes in global climatic conditions due to spreading and retreating of glaciers. The maximum of the Last Glacial Period (ca 26.5ka BP) was characterized by massive ice sheets that covered most of North America, northern Europe and Asia, storing water, causing drought, desertification and a dramatic drop in sea levels. On the contrary, the Dead Sea region experienced increased precipitation during glacial periods, and arid conditions during interglacials (Enzel et al., 2008; Waldmann et al., 2010).

Few anomalic climatic events that occurred during the glacial periods are called Heinrich events. Exceptional amounts of freshwater were supplied to the North Atlantic by eroded and melted icebergs, alternating the density-driven thermohaline circulation patterns of the ocean. The global extent of records illustrates the dramatic impact of Heinrich events (e.g., $\delta^{18}O$ speleothems from Soreq Cave, Israel, Bar-Matthews et al., 1997).

The Younger Dryas, at the end of the Pleistocene, lasted from 12,900 to 11,700 years ago BP., and was characterized by a sharp decline in temperature over most of the northern hemisphere (Walker et al., 2009).

Geochemistry, minerology and stratigraphich study of deposites from deep water and shorezone in lakes are used to indicate water level fluctuations and temporal variations in the hydrologic balance of lakes during Last Glacial Maxima, H2 and YD periods (e.g., Benson et al., 1996, Magny, 2001, Magny and Ruffaldi, 1995, Oviatt, 1997). These events are well shown in the sediments recovered from the cores, as will be elaborated in this work.

1.5 Ostracods

Ostracods are small (0.3-3 mm) bivalve crustaceans that live in most types of aquatic environments (Athersuch et al., 1990). They have an inner soft body, encased in two chitinous or calcareous low magnesium valves. The two valves are asymmetrical, with one valve fitting inside the other. Ostracods can reproduce sexually and asexually. During their lifetime (less then one year), they molt between growth stages having usually nine instars between egg and adult. Thus a single specimen may have a series of juvenile and two adult stages. Most ostracods are scavengers, some are herbivorous and a few are carnivores. The majority of the ostracods are benthic or epibenthic, living on the substrate or on other organisms, however, one group has developed some pelagic species. The biodiversity of ostracods is very high. It is composed of more than 2000 species. They live in a variety of water bodies (e.g., hot springs, fresh water, marine), characterized in different environmental parameters (e.g., temperature, salinity, nutrients) (Athersuch et al., 1990). Ostracod shells are archives of isotopic and chemical composition of their environment and have been widely used to reconstruct paleo-salinity and water temperature (e.g. Carpenter et al., 1991; Hu et al., 1998; Rosenfeld et al., 2004).

Shells of *Cyprideis torosa* (Jones, (1857) are used as a major source for tracing fluctuations in the paleo-hydrology and paleo-limnology of the late Quaternary Lake Kinneret. The species first appeared in the Miocene, it is widely distributed and is tolerant to a wide range of salinities. Ostracods assemblage composition and *Cyprideis torosa* shell chemistry play a great role in the identification of brackish water environments (e.g. Boomer and Godwin, 1993; Mischke and Wunnemann, 2006). Because Lake Kinneret is a stratified lake, ostracods are absent in the modern lake below water depth of ~15 m, where the environment is anoxic during most of the year.
The methods used in this work assessing ostracods as paleo-environments proxies are ostracod assemblage composition and trace element geochemistry and isotope ratios (Sr/Ca, Mg/Ca, $\delta^{18}O$ and $^{87}Sr/^{86}Sr$). These methods are elaborated in the material and methods chapter.

Chapter 2: Materials and Methods

2.1 Sampling sites

Modern water and surface sediment samples containing living ostracods were collected from four sites around Lake Kinneret (Ginosar, Ma'agan, Shitim and Tabgha, figure 2.1) at the end of December 2009, when water temperature was ~19 ^{0}C and the lake level 214.0 m bsl. For trace element analysis, water samples were filtered through 0.45 μm filters at the field.

KIN2 borehole and OH trench were drilled in spring 1999 by a joint group from GFZ-Potsdam and the Hebrew University, Jerusalem. They were recovered adjacent to the Ohalo II archeological site (coordinates 52039, 502325 New Israeli grid, figure 2.1). The surface elevation of KIN2 borehole is 213.0 m bsl and the drilling reached the elevation of 222 m bsl (Figure 2.2). The top of the borehole (~2m) is composed mostly of alternating dark and light gray marls. Underneath there is a ~1.5m interval of alternating massive and fine laminated sediments, and the rest are mainly fine laminated sediments. At the bottom of KIN2, a layer of pebbles was reached and warm and saline waters were leaking. The KIN2 borehole was divided into 10 segments of different lengths, some of which are overlapping. Segments are marked 1, 2, 3A, 3B, 4A, 4B, 5A, 5B. Sediments were sampled every 20 cm or less, each sample is 3 cm long. Samples were marked by segment and depth interval in the segment and by a serial number (from 2248 to 2302).

The OH trench is located ~1 meter west to KIN2 borehole (coordinates 52037, 502363 New Israeli grid). The surface of OH trench is at 211.5 m bsl, its length is ~5 m and the archeological layer appears at a depth of 40-70 cm, from 211.9 to 212.2 m bsl. The sediments beneath the archeological layer are predominantly highly fossiliferous gray marls. In the lower part of the sequence, below ~214.5 m bsl, alternating marls and fine laminated sediments occur. The OH trench was sampled by using seven “wall-cores”. The trench samples were cut into 2 cm segments that were marked OH (trench#) and a serial number, according to the depth below ground level (e.g., OH-2 121). OH7 is the deepest segment at the Ohalo trench.

SOG2 and SOG3 boreholes were recovered by Tahal at 1985. SOG2 is located at the southern part of the lake (coordinates 52056/502375, new Israeli grid). The surface elevation of SOG2 borehole is 224.0 m bsl, and the total length is ~10 meters. It was recovered from 2.2 m downward, and composes of light gray marly sediments. The core was cut into ~10cm segments that were marked SOG2 and a serial number, according to the depth under ground level (e.g., SOG2 676).

SOG3 is located at the northwestern part of the lake (coordinates 52019/502513, New Israeli grid). The surface elevation of SOG3 is 229.0 m bsl, and the total length is ~10 meters. The core was cut into ~10cm segments that were marked SOG3 and a serial number, according to the depth under ground level (e.g., SOG3 184).

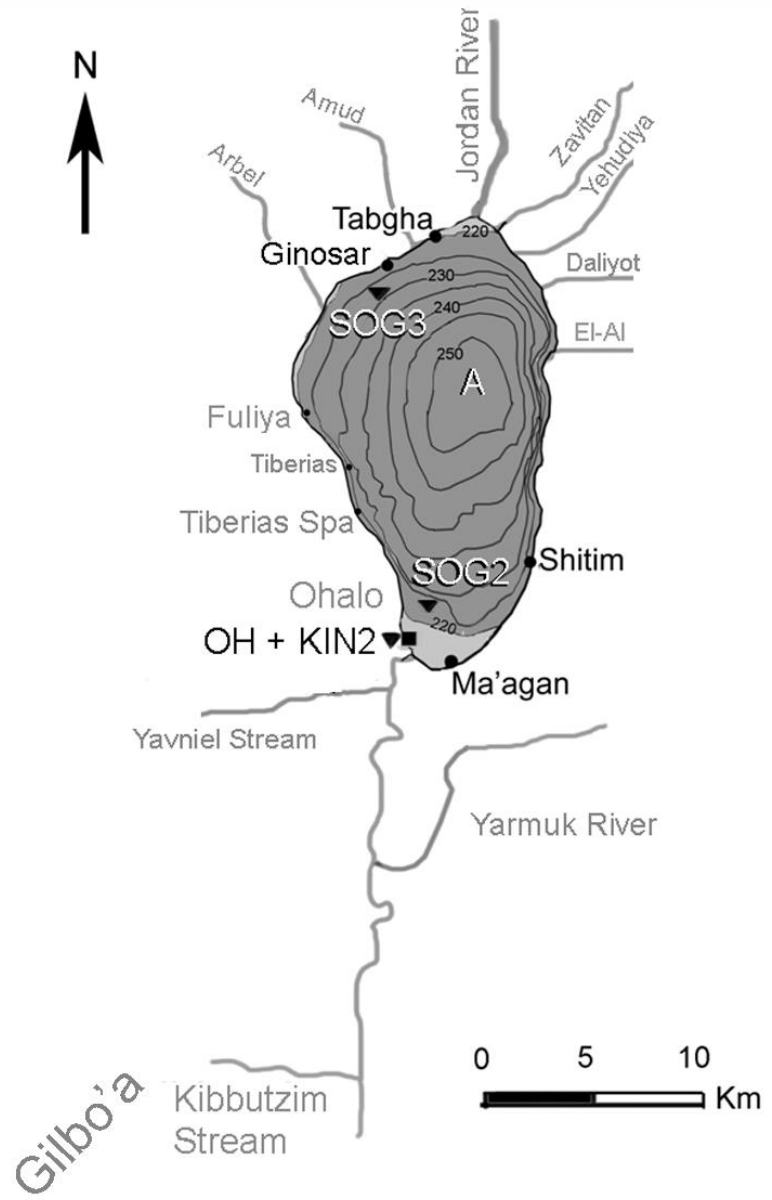

Figure 2.1 Sampling sites around Lake Kinneret. Circles mark water and sediments sampling sites, square marks the Ohalo-II archeological site, where trenching and coring were conducted. The shaded area at the south and north of the lake represents the low stand after the retreat of the lake at ~ 24 ka cal BP from its last glacial high-stand (~ 170 m bsl, Hazan et al., 2005). Bathymetry is after Ben-Avraham et al., (1990).

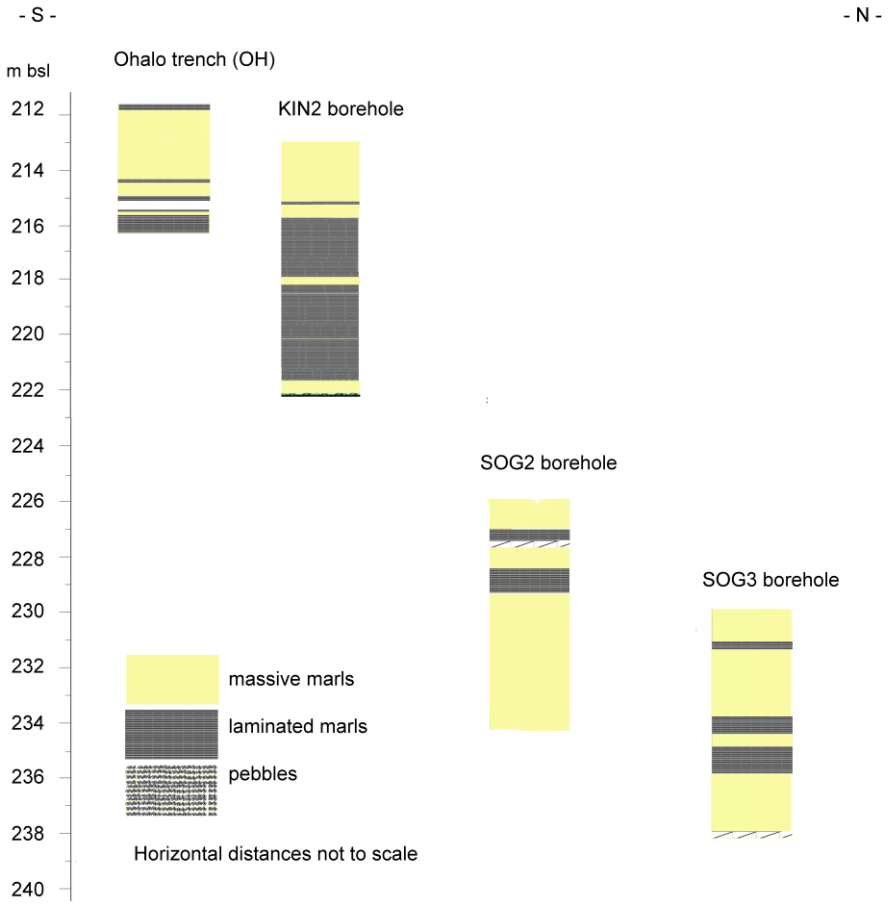

Figure 2.2 Stratigraphic locations of the Ohalo trench and KIN2, SOG2 and SOG3 boreholes. Most sediments show alternating massive and laminated marls, implying changes in environment of deposition. Definition to marls in this work is elaborated in the text.

2.2 Analytical methods

2.2.1 Bulk sediments analysis

Bulk sediment samples were measured for percent of fine sediment <63 μm and grain size. Sediments were also examined by scanning electron microscope (SEM).
Carbonate content (wt% CaCO3) – For the calculation of the carbonate content in a bulk sample, a chemical reaction with nitric acid was performed in a closed system and the resulting pressure was measured. For calibration, exact amount of calcium carbonate was reacted with the acid. Results were compared to carbonate content that was calculated from major element measurements. Calculated carbonate content based on measured CaO in bulk sediments and calibration according to:
Calculated carbonate = measured carbonate * 1.73 – 11.3.
Carbonate content at the KIN2 borehole is typically higher than the calculated values, possibly because of the use of nitric acid. Carbonate content values were calibrated according to the measured values.
XRD – X-Ray Diffraction analysis was performed using a PW 1820 diffraction spectrometer (Phillips) at the GSI. Cu Kα X-radiation (λ = 1.5418 Å) was supplied by a copper-target tube. Scan range (2 Theta) was 2 to 42° and scan speed: 2°2/ min. The mineral fractions in each sample were semi-quantitatively calculated. The intensity of the diffraction signal is plotted against the diffraction angle allowing the determination of the relative composition of the sample. Results are expressed in >5%, 5-25%, 25-50% and <50%.
Grain size analysis – Grain size analysis was performed by the Mastersizer Laser (Malvern MS-2000) at the Geological Survey of Israel for grain size < 2 mm.

2.2.2 Calcareous microfauna assemblages

Salinity is a main factor controlling the distribution of ostracods (Frenzel and Boomer, 2005). Mischke et al. (2010, 2014a,b) showed lately how ostracods assemblage composition is used for inferring the salinity of different inland water bodies in Israel.

About 30 grams from each sample were wet sieved with tap water through 63 μm screen and dried. The >150μm size fraction of 96 sediment samples from OH trench were examined under a binocular microscope, for the presence of autochthonous foraminifera. Ostracod shells in the >250μm size fraction were counted in 100 samples for assemblage analysis.

2.2.3 Ostracod and water chemical and isotope analyses

Water and ostracods were analyzed for Ca, Mg and Sr concentrations as well as $\delta^{18}O$ and $^{87}Sr/^{86}Sr$ isotope values. Trace element geochemistry and isotope ratios can provide information on the chemistry of paleo-environments, assuming that the mechanism of incorporation of trace elements into the ostracod shell and the relationship between the ionic composition and the lake's temperature/salinity are well known. Mg/Ca and Sr/Ca ratios, O_2 and C stable isotopes and $^{87}Sr/^{86}Sr$ isotope ratios are the main tools used in this work.

Sr/Ca – Sr/Ca values in ostracod shells is used to calculate past Sr/Ca in the water using partition coefficient (Kd). Past water Sr/Ca can be related to evaporation/precipitation changes, variations in the chemistry of the water and salinity variations (i.e., Sr/Ca ratio increases with salinity, (Chivas et al., 1986; Engstrom and Nelson, 1991). $SrCO_3$ has an orthorhombic structure (like aragonite), and the Kd for Sr/Ca is independent of temperature during formation of calcite within the range on 0-40 ^0C (Chivas et al., 1986). Kd is also constant for all ostracod species within the same genus (Chivas et al., 1983; Chivas et al., 1986; Engstrom and Nelson, 1991) and it correlates with the Mg/Ca ratios of the aquatic habitat (Xia et al. (1997), (Wansard et al., 1998).

$\delta^{18}O$ - The oxygen isotope composition of calcite that precipitated at isotopic equilibrium from water with certain oxygen isotope composition $\delta^{18}O$ can be converted from VPDB to VSMOW scale using the equation of Coplen et al., (1983) equation:

$$\delta^{18}O\ (VSMOW) = 1.03091 * \delta^{18}O\ (VPDB) + 30.91$$

For the isotopic fractionation between calcite and water, the equation I use is that of Kim and O'Neil (1997):

$$1000 \ln \alpha = 18.03 * \frac{10^3}{T} - 32.42$$

Where

$$\alpha_{water-calcite} = \frac{R_{water}}{R_{cakcite}}$$

which becomes

$$\alpha_{water-clacite} = \frac{1{,}000 + \delta_{water}}{1{,}000 + \delta_{calcite}}$$

and T in is the temperature in Kelvins.

Any mineral composition can be the result of many possible combinations of water composition and temperature. For example, calcite with $\delta^{18}Oc$ = -8‰ relative to the VPDB standard may have been precipitated from water with $\delta^{18}Ow$ =0‰ relative to VSMOW at T = 60°C, or from a water with δ18Ow = -7.0‰ relative to VSMOW at T = 20°C. Thus, it is also important to know the water temperature.
The $\delta^{18}O$ values of ostracod shells reflect the $\delta^{18}O$ of the habitat water and the water temperature during mineralization.

$^{87}Sr/^{86}Sr$ - Several studies have successfully applied $^{87}Sr/^{86}Sr$ ratios of ostracods to infer water sources and paleo-hydrological changes assuming that changes in the Sr isotope ratios are controlled primarily by the proportion of the water source in the solution (e.g., McCulloch et al., 1989; McCulloch and De Deckker, 1989).

For ostracod analysis, About 30 grams from each sample were wet sieved with tap water through 63 μm and dried. The sieved and dried samples were sieved again (>250 μm) and ostracods, mostly *Cyprideis torosa* and *Candona* valves were identified and separated under a binocular microscope. For ostracod elemental and isotopic analysis, only adult or A-1 specimens of *C. torosa* were used. When possible, 10 or more valves were used in order to measure the chemistry and $^{87}Sr/^{86}Sr$ isotope ratio in the same sample. At least 4 shells were used for Sr, Mg and Ca measurements when ostracods were rare. Twenty three ostracod samples from SOG2 borehole and 11 samples from SOG3 borehole were measured for their chemistry (Sr, Mg and Ca). Four of these measurements are replicates from 3 samples. The $^{87}Sr/^{86}Sr$ isotope ratios were analyzed in 22 samples.

Each ostracod was washed in distilled water, cleaned ultrasonically, dissolved in 3.5 N HNO_3 and analyzed for Ca and Sr concentrations by ICP-AES using Optima 3300 machine in the Geological Survey of Israel (GSI). Each run included repeated determinations of the international standards SO-3. Estimated precision is less than 5%.
The preparatory work for the Sr isotopic analysis included dissolution of the cleaned shells in 1.5 ml of 3.5 N distilled HNO_3 and extraction of Sr by column filled with Sr-Spec 50-100 mesh resin (e.g. Stein et al., 1997). Strontium isotope ratios were measured with Multi-Collector Inductively Coupled Plasma Mass Spectrometer (MC-ICP-MS) NU instruments at the GSI. During the course of the study the NBS987 standard yielded $^{87}Sr/^{86}Sr$ = 0.71029±0.00002 (n= 9, 1σ).

For $\delta^{18}O$ measurements, about 20 ostracod shells from each sample were selected. Samples were dissolved in 100% phosphoric acid before measuring. Oxygen isotope ratios were measured using a

Gas Bench system attached to a Delta Plus mass spectrometer at the GSI. $\delta^{18}O$ values were calibrated against the international standard NBS-19 and are reported in permil (‰) relative to VPDB standard. Analytical reproducibility of duplicates is better than 0.1‰. Water values are reported in VSMOW.

2.2.4 Bulk carbonate chemical and isotope analyses

Fifty-seven samples of bulk carbonate from KIN2 borehole were analyzed for their Ca, Sr, Mg and U concentrations assuming that the bulk carbonate is composed of autigenic calcite. About 60 mg of bulk sediments were dissolved in acetic acid, centrifuged to separate the carbonate fraction, dried on a hot plate, dissolved with concentrated HCl, dried again, dissolved with concentrated HNO_3, dried and dissolved with 3.5N HNO_3 before measurement by ICP-AES using Optima 3300 machine in the Geological Survey of Israel (GSI). Errors are less than 5%. Sc, Ru and Rh are added as internal standard.
The preparatory work for the strontium and $\delta^{18}O$ isotopic analysis is elaborated in the ostracod analysis section.

2.2.5 ^{14}C dating

Three samples of coal chunk (charcoal) and one sample of ostracod shells from Ohalo trench, four samples of coal chunk and two samples of ostracod shells from KIN2 borehole were radiocarbon dated. Five radiocarbon ages of organic debris and three radiocarbon ages of ostracod shells from SOG2 and six samples of coal chunk and wood from SOG3 were dated by radiocarbon.
Coal chunk, wood samples and ostracod shells were dated by radiocarbon at ANSTO, Austratlia. Additional 6 samples of organic debris and *Melanopsis* shells from Ohalo trench and one sample of *Melanopsis* shell from KIN2 borehole were modified after Hazan et al., (2005) according to OXCAL 4.2.

2.2.6 U-Th dating

Eight stem casts samples from Ohalo trench, composed of 100% aragonite confirmed by XRD were dated by U-Th at the GSI. Prior to measuring, 10-50 mg from each sample was dissolved in 5 ml HNO3 7N and weighted ^{229}Th-^{236}U was added to each sample. Extraction of uranium and thorium by column filled with Bio-Rad AG 1X8 200-400 mesh resin (e.g. Stein et al., 1997). Uranium isotope ratios were measured with Multi-Collector Inductively Coupled Plasma Mass Spectrometer (MC-ICP-MS) NU instruments at the GSI.

Chapter 3: Results

3.1 Lithology

Three boreholes and one trench were examined for their lithology. For that I analyzed their structure (massive or laminated), the mineralogy (by XRD), the grain size and carbonate content. I noticed that most of the samples were similar in their mineralogy and contain up to 75% calcite, 5-25% quartz and 5-25% clays. Although marl is usually used for sediments that contain no quartz, in this study I will use the term marls for sediments that contain up to 25% quartz.

I use the lithology to discuss paleo-environment, and in particular to evaluate changes in water level through time. I also use the lithology to estimate detritus material sources and compare it to Lake Lisan.

3.1.1 Ohalo trench

The main lithological units comprising the OH trench are marls (massive and laminated) that contain various amounts of ostracod shells of which *C. torosa* make up >98% (Figure 3.1). XRD results show high calcite content (~50%) and minor amounts of dolomite (less than 5%). Quartz and clay content are in the range of 5-25%. The fine grain size fraction (<63μm) is less than 90% at the top 2 meters and at the base (50 cm) of the borehole.

The lithology of the trench and ostracod-assemblages show four distinct sub-sections implying changes in the environmental and depositional conditions during the period under discussion. Toward the bottom of the core, between 216.5 and 215.0 m bsl, no ostracods were observed. Most of this section is composed of mm-thick laminated marls. Between 215.0 and 214.0 m bsl the large number of ostracods is accompanied with appearance of massive marls. The interval from 214.0 to 212.3 m bsl is dominated by massive marls, and the decrease in the ostracod shell abundance implies a change in the environment. The top of the core, from surface to 212.3 m bsl, the sediments are composed mostly of calcareous marls.

Foraminifera were also present throughout the trench section (Figure 3.1) with excellently preserved tests though some show an abnormal growth mode (cf. Almogi-Labin et al., 1992; Flako-Zaritsky, 2006). Maximum numbers of foraminifera, mostly *Ammonia tepida* occur between 214.5 and 213.7 m bsl. In between 213.7 m and 212.5 m foraminifera occur in extremely low numbers. At 212.8 m and between 212.5 and 212 m bsl *Cribroelphidium* cf. *C. vadescens* is the dominant foraminifera and at the top of the trench *A. tepida* is again predominant. The abundance variation of the foraminifera with depth in the trench resembles that of ostracod shells. This suggests a higher salinity than modern Lake Kinneret for the time interval represented at 214.5-212 m, since foraminifera are usually found in saltier water (e.g. >1200 mg Cl/l as evident in the Timsah springs, Almogi-Labin et al., 2004; Flako-Zaritsky et al., 2011). Predominance of *C.* cf. *C. vadescens* indicates somewhat fresher water compared with intervals rich in *A. tepida* (Sivan et al., 2011).

Aragonite (as determined by XRD analysis) stem-casts of undetermined biogenic origin were also observed throughout the trench, mostly in considerable numbers (Figure 3.2).

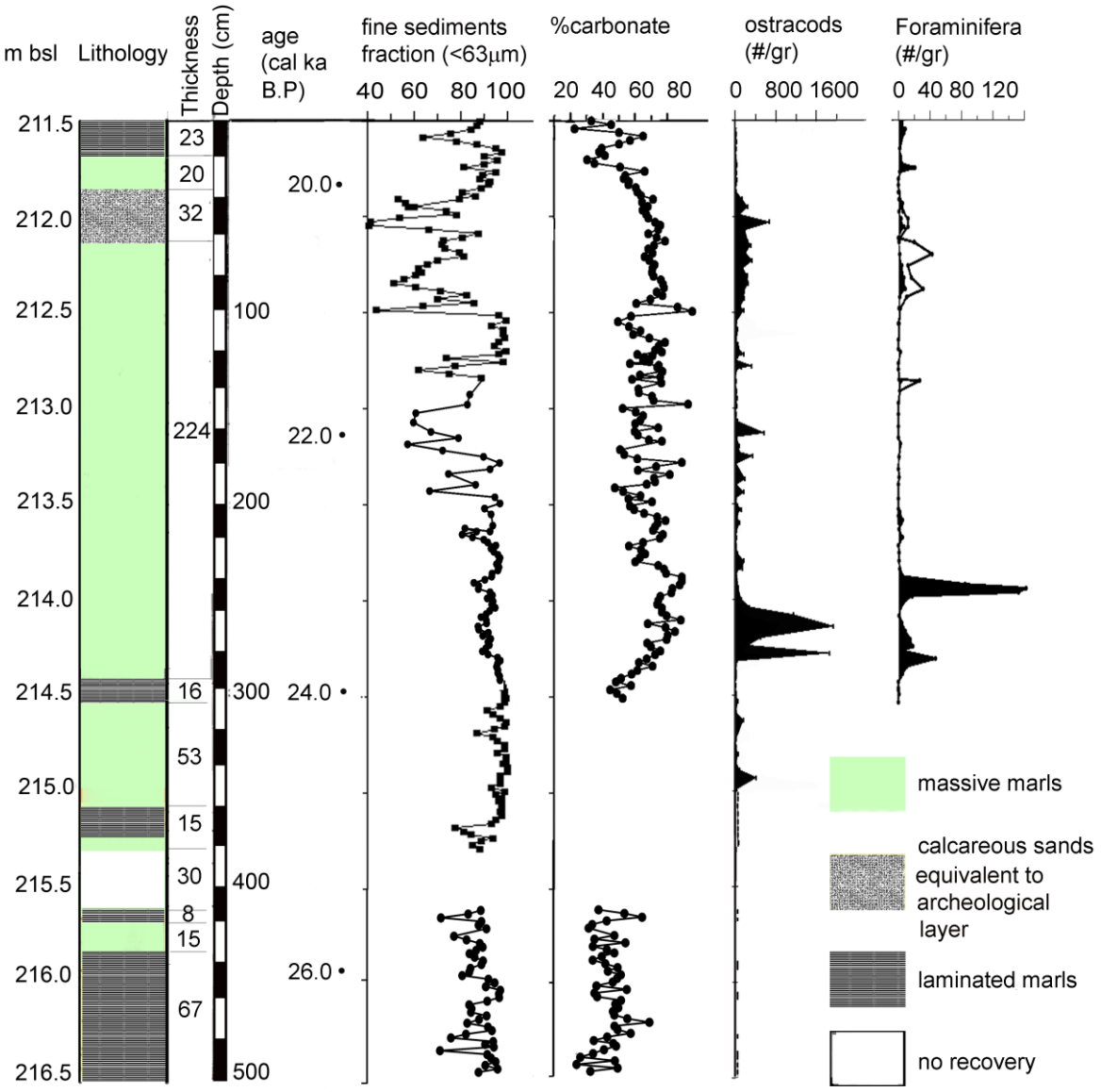

Figure 3.1 Percent of fine sediment <63 μm, carbonate content, and number of ostracods and foraminifera (per gram dry sediment) in the OH trench. The fine fraction comprise ~90% of the sediment at the bottom of the trench and shows fluctuations at the top. The carbonate content usually ranges from 40 to 60%. Ostracods and foraminifera show higher numbers at the top and mainly between ~214.0 and ~214.5 m bsl. Among the benthic foraminifera, the black filling represents the abundance of *Ammonia tepida* and the white filling of *Cribroelpidium* cf. *C. vadescens*.

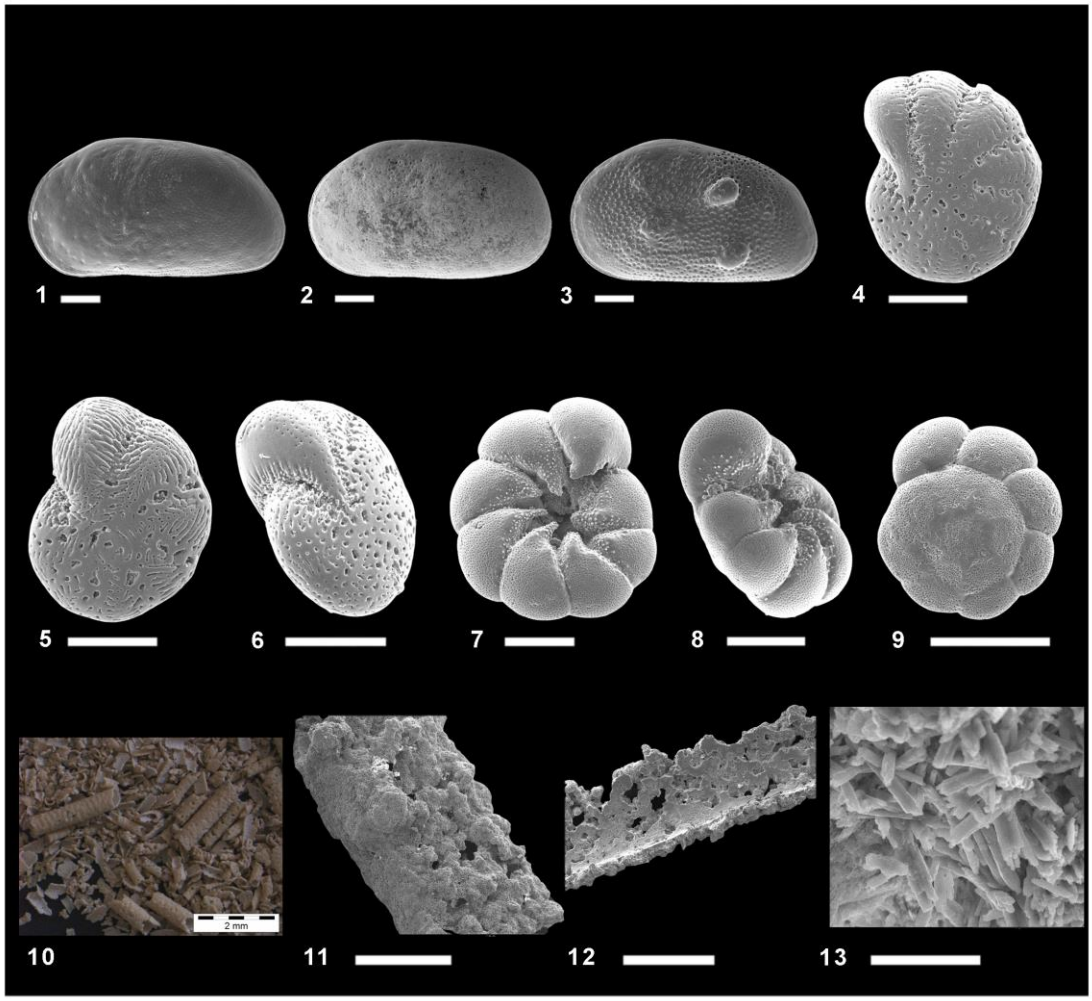

Figure 3.2 Foraminifera, ostracod and aragonite stem cast. All scale bars are 100 μm except fig. 13, 10 μm, fig. 9, 200 μm, figs. 11-12, 500 μm and fig. 10, 2 mm. 1-3. *Cyprideis torosa* (Jones, 1850): 1. Male, left valve; 2. Female, left valve; 3. Noded juvenile, left valve. 4-6. *Cribroelphidium* cf. *C. vadescens* (Cushman and Brönnimann): 4-5. Lateral view; 6. Profile view. 7-9. *Ammonia tepida* (Cushman): 7. Umbilical view; 8. Profile view; 9. Spiral view. 10-13. Stem casts made of aragonite: 10. General view of well preserved cylndrical casts; 11. Surface morphology; 12. Inner part view; 13. Magnification of aragonite needls of the casts.

3.1.2 KIN2 core

The KIN2 core comprises of two main sedimentary lithologies (Figure 3.3). Most of the core consists of mm thick laminated sediments (green/gray, yellow/gray, black/gray) that dominate from 221.5 to 215.5 m bsl. Thin layers of massive marls appear occasionally below and above the laminated sequence. From 222.0 to 221.5 m bsl the massive sediments alternate with thin layers of black and gray/white and gray laminas. From 215.5 m bsl to the top of the borehole coal grains were identified at times. At the bottom of the borehole, at 222 m bsl, a pebbly layer that contained leaking warm and saline waters was found (Hazan et al., 2005).

XRD results show high calcite content (~50%) and minor amounts of dolomite (less than 5%). Quartz and clay content are in the range of 5-25%. The fine grain size fraction (<63μm) is less than 90% at the top 2 meters and at the base (50 cm) of the borehole. The rest of the borehole is characterized by high content of fine sediment, typically with grain size mode of 4-8μm (<98%, figures 3.3, 3.4). One sample from the bottom of the borehole is characterized by coarser sediments with mode value of grain size of 23μm.
The carbonate content values at the top of the borehole are 50-60%. Throughout the rest of the borehole the carbonate content is on average 35% but shows large fluctuations, with minimum values of 20% and maximum values of ~80%.
Ostracods are scares throughout the borehole, and were recovered from the depth of 150 cm from top (214.5 m bsl) and from the bottom of the borehole.

3.1.3 SOG2 core

The SOG2 borehole comprises mostly massive and laminated marls, with some ostracods and diatoms (Figure 3.5). XRD results exhibit ~50% calcite, and varying amounts of quartz (usually in the range of 5-25%). Few samples from top of the core also consist of minor amounts of gypsum.

The core is divided into four units.

(1) In the interval from 234.0 (the bottom of the borehole) up to 228.2 m bsl the core contains massive and laminated marls. The carbonate content is usually ~ 40% with minimum values of ~20% (at 232.0 m bsl, figure 3.5). Grain size mode value of bulk sediments is ~10 μm (Figure 3.6).
(2) Between 228.2 and 227.9 m bsl the carbonate content decreases to ~20%, the mode of the bulk sediments is ~10 μm.
(3) From 227.4 to 226.05, the sediments are similar to those composing the bottom of the borehole.
(4) In the top of the core, from 226.05 to 226.0 m bsl the carbonate content is higher than 60%, the percent of fine grains sharply decreases to 25-50% and the grain size mode value is ~40μm.

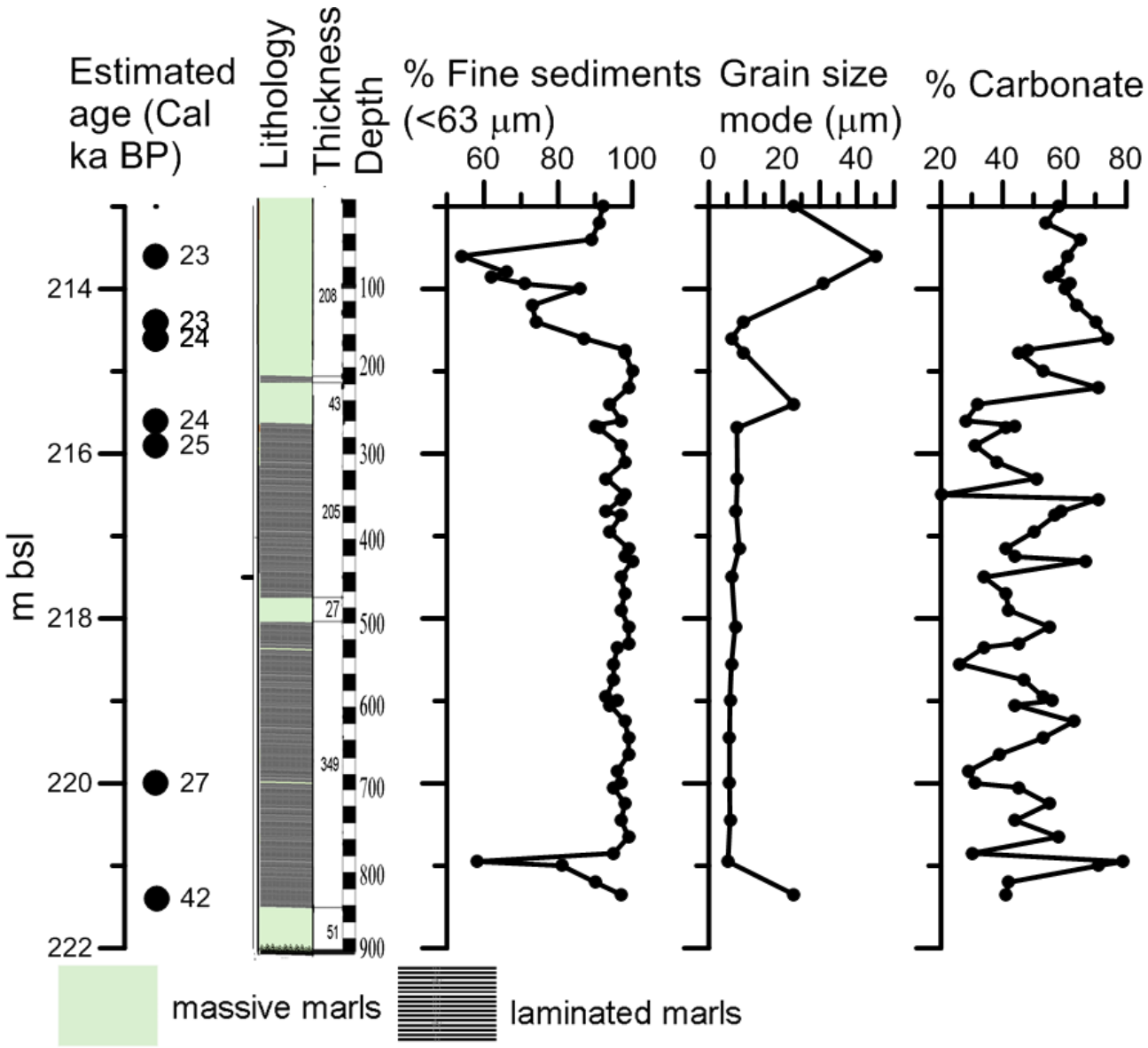

Figure 3.3 Lithology, percent of fine sediment <63 μm, mode value of grain size and carbonate content at the KIN2 borehole. The fine fraction comprises more than 90% of the sediment between 216 and 221.5 m bsl and the mode value of grain size is typically 4-8μm. The carbonate content fluctuates from 20 to 80%. A change in all parametes is noted above ~216.0 m bsl, implying some environmental change. Black ages are calibrated radiocarbon ages (Figure 4.3).

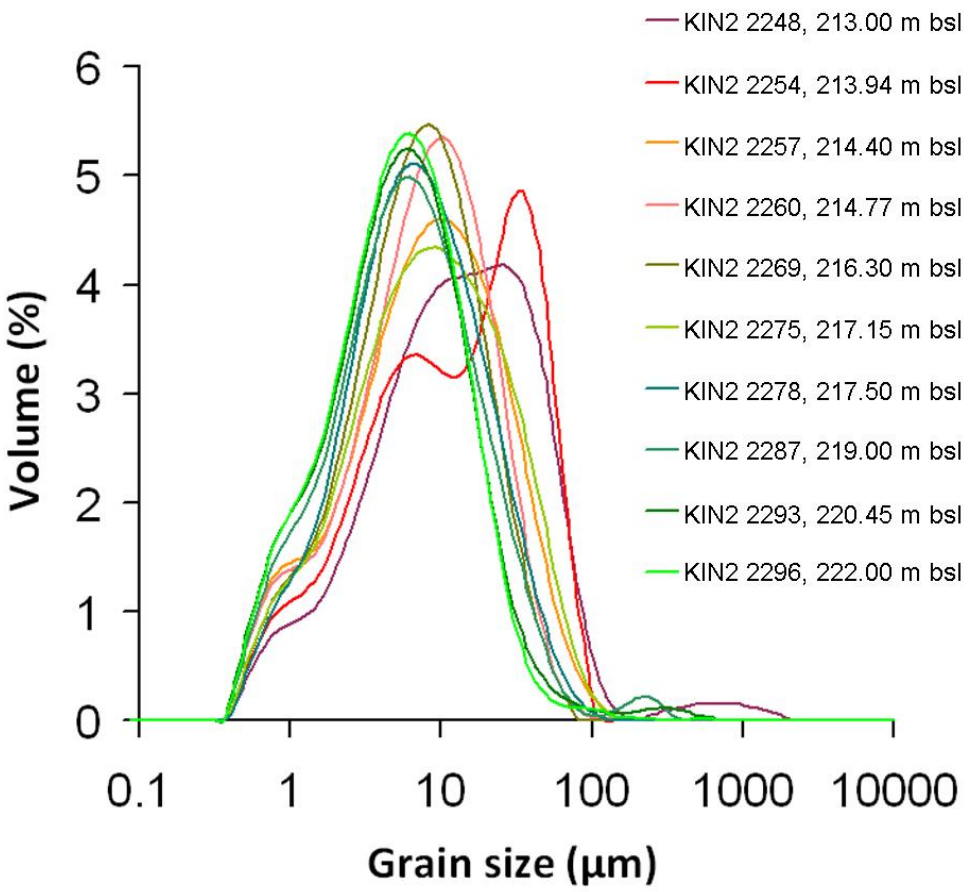

Figure 3.4 Grain size analyses of bulk sediments from KIN2 borehole. Most of the borehole is characterized by uni-modal distribution of grain size, typically with a peak at 5-8µm. Samples from the top of the borehole and one sample from the bottom of the borehole are characterized by coarser sediments.

Few samples at the top of the core contain small amounts of mollusks. Most of the sediments contain small *C. torosa* shells. Only 16 samples contain sufficient amounts of shells for chemical and isotope analysis. The top of the core, from 226.00 to 226.05 m bsl is rich in benthic freshwater diatoms and show somewhat higher amounts of *C. torosa*. Below 224.05 m bsl the core is composed of layers rich in, mostly brackish benthic diatom species, alternating with layers barren of diatoms (Ehrlich, 1985).

3.1.4 SOG3

The SOG3 borehole lithology is quite homogeneous, with alternating massive and laminated marls (Figure 3.7). The lithology in the bottom of the borehole, up to 235.80 m bsl is composed of massive marls, the carbonate content is high, usually in the range of 50-80% and the % fine fraction < 63 μm is lower than 90% and shows an increasing trend. The grain size mode values are of ~5 μm (Figure 3.8). Between 235.80 and 234.90 m bsl the lithology changes to laminated marls, the carbonate content decreases to ~20% and the fine grain size content of is ~ 95%. From 234.90 to the top of the borehole, the sediments are mostly massive marls with some laminated sequences. The carbonate content stabilizes around 40%, the % fine sediments (<63μm) is typically higher than 90% and the grain size mode values range between 10 and 20μm.
According to XRD, most samples contain less than 25% calcite, which is in agreement with the carbonate content, and varying amounts of quartz (usually in the range of 25-50%). Few samples also consist of minor amounts of dolomite.
Small amounts of *C. torosa* were recovered in most samples. Most of the sediments contain young specimens of *C. torosa* shells and only 11 samples contain sufficient amounts of shells for analysis. At the bottom of the borehole up to 235.80 m bsl no ostracods were recovered. Between 235.80 and 234.90 m bsl Ostracods are scares. Small amounts of ostracods were recovered from 234.90 m bsl to the top of the borehole.
The top of the core (down to 233.65 m bsl) is barren of diatoms. From 233.65 to 235.65 m bsl various amounts of diatoms were observed, mostly brackish specie (Ehrlich, 1985). The interval from 235.65 to 238.0 m bsl also lack diatoms. Small amounts of broken valves of euryhaline benthic forms of diatoms were recovered.

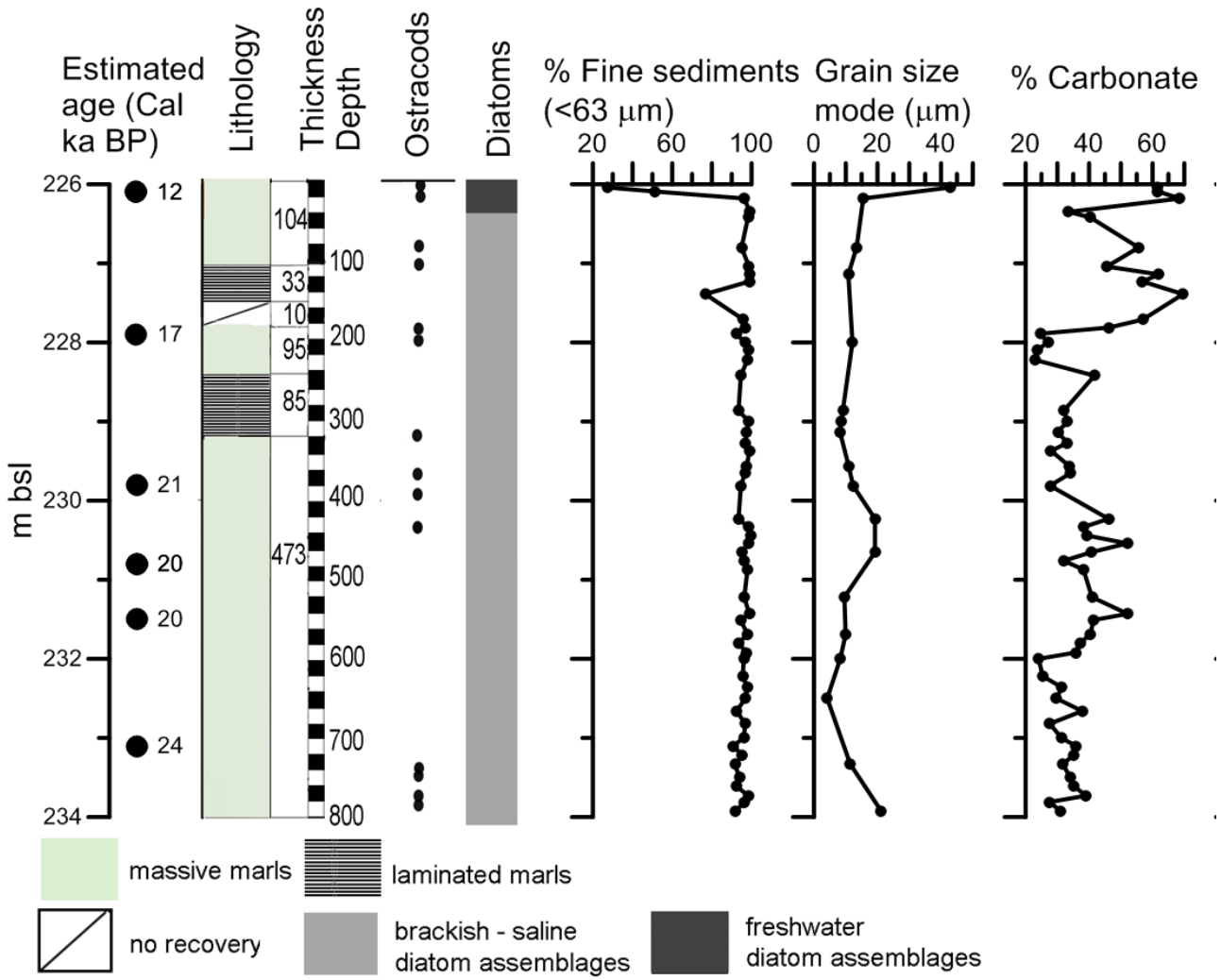

Figure 3.5 Lithology, percent of fine sediment <63 μm, carbonate content, grain size, presents of ostracod shells and presents of brackish/freshwater diatoms (Ehrlich, 1985) at SOG2 borehole. According to Ehrlich, 1985, the top of the core was at 224.0 m bsl, however sediments were recovered below 226.0 m bsl only. Except for the top of the borehole, the fine fraction comprises ~99% of the sediment. The carbonate content is typically less than 50% from bottom to 228 m bsl, and higher at the top of the borehole. Brackish diatoms were recovered at most of the borehole. Black ages are radiocarbon ages (Figure 4.1).

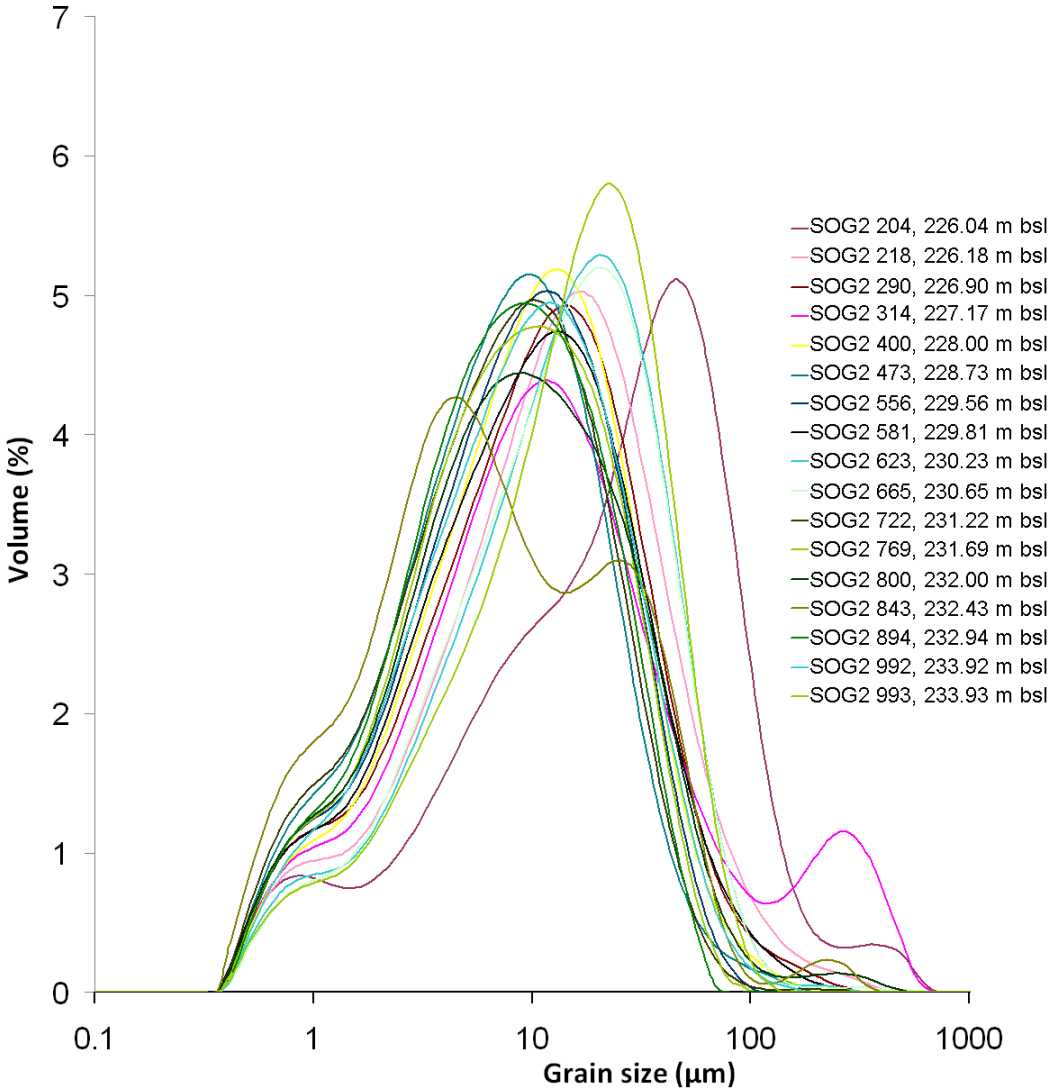

Figure 3.6 Grain size of SOG2 borehole. One sample at the top of the borehole shoes coarse grain size (>40µm). Most of the borehole is characterized by uni-modal distribution of grain size, typically with a peak at ~10µm.

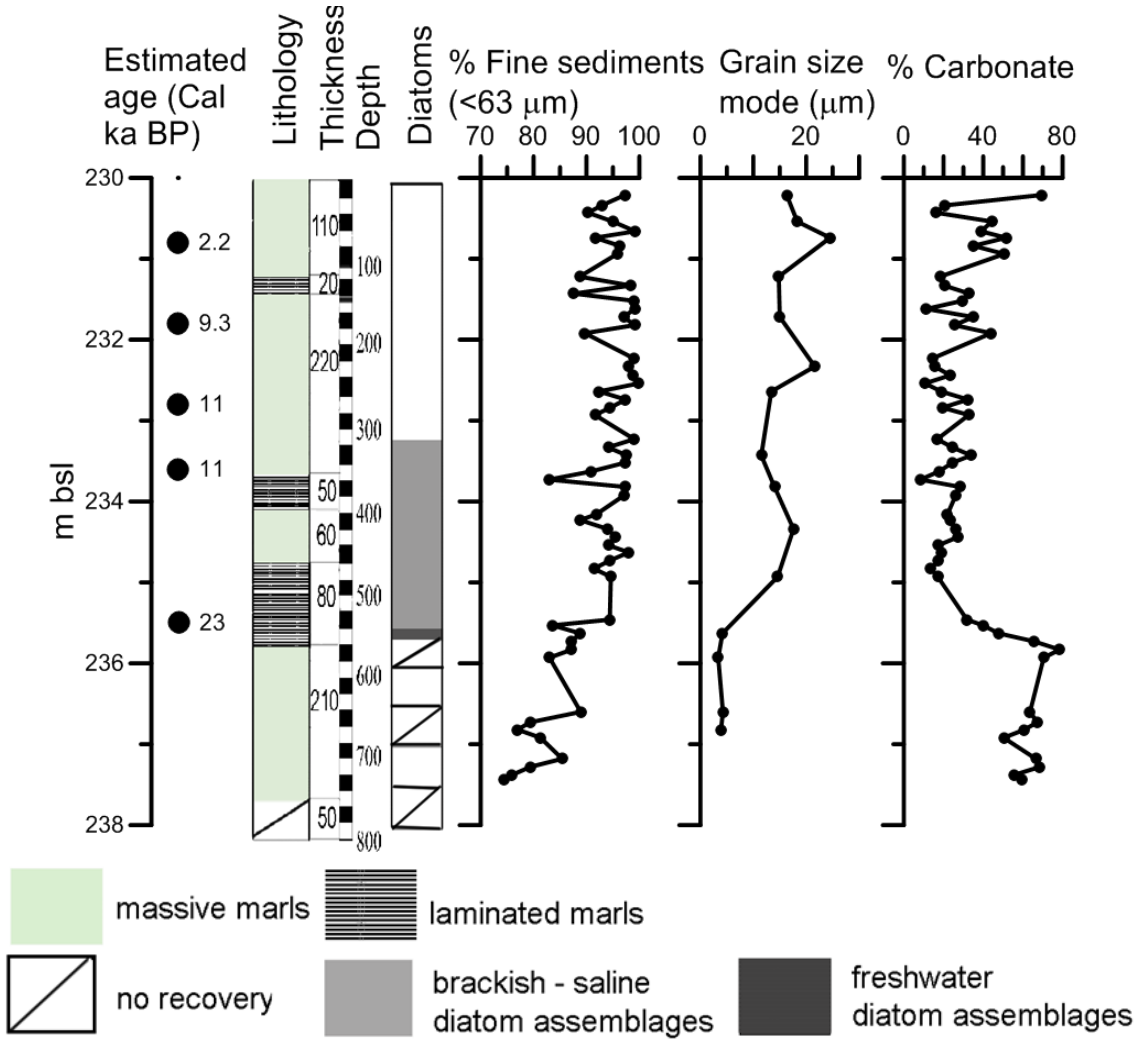

Figure 3.7 Lithology, percent of fine sediment <63 μm, carbonate content, grain size, presents of ostracod shells and presents of brackish/freshwater diatoms (Ehrlich, 1985) at SOG3 borehole. According to Ehrlich, 1985, core top of the core was at 229.0 m bsl, however, the sediments were recovered below 230.0 m bsl. The fine fraction comprises ~90% of the sediment at the top of the trench and less than 85% from 236 m bsl to the bottom. The carbonate content usually fluctuates around 40% at the top of the borehole and ~80% at the bottom. Black ages are radiocarbon ages (Figure 4.4).

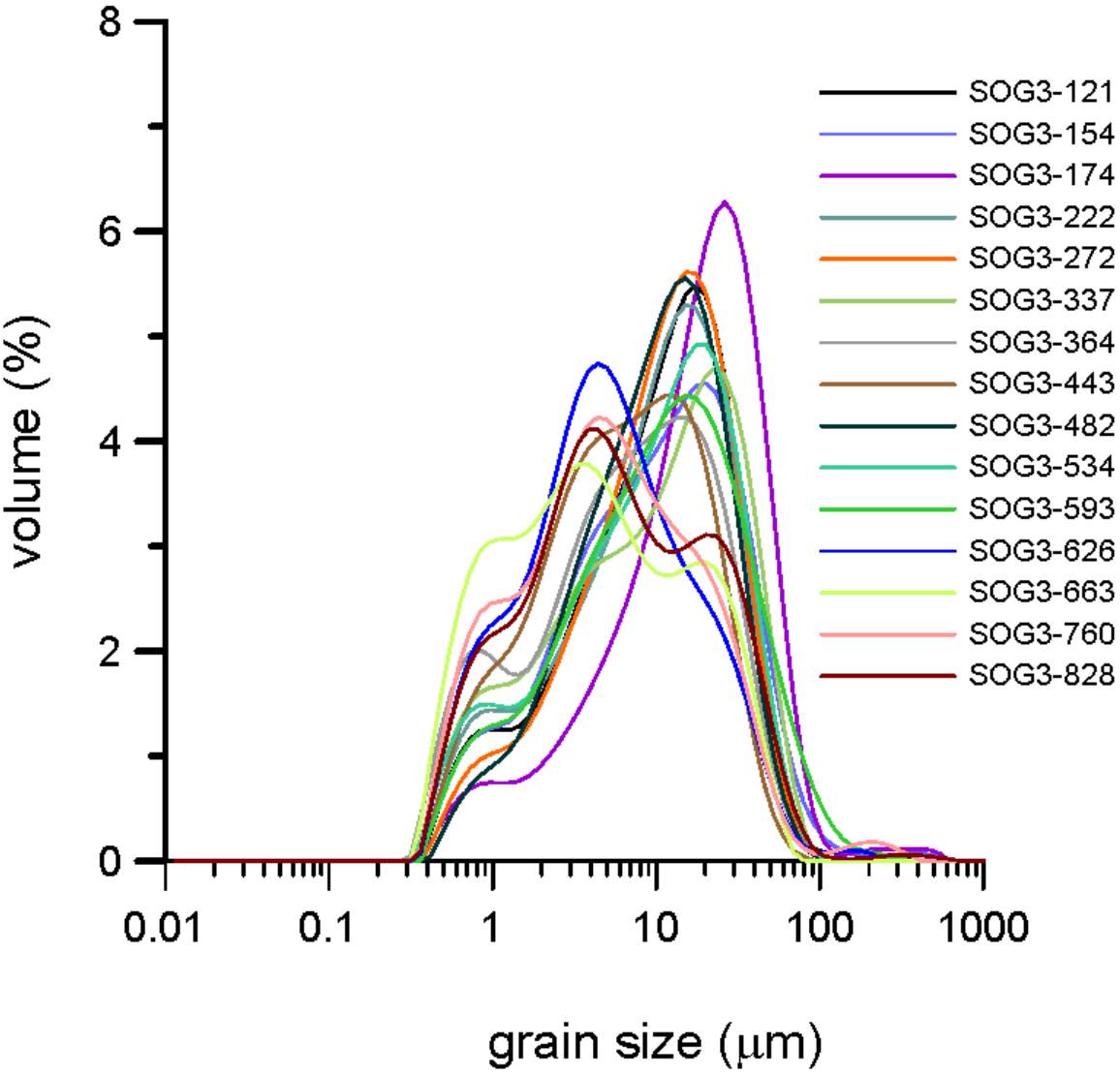

Figure 3.8 Grain size of SOG3 borehole. Up to 235.80 m bsl, grain size mode values are of ~5 μm. Between 235.80 and 234.90 m bsl the fine grain size content of is ~ 95%. From 234.90 to the top of the borehole grain size mode values range between 10 and 20μm.

3.2 Chemistry

3.2.1 Mg/Ca, Sr/Ca and $^{87}Sr/^{86}Sr$ ratios in lake water and ostracod shells

3.2.1.1 Recent Lake

Sr/Ca and Mg/Ca ratios of ostracod valves and ambient water from Lake Kinneret have average values of 0.0048 and 0.012 in the ostracods and 0.007 and 1.07 in the water (table 3.1).
$^{87}Sr/^{86}Sr$ ratios in ostracods from modern Lake Kinneret lie between 0.70749 and 0.70765.

3.2.1.2 Ohalo trench

Sr/Ca and Mg/Ca ratios in *C. torosa* shells from the trench range from 0.0017 to 0.0030 and from 0.0075 to 0.0250 respectively (Figure 3.9). An increase in the Mg/Ca values is observed from 214.5 to 213.7m and fluctuating but non-trending values occur above 213.5m. Sr/Ca values are higher at the base of the section, decrease towards 214.5 m bsl, increase upward to 213.5m and fluctuate around 0.003 from 213.5 m bsl to 212.0m, and decreases from there to the top of the trench.

$^{87}Sr/^{86}Sr$ ratios in *C. torosa* from OH trench range between 0.70790 and 0.70810 (Figure 3.9), showing lower values below 214.5 m bsl.

3.2.1.3 SOG2

Sr/Ca and Mg/Ca ratios in ostracod shells from SOG2 borehole range from 0.0016 to 0.0039 and from 0.0069 to 0.198 respectively (Figure 3.10). The top of the core (down to 226.10 m bsl) are characterized by higher Sr/Ca values, and a sharp decrease to quite constant values of ~0.0020 from 226.10 m bsl and downwards. Mg/Ca values show somewhat lower values in the top part of the core. $^{87}Sr/^{86}Sr$ ratios in the ostracods range from 0.70771 to 0.70807, showing the lowest values at the top of the borehole and the highest values between 227 and 230 m bsl.

3.2.1.4 SOG3

Sr/Ca and Mg/Ca ratios in ostracod shells from SOG3 borehole range from 0.0044 to 0.0060 and from 0.0066 to 0.133 respectively (Figure 3.11), with a much higher Sr/Ca ratio compared with SOG2. Sr/Ca values show a small increase from bottom to 233.5 m bsl. $^{87}Sr/^{86}Sr$ ratios in ostracods range from 0.70765 to 0.70773, showing slightly lower values at the top of the borehole and lower values compared with SOG2.

Table 3.1 Mg, Sr, Ca, Sr/Ca, Mg/Ca, $^{87}Sr/^{86}Sr$ and $\delta^{18}O$ in water and living ostracods, this study

Sampling sites	Ostracods*							Water						
	#	Mg++ (ug/L)	Sr++ (ug/L)	Ca++ (mg/L)	Mg/Ca (eq)	Sr/Ca (eq)	$^{87}Sr/^{86}Sr$	$\delta^{18}O$ ‰VPDB	Mg++ (mg/L)	Sr++ (mg/L)	Ca++ (mg/L)	Mg/Ca (eq)	Sr/Ca (eq)	$\delta^{18}O$ ‰VSMOW
KG-1	10	175	248	24	0.012	0.0047	0.70752	-0.22	35	0.7	56	1.03	0.006	+0.26
KT-1	10	164	270	25	0.011	0.0050	0.70757	-0.35	37	0.8	55	1.11	0.007	+0.12
KS-1	5	101	150	14	0.012	0.0048	0.70765	-0.13	37	0.8	52	1.17	0.007	+0.36
KM-1	10	179	230	24	0.012	0.0044	0.70749	+0.07	34	0.8	58	0.96	0.006	+0.56

*Values that were measured in the solution; KG=Ginosar, KM=Ma'agan, KS=Shitim, KT=Tabgha; # Number of species

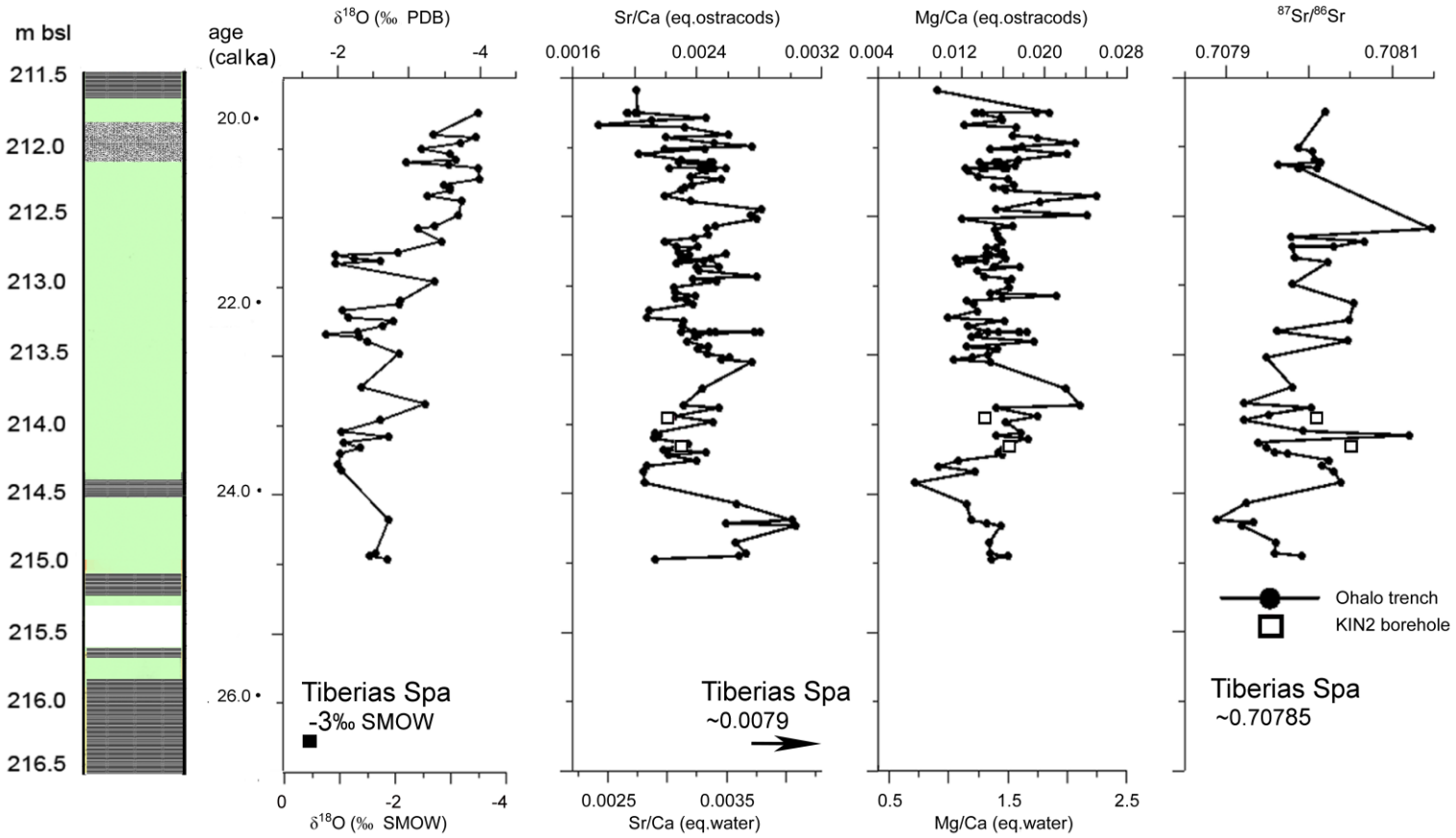

Figure 3.9 $\delta^{18}O$, Sr/Ca, Mg/Ca and $^{87}Sr/^{86}Sr$ values of ostracod shells and inferred water values from the OH trench (black dots) and KIN2 borehole (squares). The $\delta^{18}O$ water shows a decrease in values from ~ -2.0‰ VSMOW below 212.5 m bsl to ~ -3.5‰ at the top of the trench. The values are lower than modern lake (~0.0‰). Sr/Ca in the water is lower than modern LK (~0.007), showing a wiggle in the values above ~214.5 m bsl, and somewhat higher values below that point. Mg/Ca values in the water are similar to the values in the modern lake (~1.0). $^{87}Sr/^{86}Sr$ in the water is higher than modern values, and shows a small increase in values from bottom to top. The lithologic legend is given in figure 3.1.

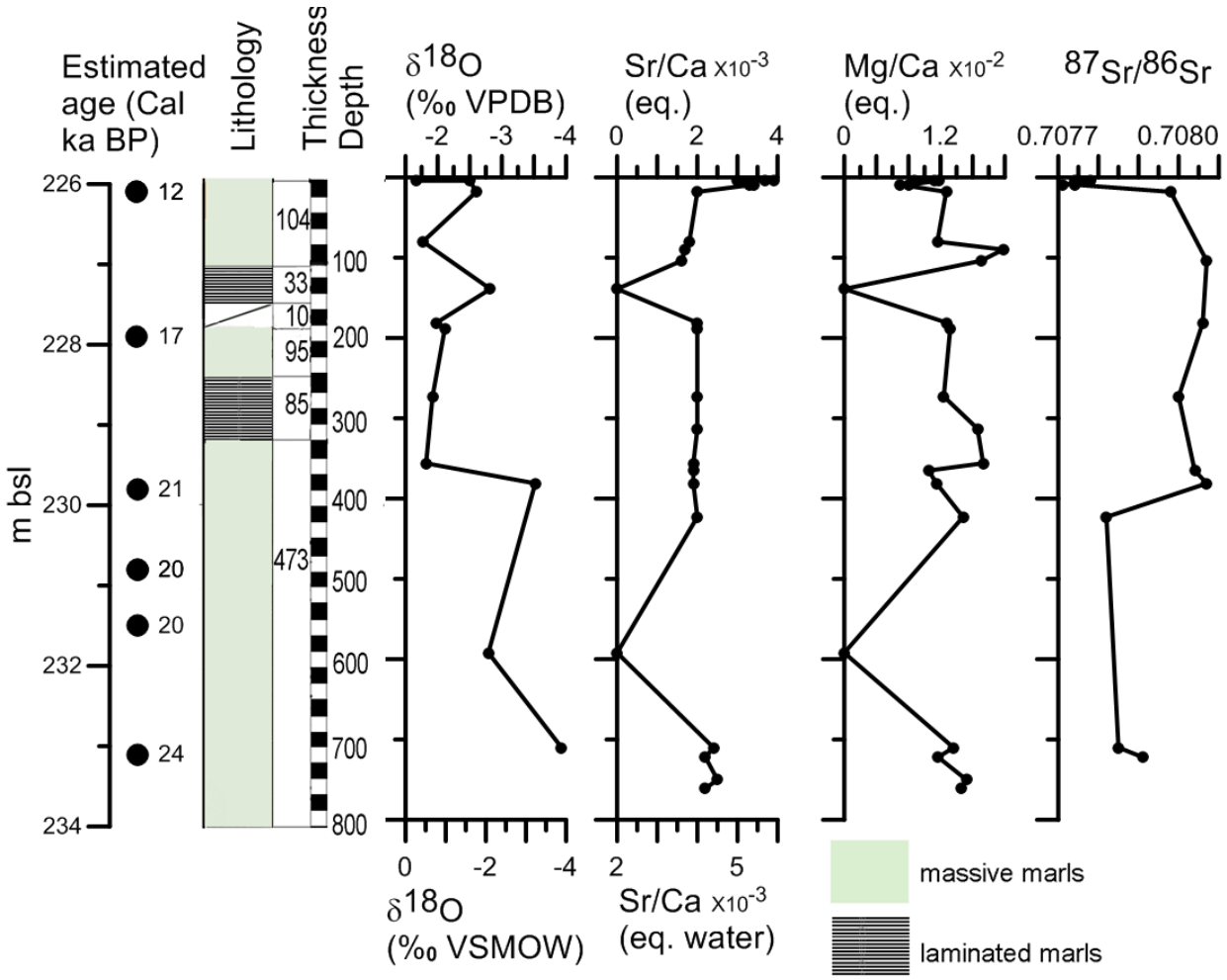

Figure 3.10 $\delta^{18}O$, Sr/Ca, Mg/Ca and $^{87}Sr/^{86}Sr$ values of ostracod shells and inferred water values from the SOG2 borehole. The $\delta^{18}O$ water shows an increase in values from ~ -3.5‰ VSMOW below 229.5 m bsl to ~ -1.5‰ at the top of the trench. Sr/Ca in the water is similar to the values that were inferred from Ohalo trench. The top of the borehole show higher values. Mg/Ca values in the water are similar to the values in the modern lake (~1.0). $^{87}Sr/^{86}Sr$ in the water are also similar to values from Ohalo trench, and show low values at the top of the borehole. The lithologic legend is given in figure 3.5.

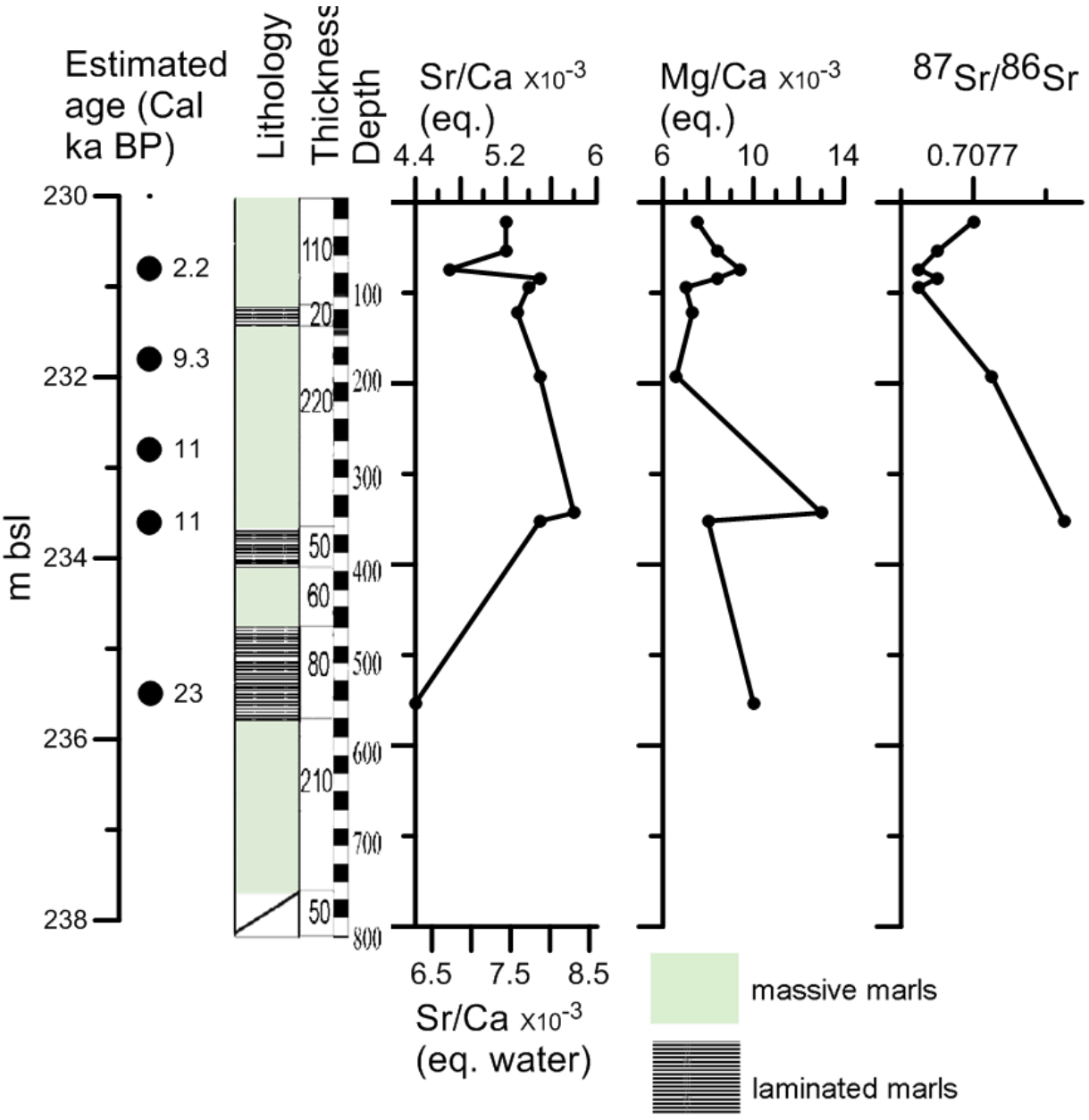

Figure 3.11 $\delta^{18}O$, Sr/Ca, Mg/Ca and $^{87}Sr/^{86}Sr$ values of ostracod shells and inferred water values from the SOG3 borehole. Sr/Ca in the water is higer than modern LK (~0.007). Mg/Ca values in the water are lower from the values in the modern lake (~1.0). $^{87}Sr/^{86}Sr$ in the water is higher than modern values, and shows a small decrease in values from bottom to top. The lithologic legend is given in figure 3.7.

3.2.2 $\delta^{18}O$ in the lake water and ostracod shells

3.2.2.1 Recent Lake

$\delta^{18}O$ values in modern Lake Kinneret water lie between 0.12 and 0.56‰ (VSMOW) (table 3.1). $\delta^{18}O$ in living ostracod shells from the same localities lie between -0.37‰ and +0.07‰ (VPDB). Values of ostracod shells (VPDB) were ~0.5‰ lighter than the lake water reflecting a fractionation factor.

3.2.2.2 Ohalo trench

The $\delta^{18}O$ values of *C. torosa* shells from the OH trench lie between -4‰ and -2‰ (VPDB, figure 3.9). Ostracod values correspond to water values of -3.5‰ to -1.5‰ (VSMOW) at 19^{o}C assuming isotopic equilibrium between calcite and water.
The $\delta^{18}O$ values show an overall decrease along the section, with some shifts to more positive ratios, e.g. at 22.2 ka BP.

3.2.2.3 SOG2

The $\delta^{18}O$ in ostracod shells from SOG2 borehole lie between -3.93‰ and -1.66‰ (VPDB), corresponding to -3.5‰ to -0.5‰ (VSMOW) at 19 ^{o}C (Figure 3.10).

3.2.3 Mg/Ca, Sr/Ca, $^{87}Sr/^{86}Sr$ and $\delta^{18}O$ ratios in bulk carbonate

Mg/Ca in bulk carbonate from OH7 trench ranges from 0.026 to 0.093, showing an increasing trend from bottom to top (Figure 3.12). Sr/Ca in the sample ranges from 0.0012 to 0.0013 showing a decreasing trend from bottom to top. $^{87}Sr/^{86}Sr$ values that were measured on bulk carbonate range from 0.70767 to 0.70792 showing larger fluctuations at the top of the segment.
Sr/Ca and Mg/Ca in bulk carbonate from KIN2 borehole range from 0.0012 to 0.0022 and from 0.023 to 0.129 respectively (Figure 3.12). $^{87}Sr/^{86}Sr$ values range from 0.70771 to 0.70796, with average value of 0.70778 and showing slightly lower values at the base of the core. One sample from depth of 221.20 m bsl shows higher value (0.70786) in accordance with higher Sr/Ca values (0.0020).

$\delta^{18}O$ at OH trench fluctuates from -3.89‰ to -3.07‰ (VPDB). These values correspond to -2.0‰ to -3.0‰ (VSMOW) at 19 ^{o}C.
$\delta^{18}O$ of bulk carbonate from KIN2 borehole range from -5.67‰ to -2.9‰ (VPDB), corresponding to -2.0‰ to -4.5‰ (VSMOW) at 19 ^{o}C. One sample at the base of the core (221.35 m bsl) show lower value of -8.44‰ VPDB (-7.5‰ VSMOW). This coincides with higher values of Sr/Ca in the bulk carbonate.

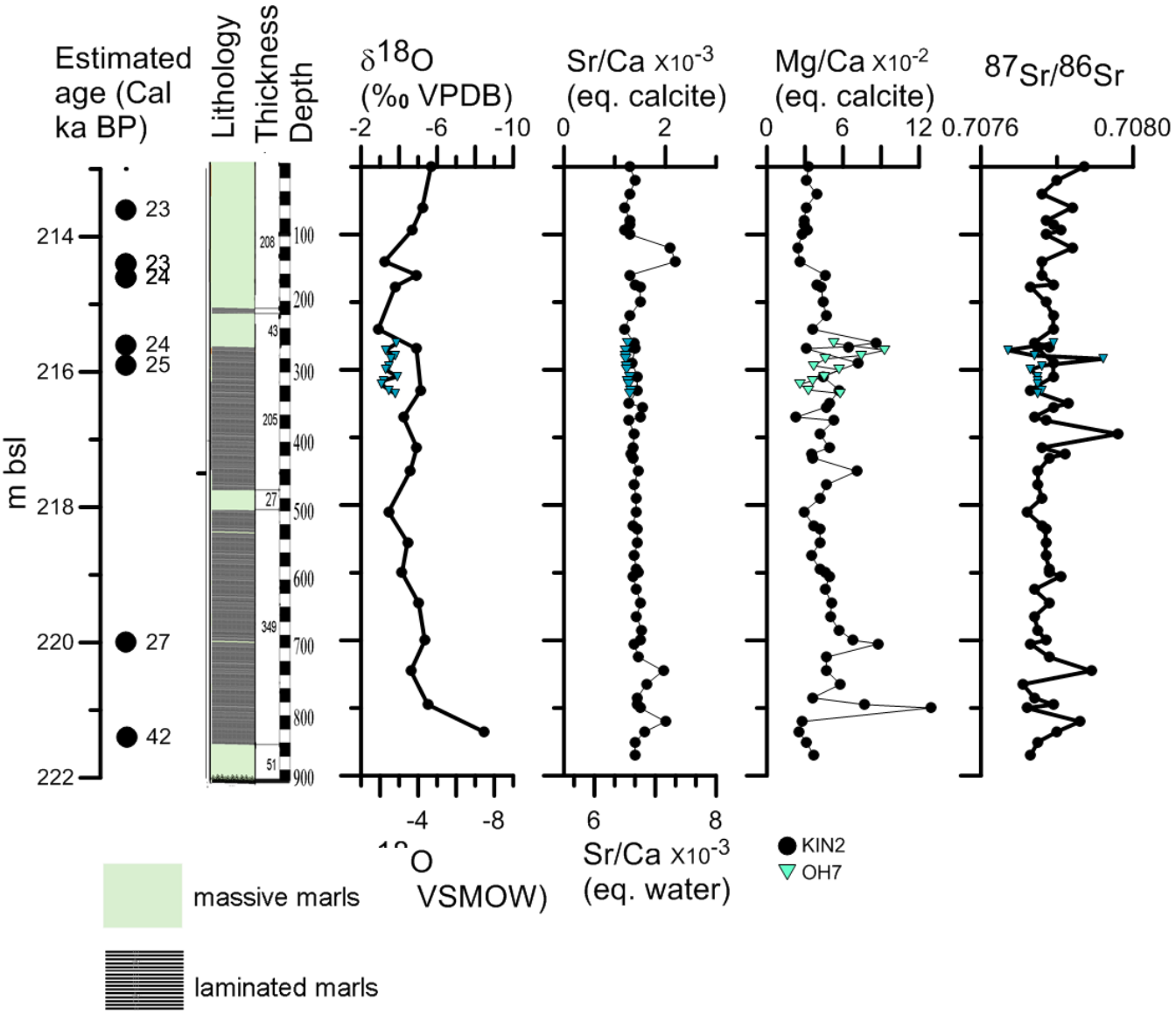

Figure 3.12 $\delta^{18}O$, Sr/Ca, Mg/Ca and $^{87}Sr/^{86}Sr$ values of bulk sediments and inferred water values from the OH7 segment from Ohalo trench and from KIN2 borehole. The $\delta^{18}O$ water shows values of ~ -6.0‰ VSMOW to ~ -3‰ between 215.5 to 221.5 m bsl. The values are lower than modern lake (~0.0‰). Sr/Ca in the water is ~0.007, showing small decrease from bottom to top. $^{87}Sr/^{86}Sr$ in the water is higher than modern values. The lithologic legend is given in figure 3.3. Blue ages are based on depth-age model (Figure 4.3).

Chapter 4: Chronology

4.1 General

The establishment of the late Pleistocene and Holocene environmental history of the Dead Sea – Kinnarot basins requires a high-resolution and precise chronological framework. Ages of the cores and trench that are discussed in this study were obtained mainly by radiocarbon dating of coal chunks, wood remains and *Melanopsis* shells. Most of them lie in stratigraphic order, allowing us to obtain reasonable depth-age models. However, the reconstruction of depth-age model for the trench and the boreholes is hampered by measured ages that lie outside of stratigraphic order. This led us to examine the possibility of using carbonate shells for radiocarbon dating as well as independent dating methods such as the U-Th disequilibrium method.

Radiocarbon dating of lacustrine carbonates (sediments and shells) involves two issues that need to be taken into account: first, the reservoir age, and second – the calibration because of secular variations in atmospheric ^{14}C.

The ^{14}C of the lacustrine water is affected from contribution of old carbon, resulting in different values than atmospheric ^{14}C content. I assume that the source for ^{14}C in a sample is the water habitat, thus I need to apply reservoir age to our ages. The problem with the reservoir age is that it is not constant for all water bodies. Even more problematic is that it might show temporal changes, thus I need to evaluate the reservoir age for each period using independent ages.

Ostracods and *Melanopsis* snails are common inhabitants of Lake Kinneret (Mischke et al., 2010; Tchernov, 1975). *Melanopsis* shells were found to be reliable radiocarbon chronometers when assessing known reservoir age (Lev et al., 2007). Here, I assessed the feasibility of using ostracod shells as radiocarbon chronometers. For this, I analyzed the ^{14}C (radiocarbon) content of fossil ostracod shells that were recovered from the trench and boreholes from Lake Kinneret (Sea of Galilee), and compared them to the ages of *Melanopsis* shells and charcoal from the same depth. I conclude that ostracod shells are in radiocarbon equilibrium with their habitat waters allowing specifying reservoir ages for Lake Kinneret waters. I also compared the radiocarbon ages to U-Th ages that were obtained on aragonite stem casts and to lake's water level. I succeeded to create a chronological framework for the trench and the boreholes.

The themes that are addressed in this chapter are:

1. Assessing the potential use of ostracod shells as radiocarbon chronometers: this includes evaluation of the reservoir ages and hard water contributions to the radiocarbon content of the ostracods.

2. Constructing depth-age models for the sedimentary sequences discussed in this work. For this I date organic debris, *Melanopsis* and ostracod shells by radiocarbon. I also use U-Th ages that were obtained on aragonite stem casts.

3. Re-establishing Lake Kinneret lake curve according to the new lithology and chronology data that were obtained in this work and discuss widespread hiatuses in the sequence.

4.2 The feasibility of using ostracod shells and reservoir ages of LK

Radiocarbon and U-Th data of the ostracod shells, organic debris and stem casts are listed in tables 4.1 and 4.2. The use of the results for reconstructing depth-age model is discussed below.

First I would like to assess the potential use of ostracods shells as radiocarbon chronometers. Fossil *Melanopsis* shells from Lake Kinneret were found to yield reliable ^{14}C ages when applying known reservoir ages (Lev et al., 2007). When I examine the ostracod shells from the top of Ohalo trench (OH-1 23.7) and KIN2 sample 2257 from 214.4 m bsl, I see that applying ~800 years reservoir age for shells would yield reasonable ages, consistent with atmospheric ^{14}C ages of adjacent charcoal. This reservoir age also match the reservoir age that was found for *Melanopsis* shells of the same age. I conclude that ostracod shells can be used as reliable chronometers when applying reservoir age.

Next, I use ostracod shells and charcoal samples to estimate the variability of the reservoir age of LK through time. The radiocarbon age of ostracod shell from SOG2 (at depth of 226.1 m bsl, table 4.1, figure 4.1) is older by ~5000 years from the age of a charcoal sample from the same stratigraphic layer that yielded a radiocarbon age of ~12 ka cal BP. This implies a reservoir age of 5,000 years for carbonate samples that were deposited during the YD period. This value is significantly higher than that of the modern Lake Kinneret (~ 800 years), but closer to the value deduced for Kibbutzim stream. It may indicate that the Kinneret waters (at least at the SOG2 site) originated from the mountain aquifers where they obtained high "hard carbon" content.

In summary, I can see the difference between reservoir age during H2 low stand water level (~800 years for 24-20 ka BP) and YD high stand water level (~5,000 years for 11-12 ka BP). This is due to changes in the contribution of the water sources. This issue will be elaborated in chapter 7.

4.3 Depth-age models

For reconstructing depth-age model I use mainly radiocarbon ages on both organic debris and ostracods and a few U-Th ages on aragonite stems. In the following section I will discuss the chronology and the age-depth model of each of the studied sites.

4.3.1 OH trench

The chronology of the sedimentary section of the Ohalo trench (OH trench) that was dug at the Ohalo-II shore is based mainly on radiocarbon dating. The most robust radiocarbon age that is used as an anchor for the age-depth model is that of the archeological layer of Ohalo site. There, 40 samples of terrestrial organic debris were dated yielding an average age of 21.3±0.8 cal ka BP, (modified after Nadel et al., 2001 according to Oxcal 4.1). The bottom of the trench comprises a laminated marly sequence, which was probably deposited during the lake high-stand, prior to the lake level drop (Figure 3.1). The age of the trench bottom coincided with H2 (Hazan et al., 2005) (24.3±0.7 ka cal BP, cf. Rashid et al., 2012). In between the archeological layer and the bottom of the trench several samples were dated: four samples of organic debris from the trench were dated by radiocarbon and eight samples of stem casts composed of aragonite were dated by U-Th. The measured ages lie outside of stratigraphic order. The stem casts show relatively high ^{232}Th concentrations, implying contribution of detrital U and Th and require correction. For the detrital correction I used $^{232}Th/^{238}U$ ratios of 0.8 or 0.95 (Table 4.2, Haase-Schramm et al., 2004) and assumed secular equilibrium among the U and Th isotopes in the decay series. The error is estimated to be 10%, and overestimation of the Th/U ratio will result older ages. Most of the corrected U-Th ages lie within the age-depth model defined by the radiocarbon ages (Figure 4.2). Only the top of U-Th sample lies off age-height model. In figure 4.2 I show an age-depth model that takes into consideration the age and uncertainty of the well-dated archeological site (21.3±0.8

cal ka BP) at the top and the *Melanopsis* age (22.5±0.7 cal ka BP, corrected for 800 years reservoir age) at the bottom, which is coincident with the U-Th age of Lake Lisan retreat at H2 (Haase-Schramm et al., 2004; Lev et al., 2014; Torfstein et al., 2013). Based on this dating the accumulation rates at this site are ~ 70 cm/ka.

4.3.2 KIN2 borehole

The chronology of KIN2 is based on several radiocarbon ages from the top and a single age dated at the bottom of the core (Figure 4.3, table 4.1). The covered time period is from ~40 to 21 cal. ka BP. Additional radiocarbon ages indicate that the age at the depth of 220 bsl is ~27 cal. ka BP (Litt, personal communication) suggesting a large hiatus above the base of the core where an age of ~40 cal. ka BP was determined. The chronology of the top of KIN2 is consistent with that of the adjacent Ohalo trench (Lev et al., 2014) and in the upper part of the core, where more dates are available, the accumulation rate reach ~ 100 cm/ka.

4.3.3 SOG2 borehole

The age-depth model of SOG2 is based on radiocarbon ages of eight samples of organic debris and ostracod shells (Figure 4.1, table 4.1). The data indicates two age-intervals the first is between 24 and ~20 cal. ka BP and the other around 12 cal. ka BP. In between these intervals there is an indication of deposition from 16-17 cal. ka BP (based on an ostracod age at a depth of 227.9 m). Continuous accumulation between 24 and 12 cal. ka BP implies average sedimentation rate for this interval of ~50 cm/ka. However, the chemical and isotope data (Mg/Ca $\delta^{18}O$, $^{87}Sr/^{86}Sr$) indicate on a possible hiatus at the depth of ca 230 m bsl.

4.3.4 SOG3 borehole

The chronology of SOG3 is based on five radiocarbon ages: wood-debris from the depth of 235.5 m bsl was dated to 23.1±0.9 cal. ka BP. Three samples of charcoal from depths of 233.6 – 231.8 m bsl were dated to 9.0 – 11.3 cal. ka BP (Figure 4.4, table 4.1). In between these two intervals there is a distinct change in sediment properties (% carbonate and grain size mode) that might indicate a change in the sedimentation regime (e.g. a possible sedimentary hiatus between~22 and 11.3 cal. ka BP). The top of the borehole was dated to 2.2±0.2 cal. ka BP. Between 11 and 9 cal. ka BP the sedimentation rates is ~90 cm/ka, while at the top of the core (1.3 meters) sedimentation rate is much lower, in the order of 15 cm/ka.

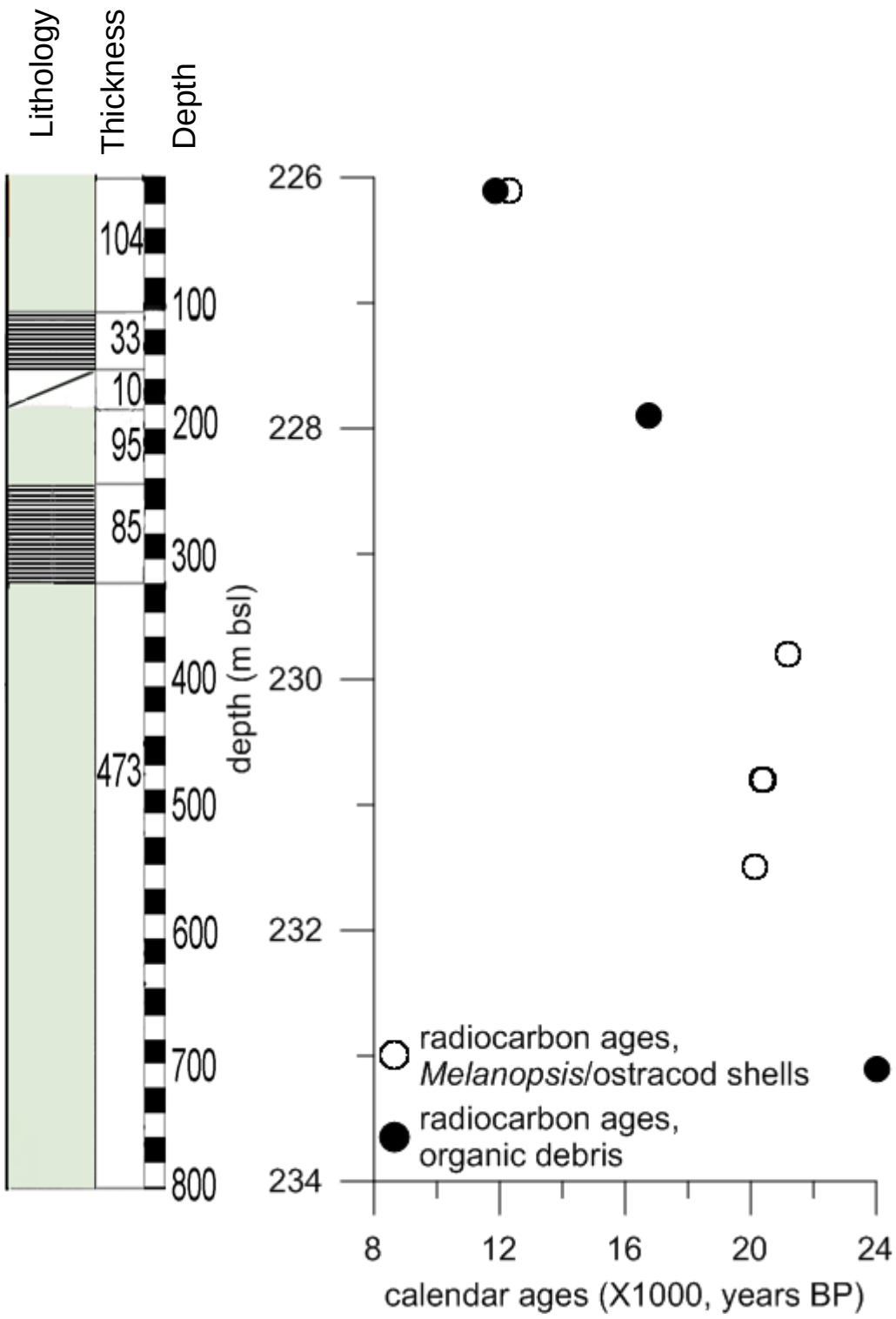

Figure 4.1 Age-depth diagram of the SOG2 borehole. The diagram shows ^{14}C data of organic debris and ostracod shells. The measured radiocarbon ages of the *Melanopsis* shells are corrected for reservoir age of 800 years (Lev et al., 2007) and 5000 years (see text for further discussion). Radiocarbon ages are calibrated according to OxCal 4.1. The lithologic legend is given in figure 3.5.

Table 4.1 Radiocarbon ages.

Sample	Location	Type	Height (m bsl)	Age (^{14}C ka B.P)	Calendar age (ka B.P.)
[+]	Ohalo site	organic debris	212.0		20.5 – 22.1
OH-1 23.7	Ohalo trench	ostracods	212.0	20.0±0.2	23.4 – 24.5
OH-1 23.7	Ohalo trench	charcoal	212.0	19.1±0.1	22.5 – 23.3
OH-1 38.5	Ohalo trench	charcoal	212.2	19.6±0.1	23.0 – 23.9
OH-1 42	Ohalo trench	charcoal	212.2	19.5±0.1	22.7 – 23.7
OH-2 70[*]	Ohalo trench	charcoal	212.5	19.5±0.2	20.5 – 22.5
OH-3 175[*]	Ohalo trench	charcoal	213.3	21.2±0.2	22.5 – 24.1
OH-3 185[*]	Ohalo trench	charcoal	213.4	21.8±0.2	23.1 – 25.6
OH-4 212[*]	Ohalo trench	charcoal	213.7	20.6±0.2	21.8 – 23.2
OH-5 310[*]	Ohalo trench	*Melanopsis*	214.6	21.1±0.2	21.4 – 23.2
OH-5 400[*]	Ohalo trench	charcoal	215.5	21.1±0.2	22.3 – 24.4
KIN2 2251	KIN core	charcoal	213.6	19.4±0.1	22.7 – 23.6
KIN2 2257	KIN core	charcoal	214.4	19.6±0.1	23.0 – 23.9
KIN2 2257	KIN core	ostracods	214.4	19.6±0.2	22.7 – 24.0
KIN2 2258	KIN core	ostracods	214.6	19.9±0.4	22.7 – 24.8
KIN2 2258[*]	KIN core	*Melanopsis*	214.6	20.7±0.2	23.2 – 24.5
KIN2 2264	KIN core	charcoal	215.6	20.0±0.1	23.5 – 24.3
KIN2 2267	KIN core	charcoal	215.9	20.8±0.1	24.5 – 25.2
KIN2 2302[*]	KIN core	*Melanopsis*	221.4	40.5±1.3	40.2 – 42.8
SOG2 209	SOG2 core	wood	226.1	10.4±0.1	12.0 – 12.6
SOG2 209	SOG2 core	ostracods	226.1	15.1±0.2	11.2 – 12.5
SOG2 389	SOG2 core	ostracods	227.9	18.8±0.2	16.1 – 17.4
SOG2 581	SOG2 core	wood	229.8	17.8±0.1	20.8 – 21.6
SOG2 676	SOG2 core	wood	230.8	17.1±0.1	20.1 – 20.6
SOG2 676	SOG2 core	wood	230.8	17.2±0.1	20.2 – 20.6
SOG2 753	SOG2 core	wood	231.5	16.9±0.1	19.9 – 20.4
SOG2 910	SOG2 core	ostracods	233.1	20.0±0.2	23.5 – 24.5
SOG3 184	SOG3 core	charcoal	230.8	2.2±0.1	2.05 – 2.41
SOG3 282	SOG3 core	charcoal	231.8	8.2±0.1	9.03 – 9.47
SOG3 384	SOG3 core	charcoal	232.8	9.3±0.1	10.3 – 10.7
SOG3 463	SOG3 core	charcoal	233.6	9.7±0.1	10.8 – 11.3
SOG3 646	SOG3 core	wood	235.5	19.3±0.1	22.3 – 24.0

[+]Terrestrial organic debris from the archeological site (212-213 m bsl). Modified after Nadel et al., 2001 according to Oxcal 4.1.
[*]Ages are modified after Hazan et al., (2005) according to OXCAL 4.2.
Ostracods and *Melanopsis* shells ages are corrected for reservoir age of 800/5000 years (Lev et al., 2007).

Table 4.2 Uranium-Thorium ages performed on aragonite stem casts from OH trench.

Sample	Absolute depth (m bsl)	^{232}Th (ppm)	^{238}U (ppm)	$[^{234}U/^{238}U]$	2-sigma	$[^{230}Th/^{238}U]$	2-sigma	Uncorrected age (ka)	Corrected age (ka)
OH-2(63)	212.1	0.52	1.94	1.516	0.010	0.511	0.003	43.6±0.3	20.6-21.7
OH-2(102)	212.5	0.27	2.17	1.569	0.009	0.417	0.003	32.9±0.2	20.7-21.9
OH-2(128)	212.8	0.42	2.31	1.541	0.010	0.468	0.004	38.5±0.4	20.4-21.6
OH-3(183)	213.3	0.24	2.84	1.583	0.005	0.381	0.002	29.4±0.2	21.3-22.6
OH-3(205)	213.5	0.27	2.09	1.572	0.006	0.435	0.003	34.6±0.3	21.9-23.2
OH-4(230)	213.8	0.20	2.10	1.584	0.008	0.403	0.002	31.4±0.1	22.1-23.4
OH-4(235)	213.9	0.21	2.28	1.606	0.006	0.409	0.002	31.4±0.1	21.6-22.9
OH-5(321)	214.7	0.36	2.93	1.548	0.007	0.403	0.002	32.2±0.3	22.0-23.2

2-Sigma error of $^{230}Th/^{238}U$ and $^{234}U/^{238}U$ are calculated according to the error of ^{230}Th and ^{234}U, respectivaly. Ages are corrected for detritus contamination applying Th\U ratios of 0.80 or 0.95 at secular equilibrium in the detrital component (Haase-Schramm et al., 2004).

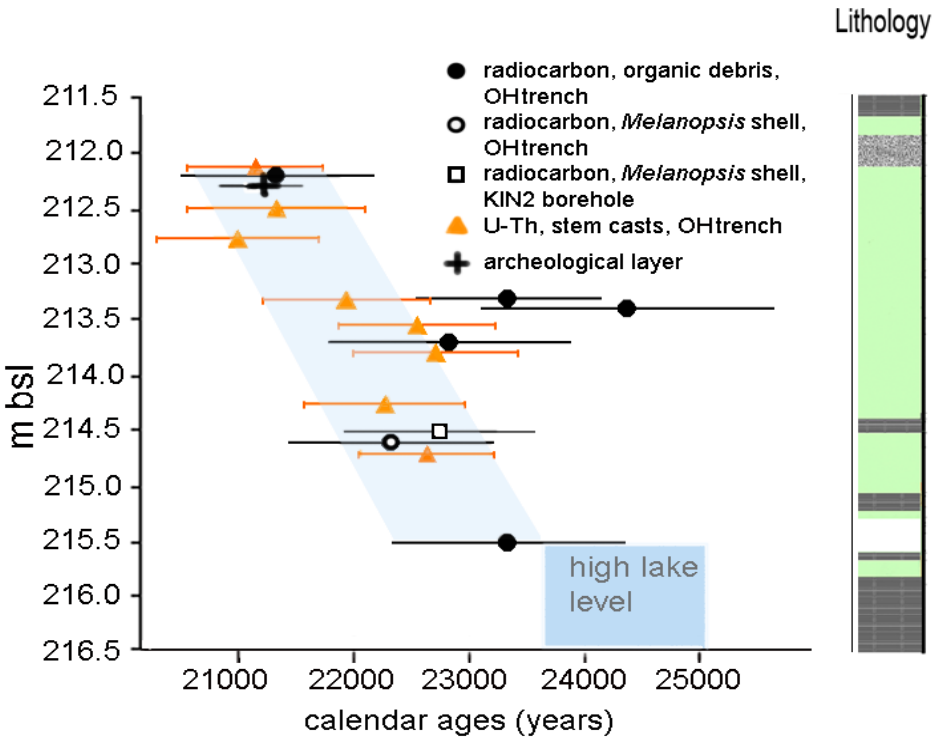

Figure 4.2 Age-depth diagram of the Ohalo trench. The diagram shows ^{14}C data of organic debris, *Melanopsis* shells and U-Th ages of aragonite stem casts. The measured radiocarbon ages of the *Melanopsis* shells are corrected for reservoir age of 800 years (Lev et al., 2007). Radiocarbon ages are calibrated according to OxCal 4.1. U-Th data are corrected for detritus contamination applying a range of U/Th ratios of 0.80 and secular equilibrium in the detrital component. The blue square represent the high lake stand period (Hazan et al., 2005). The gray area represents the range of the age-depth model based on the calendar age of the archeological site and the estimated age of the high-stand (see text for further discussion). The lithologic legend is given in figure 3.1.

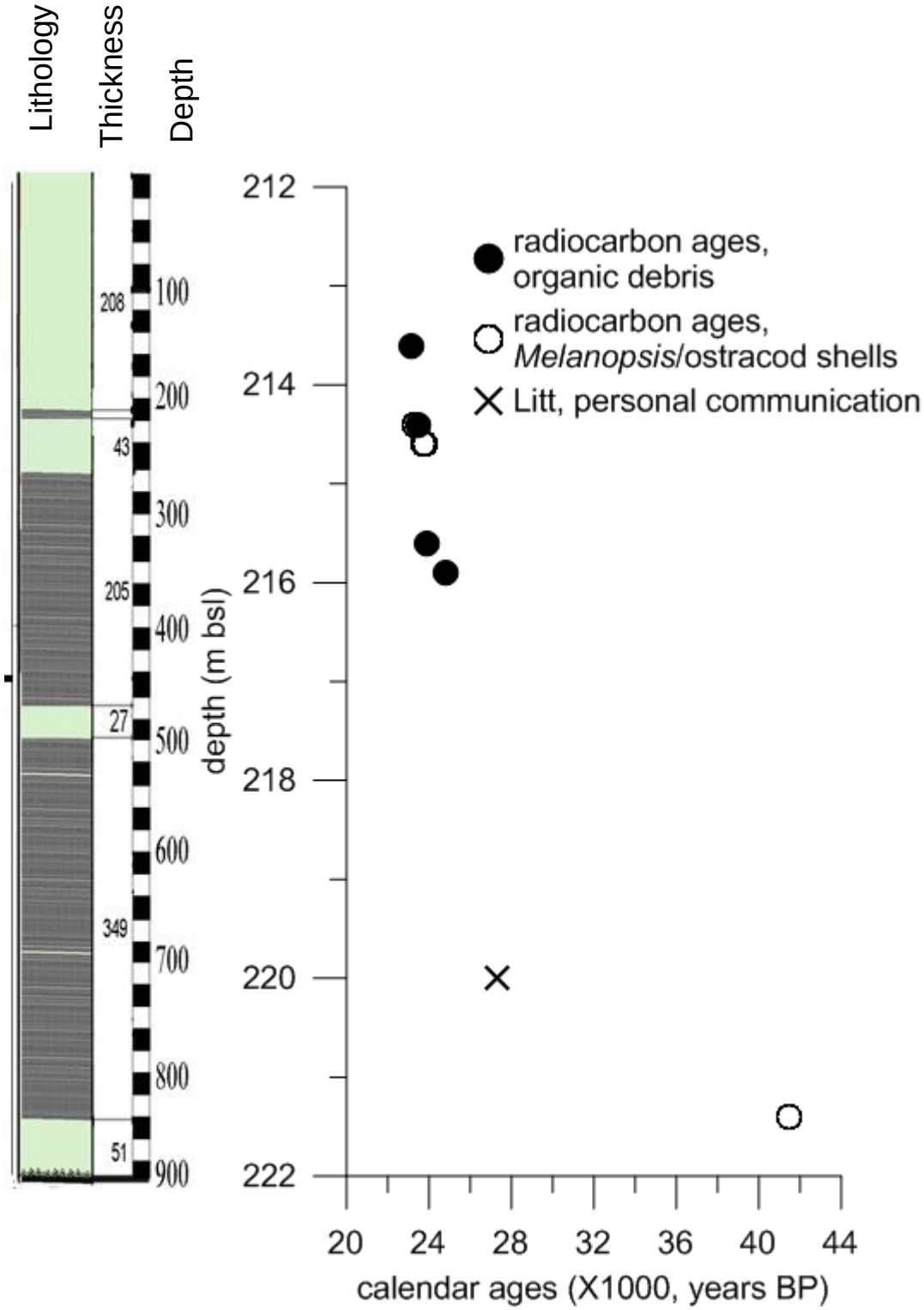

Figure 4.3 Age-depth diagram of the KIN2 borehole. The diagram shows ^{14}C data of organic debris and *Melanopsis* shells. The measured radiocarbon ages of the *Melanopsis* shells are corrected for reservoir age of 800 years (Lev et al., 2007). Radiocarbon ages are calibrated according to OxCal 4.1. The lithologic legend is given in figure 3.3.

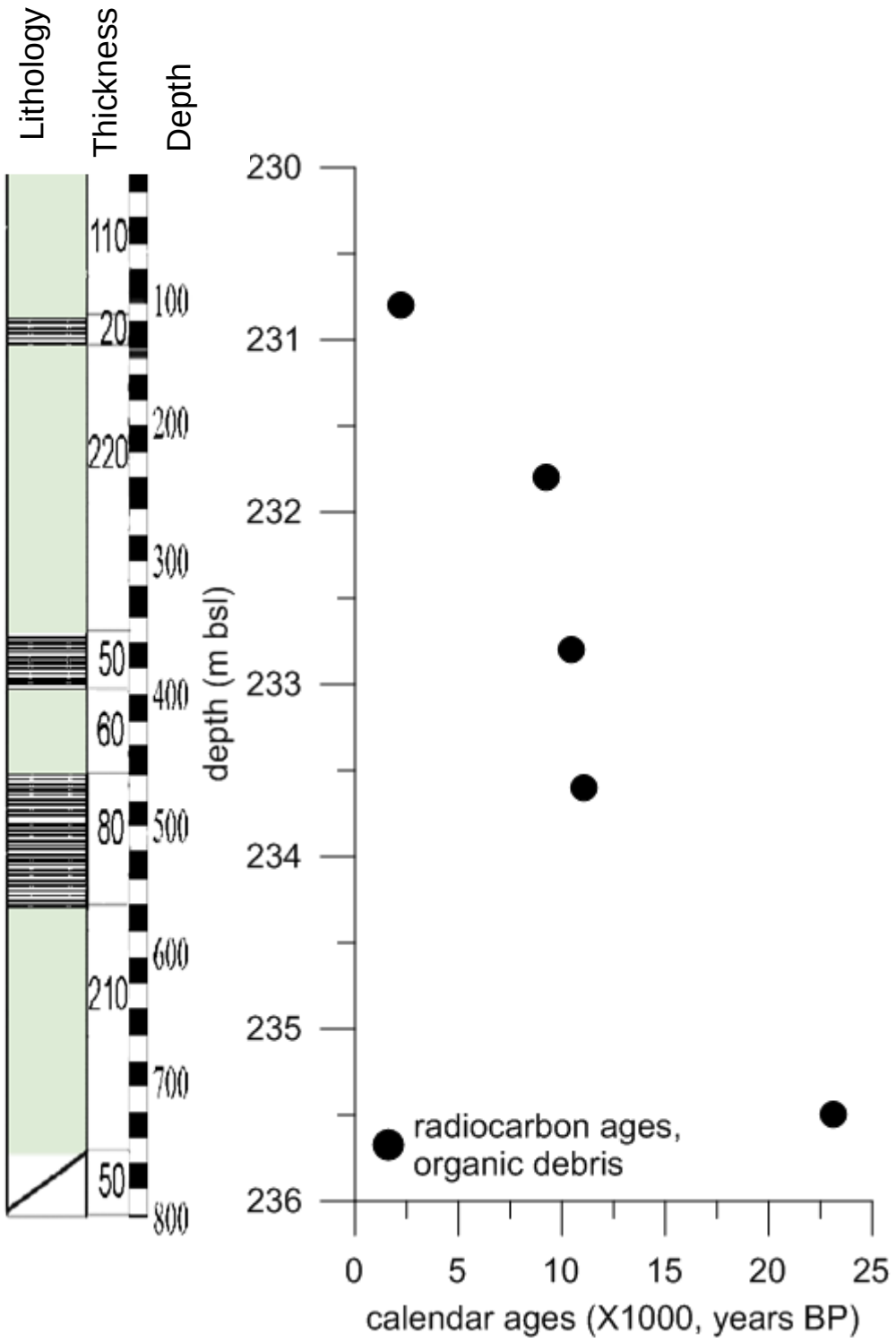

Figure 4.4 Age-depth diagram of the SOG3 borehole. The diagram shows ^{14}C data of organic debris. Radiocarbon ages are calibrated according to OxCal 4.1. The gray area represents the range of the age-depth model (see text for further discussion). The lithologic legend is given in figure 3.7.

4.4 Implications for Lake Kinneret lake level curve

The sedimentary record of the cores cover the time span from ~40 cal ka BP to ~9 cal ka BP, and late Holocene (~2.2 cal ka BP), enabling us to characterize the lake during last glacial time, including H2, and indicate the differences from the YD interval and the Holocene lake. Lake level curve of Lake Kinneret during the past 40 ka was established by Hazan et al., (2005) who identified and radiocarbon dated paleo-shorelines at the exposed margins of the modern lake and in drilled cores. The Kinneret curve was compared to that of Lake Lisan, which was reconstructed independently (Bartov et al., 2003; Bartov et al., 2002; Torfstein et al., 2013). Both lakes (and curves) converge between 27 and 25 ka cal BP when their levels reached the highest stand of ~ 170 m bmsl with Lake Lisan crossing the Wadi Malih and Yarmouk sills at ~ 280 and ~ 200 m bmsl. Lake levels dropped in both of them at the Heinrich event H2 (~24 ka cal BP, figure 4.5). This behavior clearly indicate a inter-dependence of both lakes, the Kinneret – flow through lake and the Lisan- a terminal lake, on the hydrological conditions in their common northern and western watershed, which receives mostly winter Mediterranean rains (Stein, 2014a, b). This conflicts with the dry conditions that persisted during MIS2 at the north part of the Levant (e.g., Yemmouneh basin, Develle et al., 2011). It was suggested to be either because of local factors or due to changes in the atmospheric circulations (Develle et al., 2011,; Enzel et al., 2008).

Water level dictates changes from marginal to deep water environment. These vertical changes are clearly reflected in the lithology. Here, I use the depth-age models of the cores combined with their lithology to refine the Lake Kinneret level curve during the time interval of ~19 to ~11 ka cal BP, including the H1 period. Figure 4.6 depicts the size of Lake Kinneret at ~ 25-27, 24 and 13-14 ka cal BP. The lithology of the cores and the Ohalo trench is used as a marker for relative water level: Massive marls, high content of coarse grain size (>63μm) and presence of ostracod shells mark shallow waters environments (e.g. of less than ~ 15, the present day maximum depth of living ostraocds in the lake and location of the lake level at or below the Ohalo-II shore (at 212 m bsl). Laminated and fine sediments were probably deposited when no bioturbation occurs. This in turn becomes possible when anaerobic conditions prevail, and it is also reflected in the absence of ostracod shells. Annual stratification in the modern lake causes anoxic conditions to prevail at water depth deeper then 15 meters. Therefore, laminated sediments rich in fine grain size <63μm and absent ostracod shells imply high level periods. When lamination appears at SOG3 solely, I conclude that water level rose but probably did not exceed 200 m bsl. The lamination at KIN2 implies higher water level (e.g. ~ 170 m bsl at ~ 27-25 ka cal BP).

The laminated segment at most of KIN2 borehole was deposited during the lake high stand (~25-27 ka B.P, ~ 170 m bsl) when it merged with the Lake Lisan to the south (Hazan et al., 2005). Massive marls at the top of KIN2 borehole (between 216.0 and 213.0 m bsl) and at the bottom of SOG2 borehole in the lake reflect low-water level at the post high-stand period.
KIN2 borehole and the Ohalo trench are located at the margins of the lake (figure 2.1), where erosion conditions did not allow sediments to be preserved when lake level dropped, and the youngest sediments recovered are ~20 cal ka BP. The next period that is represented in the sediments of SOG2 and SOG3 is correlated with the Younger Drays (YD) interval (12,800-11,500 years BP, Rasmussen et al., 2006), which is known is an abrupt return to glacial-like conditions. The sediments that were deposited during the YD interval are massive marls, indicating that increase in water level was limited. The Holocene time is represented in our cores only in a short interval at SOG3 and covers only ~4,000 years. The lithology of SOG3 at that segment shows laminated and massive marls, reflecting closed fluctuations in lake level.
The continuous sedimentation at SOG2 between 25 and 12 ka cal BP implies that lake level did not fall below the depth of this core ~226 m bsl. On the other hand, from the missing sediments at KIN2 and the Ohalo trench I conclude that water level did not rise above 212 m bsl after 21 ka cal BP (Figures 4.5, 4.7).
I will refer to water level in context of global climate in the chapter 7.

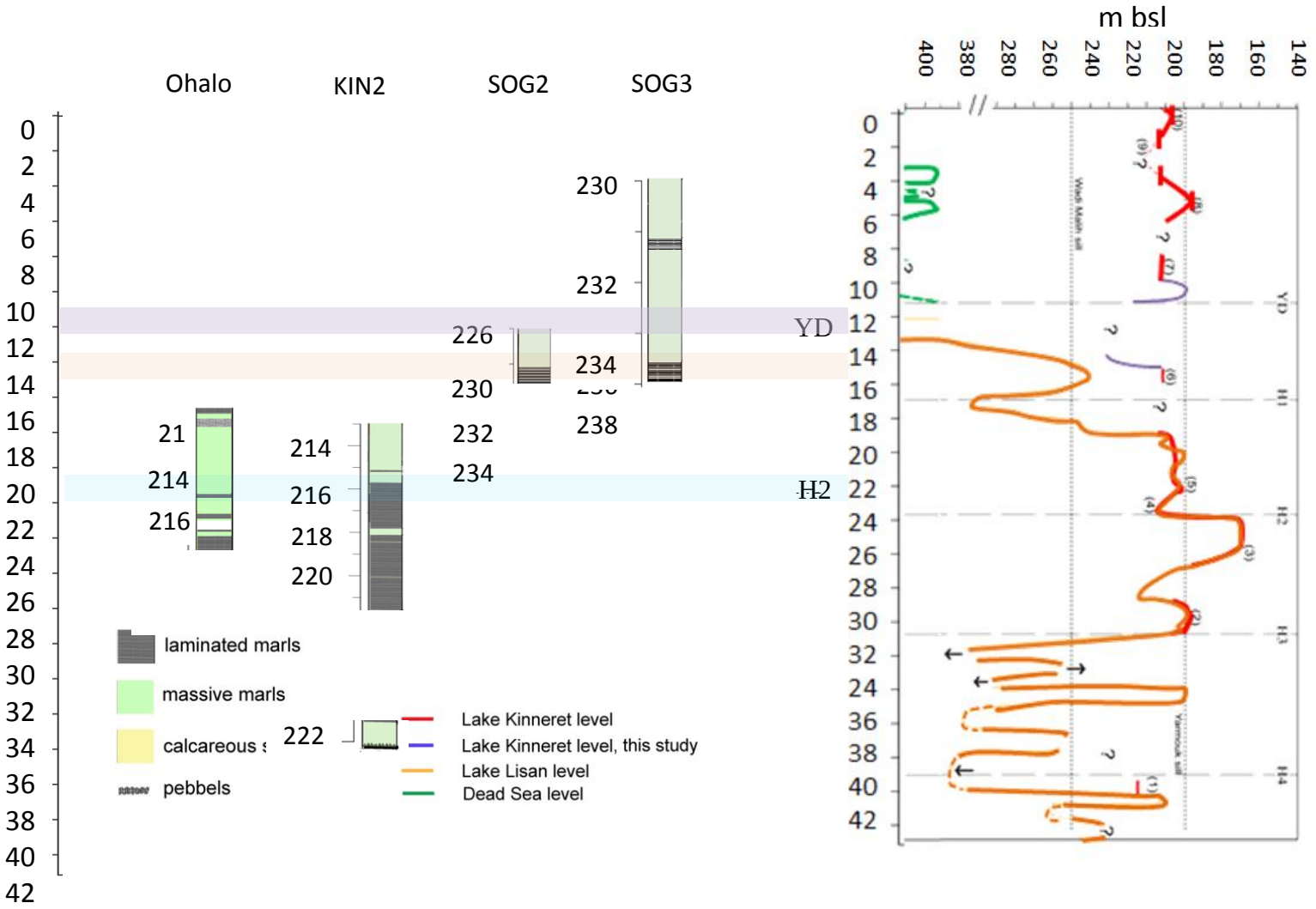

Figure 4.5 Ohalo trench, KIN2, SOG2 and SOG3 boreholes presented with calendar ages and lake level curve. Vertical changes in lake level are reflected in the lithology, alternating from massive to laminated marls. Depth-age models of the cores and lithology are being used to refine the Lake Kinneret level curve (Hazan et al., 2005) during the time interval of ~19 to ~11 ka cal BP, including the H1 period.

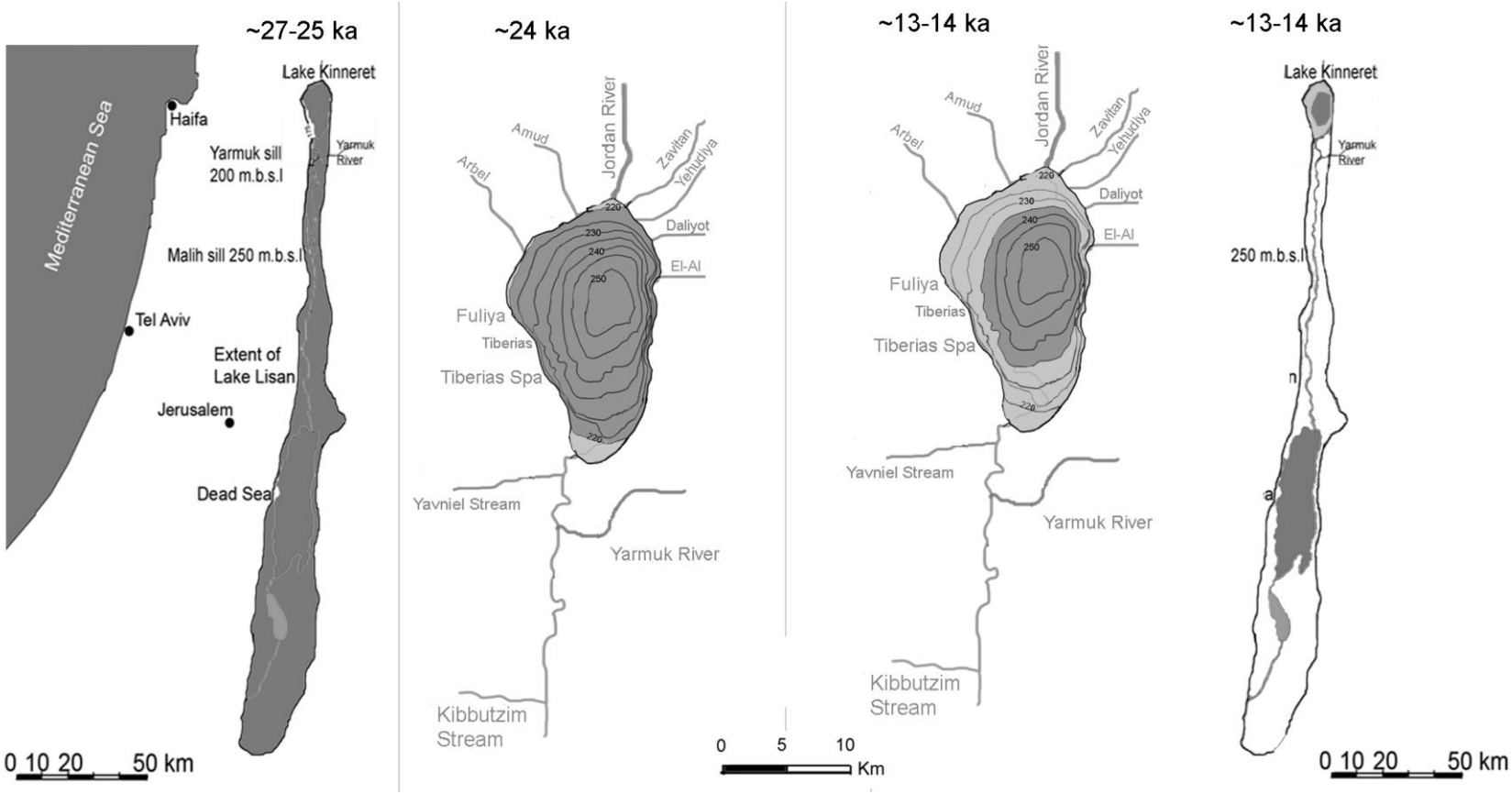

Figure 4.6 Water level of Lake Kinneret when water reached its highest level and merged with Lake Lisan at 27-25 ka, when lake level dropped at H2 event (24 ka) and when it reached it lowest level at 14-13 ka. Modified after Bartov et al., (2002).

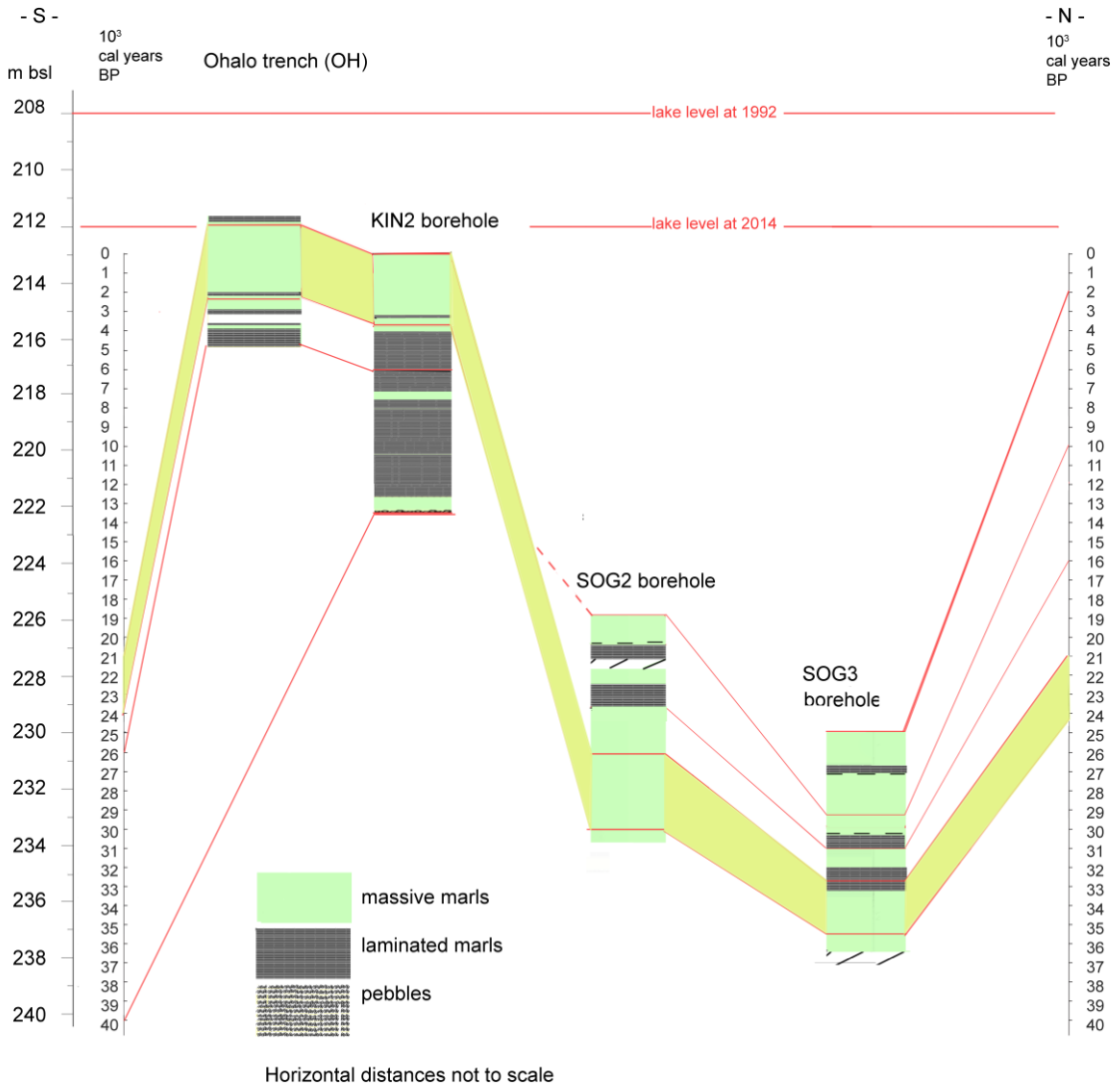

Figure 4.7 Stratigraphic correlation of the Ohalo trench and KIN2, SOG2 and SOG3 boreholes, showing absolute depth and calendar ages. Post high stand period (yellow area) is the only period that is in reflected in the trench and all boreholes. The youngest sediments recovered KIN2 borehole and the Ohalo trench are ~20 cal ka BP, posing an upper limit on lake level.
The Holocene time is represented in the cores only in a short interval at SOG3 and covers only ~4,000 years. The lithology of SOG3 at that segment shows laminated and massive marls, reflecting closed fluctuations in lake level.

4.5 Conclusions

1. Organic debris (branches, wood remains, grains) and ostracod calcitic shells and *Melanopsis* aragonitic shells were dated by radiocarbon, aragonite stem casts were dated by U-Th to reconstruct depth-age model for the Ohalo trench and other 3 boreholes drilled in Lake Kinneret.
2. The Ohalo trench covers the period from 27 to 20 ka cal BP. The KIN2 core lies between ~40 and 21 ka cal BP. The SOG2 covers the time interval of 25 to 12 ka cal BP. SOG3 covers the time between 25 to 2 ka cal BP.
3. The Ohalo trench and KIN2 core are sensitive to lake level declines. At ~ 23.8 ka cal BP (the H2 event) the lake declined to ~ 212 m bsl (from the Ohalo site). Lake level fluctuated between 230 and 200 m bsl between 24 and 14 ka cal BP.
4. Reservoir ages of Lake Kinneret changed through time and were ~800 years at 24-20 ka BP and ~5,000 years at 11-12 ka BP.

Chapter 5: Sources of detrital material

5.1 General

The climate during the Pleistocene and Holocene is characterized by cyclic shifts between cold, warm, humid and dry conditions. These shifts have influence on desert dust transport and they are recorded in the sedimentary sections that were deposited in Lake Kinneret. The main sources of desert dust in Israel today are the distanced Saharan dust storms, the rarer Arabian Desert storms and the proximal Sinai-Negev deserts (Crouvi et al., 2008; Ganor et al., 1991). The first are associated with winter low pressure systems, which are also responsible for most of the rain over Israel while the second dust storms are generated when a high barometric pressure exists over Northern Israel and the Persian Gulf Depression is situated over the Red Sea. Grain size distribution of loess material from the Negev desert of Israel typically showed bi-modal distribution with mode values of 2-8 and 40-60μm, implying Sahara Desert source and Negev Desert source, respectively (Crouvi et al., 2008; Ganor and Foner, 1996). Haliva-Cohen et al., (2012) combined the grain size data with mineralogy, petrography and chemical and Sr-Nd isotope values of the fine detritus material (FDM) to infer the sources of the FDM and the environmental conditions during its deposition. She pointed out that during glacial period the FDM originated in the Sahara Desert storms with mode values of grain size of 8-10 μm. The 60-70 μm is the typically grain size of the laminated detritus of Samra and Lisan formations (***ld***) that was deposited during inter-glacial periods. The latter originated in the loess material in the northern Negev desert that accumulated during glacial periods. In the following section we examine grain size in bulk sediments recovered by the boreholes and examine the possibility to use the data as proxy to detritus material source during the transition from high to low level, including the H2 and YD time intervals and compare it to the grain size in sediments from Lake Lisan and Dead Sea.

5.2 Detritus material sources

5.2.1 High level period, 27-25 cal ka BP

High lake levels between ~27-25 cal ka BP (marine Isotope Stage MIS2 of the last glacial period) reflect a wet period and enhanced rains in Lake Kinneret watershed. However, extreme arid conditions persisted in the Sahara resulting in enhanced desert dust transport to the region that accumulated in the northern Negev desert of Israel and the Judean and Galilee Mountains (Yaalon and Dan, 1974). Glacial periods at the Yemmouneh basin exhibit the highest weight percentages of wind-blown particles, indicating a strong contribution of eolian dust to sedimentation (Gasse et al., 2011). It was suggested by Haliva-Cohen et al., (2012) that during glacial periods fine detrital material was blown from the north Sahara deserts and was washed directly into the Dead Sea. Looking at the grain size of KIN2 that represent the high level period (Figure 3.4), we see uni-modal distribution, typically at 4-8μm. This grain size is close to the fine grain size peak of the loess from the Negev Desert (Crouvi et al., 2008) and to the ***add facies*** (aragonite and silty detritus laminae, 8-10μm) from the Lisan formation at the same period (Haliva-Cohen et al., 2012). The logic conclusion is that the same system influenced the two water bodies: the same Mediterranean fronts and rain systems were responsible to both Lake Kinneret and Lake Lisan water level to rise and same desert dust storms did not stop at Lake Lisan and were responsible to the travel of dust all the way to Lake Kinneret. The small difference between the ***add facies*** (8-10μm) and KIN2 sediments (4-8μm) could be interpreted as a result of the longer distance the particles have traveled from the Sahara and Arabian deserts.

The Fe_2O_3 vs. Al_2O_3 figure (Figure 5.1) indicates the degree of leaching of the soluble components from the original dust material during pedogenic processes. Washout of the carbonates from the terra rossa surface cover enriches the residual rock in Al and Fe. It is being used to support the theory regarding the sources of detritus. The similarity of the composition of the sediments from Lake Kinneret to the contemporaneous Lisan samples (~7-10 wt% Al_2O_3 and ~5-9 wt% Fe_2O_3) contribute to the above conclusion regarding the same source of the detritus. KIN2 samples from the high lake level period show slightly higher values and larger scatter. This might be a result of additional leaching of the soluble components due to a greater travel distance.

5.2.2 Post high level period, 24-20 cal ka BP

Grain size at SOG2 during post high stand period (~20-24 cal ka BP) is also uni-modal, typically ~10μm (Figure 3.6). It shows major difference from the ***ld facies*** grain size that characterize the inter-glacial periods (~60 μm). Al and Fe values (Figure 5.1) are low, implying closer dust source than the Sahara desert. This is in agreement with the wet conditions that persisted at the Sahara region during H2 event. However, for the deremination of the sources of detrital material during the H2 event, I recommend more data should be acquired.

5.2.3 YD and transition to the Holocene

The sediments from SOG3 that represent the YD show low carbonate content and also uni-modal distribution of grain size, with a peak at ~10μm (Figure 3.8). As discussed above, the YD short period was characterized by an increase in water level, as a result of returning to glacial-like conditions. These glacial like conditions persisted also at the Sahara region, thus I would expect similar grain size values. However, although differences are small, the grain size of the sediments from the YD period (~10 μm) is not identical to values of high-stand (8μm). In order to understand the difference between the high level period and the YD period I try to examine the carbonate content. The carbonate content at SOG3 during this period is extremely low (~20-30%, figure 3.7), probably expressing high contribution of detrital material to the lake. Climate conditions during YD period were not as extreme as during the high level period. In accordance, high contribution of desert dust from moderate distance is probably the source for detritus during the YD period.

5.2.4 Holocene

Grain sizes mode of samples that represent the Holocene are 16, 18 and 24 μm, showing wide distribution (SOG3 borehole, figure 3.8). It is obvious from the coarse grain size values that the distanced Sahara desert could not be the source of dust during Holocene period. However, these values are closer to the grin size of the settled dust samples that were collected at Jerusalem (~20-30 μm), implying closer source for dust storms during this period.
The high carbonate content that was measured at SOG3 during the Holocene period (Figure 5.2) could be interpreted as a regional change in the supply of bi-carbonate to the lake and an increase in carbonate precipitation, or higher supply of detrital material to the lake. The dry conditions during the Holocene, as implied from low lake level, suggest enhanced contribution of detrital carbonate to the lake. However, there are no sufficient known parameters to determine. Chemical analysis, e.g. Si/Al and K/Al can be used as tracer of wind-blown quartz grains (Develle et al., 2011).

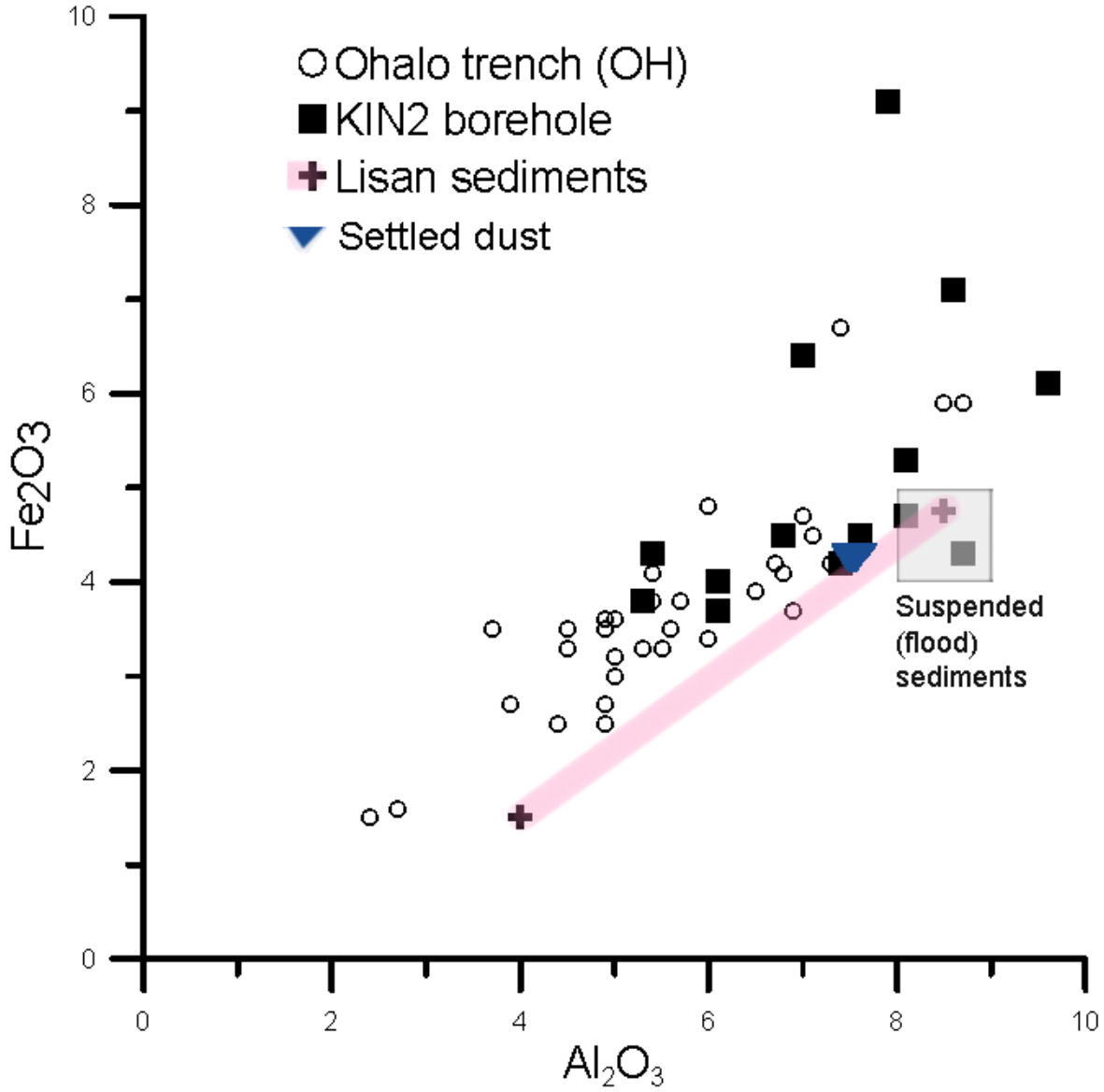

Figure 5.1 Al_2O_3 vs. Fe_2O_3 diagram. The diagram is a complimentary tool to distinguish detritus source. Note a general linear array: higher Al and Fe values reflect the leaching of the soluble components (e.g., carbonates) from the original dust material.

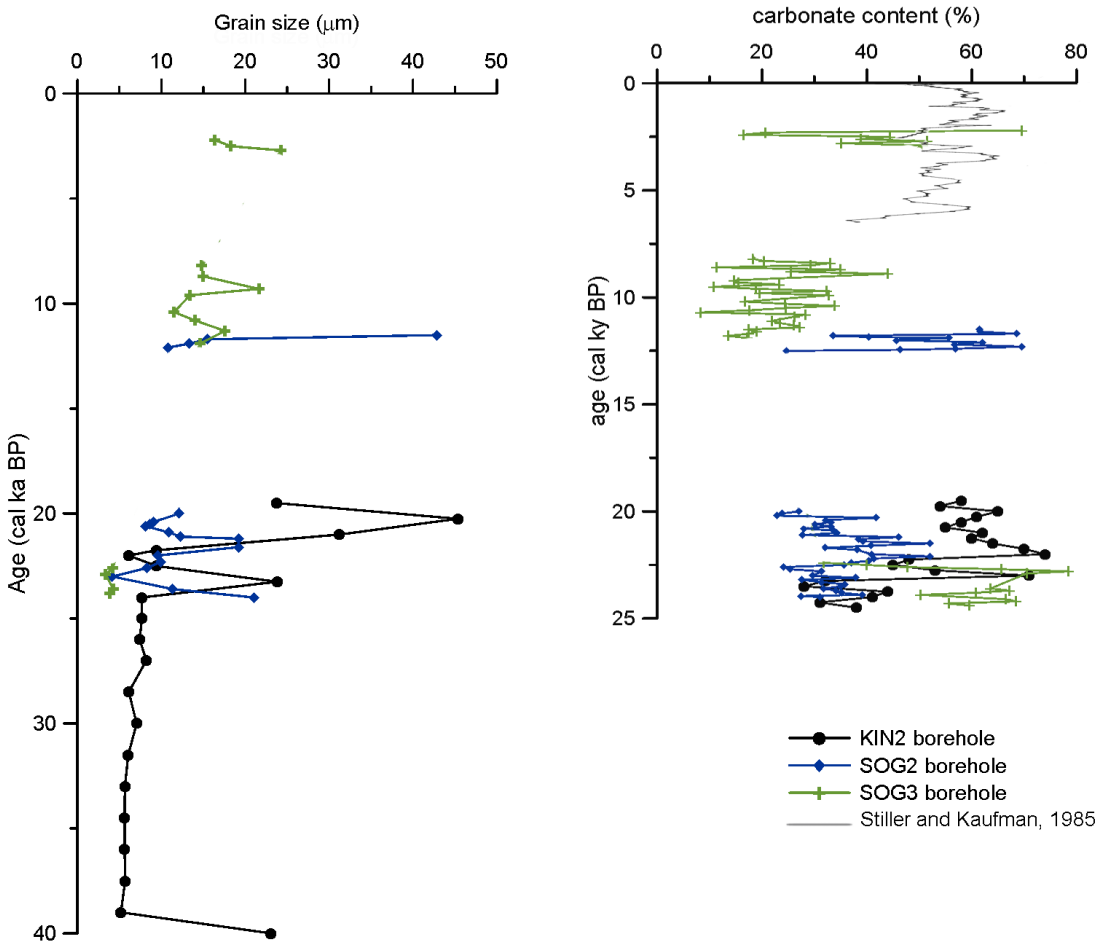

Figure 5.2 Grain size mode value and carbonate content of KIN2, SOG2 and SOG3 sediments. Carbonate content from core KINF5 from Stiller and Kaufman (1985), located ~2km south to SOG3. Carbonate content shows variable values from deep to shallow water environment. Variability in grain size implies shifts from different dust sources.

5.3 Conclusions

1. Grain size analysis was performed on bulk sediments from KIN2, SOG2 and SOG3 and show variation through time and space.
2. KIN2 sediments from the last glacial period are typically 5-8μm. Grain size of bulk sediments from SOG2 that represent the post high stand period (~20-24 cal ka BP) are typically ~10μm. SOG3 sediments that represent the YD show uni-modal distribution of grain size, with a peak at ~10μm.
3. Grain sizes of sediments from Lake Kinneret from the high stand period are similar to those of the Lisan sediments, indicating same desert dust storms responsible to the dust origin. After lake retreat and during H2 period the sediments at Lake Kinneret were mostly transported into the lake from a different source. Grain size of sediments from YD period implies moderate travel distance of dust into the lake. Holocene period is characterized by coarse sediments, implying close source of detrital matter.
4. The Fe_2O_3 vs. Al_2O_3 diagram helps us to understand the sources of dust transport: during high level lake dust was transported from distance sources (Sahara desert) and soluble components were leached out from the sediments. During H2 period, dust was carried into the lake from less distance source resulting in less leaching.
5. Low values of carbonate content are correlated with low contribution of detritus compared to primary production of carbonate during high water levels. High values of carbonate content are linked to high values of detritus to the lake during low water level periods.

Chapter 6: Paleohydrology during H2

6.1 General

Archaeological excavations and geological trenching and drilling that were performed in the drought years of 1999-2001 at the Ohalo shore (Figure 6.1) provided the opportunity to investigate the environmental and hydrological history of the transition of Lake Kinneret from high to low-stand. I studied the stratigraphy and lithology of the Ohalo trench and the adjacent KIN borehole section, studied the ostracod and benthic foraminiferal distribution in these sediments and determined their geochemical and isotope composition.
The shallow morphology of the southwestern part of Lake Kinneret where Ohalo trench is located is sensitive to changes in the lake level and in the discharge of Yavniel Stream and Jordan River. The mm-thick laminated marls at the bottom of the core (Figure 3.1) were probably deposited during the lake high stand (at ~ 160-170 m bsl) when it merged with Lake Lisan to the south (Hazan et al., 2005). The massive marls and the sharp increase in the abundance of ostracods and foraminifera between 215.3 and 213.8 m bsl coincides with subsequent lake level drop, implying that the Ohalo site was under shallow water. Moreover, the occurrence of ostracods and well preserved foraminifera continuously upwards in the section, though in lower and variables numbers, indicates the prevalence of lacustrine conditions in this part of the lake throughout most of the studied period (I bear in mind, however, that the prehistorical people stayed at the Ohalo at ~ 21.3 ka cal BP).

6.2 Water sources

6.2.1 Mg/Ca, Sr/Ca and $^{87}Sr/^{86}Sr$ ratios in the ostracods and waters

The changes in the limnological conditions and in the contribution of various water sources to the southwestern Kinneret are reflected in the elemental and Sr and O isotope composition of the *C. torosa* shells recovered from the trench and the core. In the following section I use these parameters to reconstruct the geochemical and hydrological history of this shallow, near-shore environment during the decline of the lake from its highest level between 27 and 25 ka BP to the low H2 stand.
Sr/Ca and $^{87}Sr/^{86}Sr$ ratios in *C. torosa* shells are used to constrain the sources of water that comprised the lake water at the vicinity of the trench. The translation of the *C. torosa* Sr/Ca (and Mg/Ca) to water Sr/Ca (and Mg/Ca) is done by using partition coefficients that were calculated using data for living *C. torosa* and water at Lake Kinneret (Table 3.1). The calculated values are Kd[Sr] ~ 0.7 and Kd[Mg] ~ 0.011 (Table 6.1). Kd values are likely correlated with the Mg/Ca ratios in the habitat water for the Sr/Ca and Mg/Ca range under consideration (Wansard et al, 1998; DeDeckker et al, 1999; Marco-Barba et al, 2012).

Table 6.1 Partition coefficients Kd[Mg] and Kd[Sr] in *Cyprideis torosa*.

	Kd[Mg/Ca]	Kd[Sr/Ca]
KG-1	0.012	0.82
KT-1	0.010	0.75
KS-1	0.010	0.68
KM-1	0.013	0.70
average	0.011	0.74

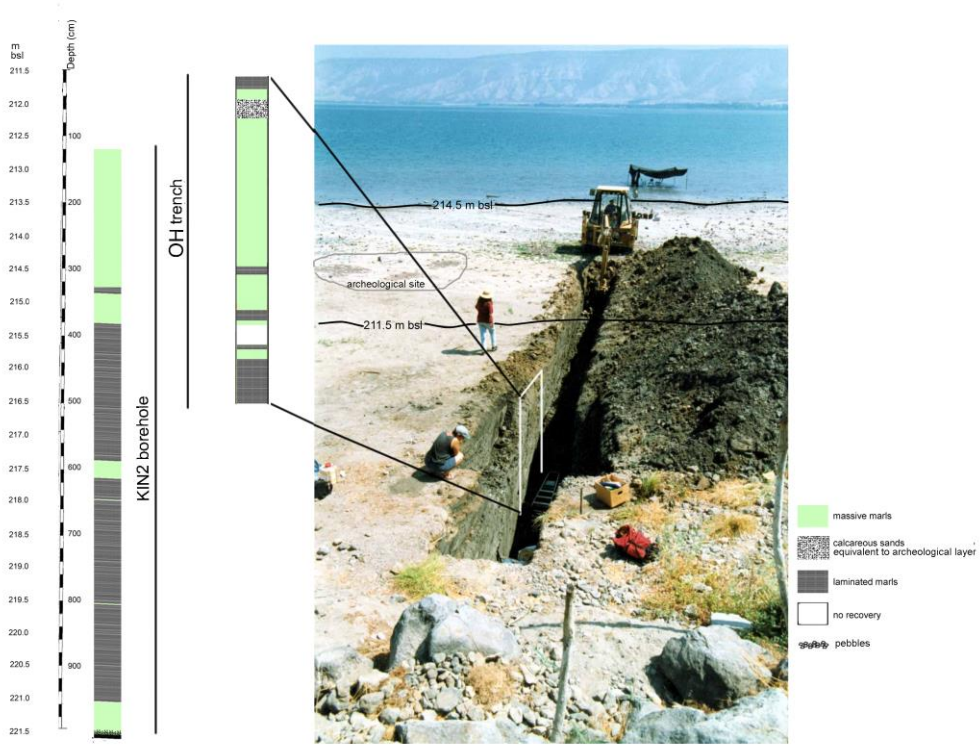

Figure 6.1 The Ohalo II archeological site (Oh) showing the location of the OH trench and site of drilling. The figure displays a detailed lithological description of the OH trench combined with the KIN2 borehole. The picture of the trench was taken in 1999 when shoreline was at 214.5 m bsl.

Sr/Ca values in the water as inferred from *C. torosa* shells from OH trench and KIN2 core lie in the range of 0.0025 to 0.0043 and they are significantly lower than ratios measured in modern Lake Kinneret (Figures 3.9, 6.2). The *C. torosa* valve data lie between the composition of Tiberias Spa ($^{87}Sr/^{86}Sr$ ~ 0.70785) and runoff from the Galilee Highlands ($^{87}Sr/^{86}Sr$ ~ 0.7082) and streams like the Kibbutzim stream ($^{87}Sr/^{86}Sr$ ~ 0.7082, Lev, 2006). The $^{87}Sr/^{86}Sr$ values of *C. torosa* can, then, be interpreted as a result of mixing of saline springs and runoff. It can be seen in Figure 3.9 that there is an overall trend of increasing contribution from the runoff from ~214.5 to ~212.5 m bsl with two significant runoff spikes occurring at 214.1 and at 212.6m bsl.
Mg/Ca ratios in the *C. torosa* valves range between 0.0075 and 0.0250 (Figure 3.9). Applying Kd = 0.011, the ambient water would have had Mg/Ca ratio close to 1, lying between runoff and Tiberias Spa water. Thus, Sr/Ca, Mg/Ca and $^{87}Sr/^{86}Sr$ are all consistent with the interpretation that the habitat waters of the *C. torosa* was a mixture between waters with compositions similar to Tiberias Spa and runoff from the Galilee Highlands. Modern Lake Kinneret waters show distinctly lower $^{87}Sr/^{86}Sr$ and higher Sr/Ca ratios and indicate enhanced contribution from other water sources (discussed below).

6.2.2 $\delta^{18}O$ values in the lake's waters

The $\delta^{18}O$ values found in the lake water, as inferred from the ostracods, decrease from -2‰ to -3.5‰ during the time interval ~24-21 ka BP (Figure 3.9). This general trend is overprinted by several shifts to more positive values (Figure 6.3). The figure shows comparison between the $\delta^{18}O$ values of lake waters, speleothems from the Judea –Galilee caves and foraminifera from east Mediterranean deep-sea cores. The speleothems and Mediterranean forams co-vary, pointing to the dominance of the Mediterranean-rain sources on the speleothems $\delta^{18}O$ values (Kolodny et al., 2005). Yet, while the ostracods' habitat-waters show a general decline over the entire time interval (~ 24-21 ka BP), the speleothems increase during the interval ~ 23.5 to 22.2 ka BP and then decline and co-vary with the ostracods. The slight increase in speleothems and Mediterranean $\delta^{18}O$ values comes after the negative anomaly at ~ 24 ka BP that possibly reflects the effect of melting ice during the H-event. There is no counterpart to this part of the record at Ohalo. The subsequent return of the speleothem to heavier $\delta^{18}O$ values (between ~ 23.5- 22.2 ka BP, figure 6.3) possibly marks a return to "normal glacial conditions". Lake Lisan, a sensitive recorder of the glacial-world responded by a level rise during this time interval (~ 23-22 ka BP, Torfstein et al., 2013). It appears that Lake Kinneret did not or only slightly recovered from the H2 drop and the Ohalo-shore remained a shallow-water environment that was almost dried when the Ohalo-II people settled there.
The waters in the marginal environment of the (post-H2) Ohalo shore were dominated by regional run-off whose $\delta^{18}O$ values respond to the changes in the composition of regional rains. This is consistent with the $^{87}Sr/^{86}Sr$–Sr/Ca data that calls for significant run-off contribution to the Ohalo environment. Thus, the environment can be described as a fluvial plain or small estuary, possibly of the Yavniel River.
The modern Lake Kinneret $\delta^{18}O$ values are significantly *more positive* than the late Glacial (post-H2) lake lying at ~ 0.0‰. During most of the late Holocene the lake covers the Ohalo shore and the $\delta^{18}O$ values reflect the "main lake" composition, which is dictated by higher temperature and evaporation compared to the post - H2 marginal environment.

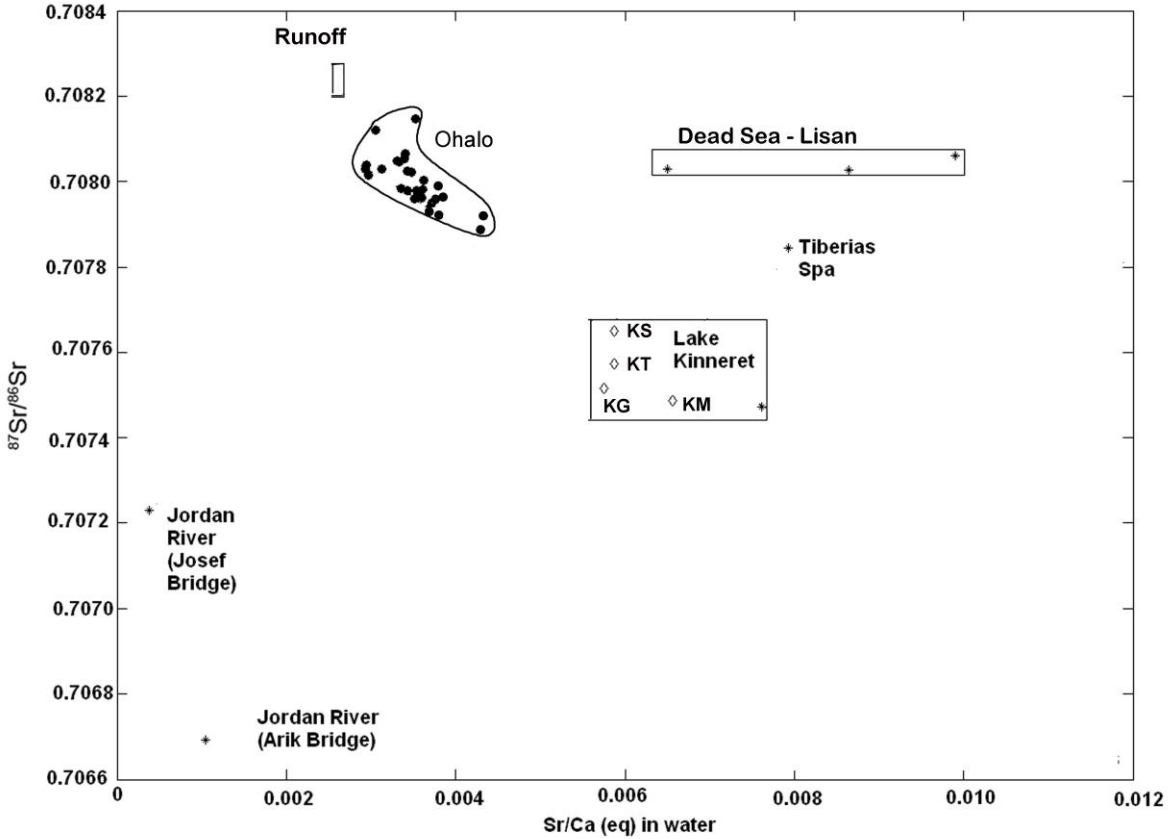

Figure 6.2 Sr/Ca vs. $^{87}Sr/^{86}Sr$ values shown for the different water sources of the modern Lake Kinneret and the water at the Ohalo site after the retreat of the lake from its highest level. Stars indicate water samples from the Jordan River, Tiberias Spa and the Dead Sea and Lisan Lake (Stein et al. 1997), square indicates water sample from Fuliya springs (Bergelson et al., 1999; Klein-BenDavid et al., 2005), diamonds indicate water samples of this study and full circles are for water composition based on ostracods analysis (this study). Note the general trend from modern lake water to more runoff contribution in the studied material.

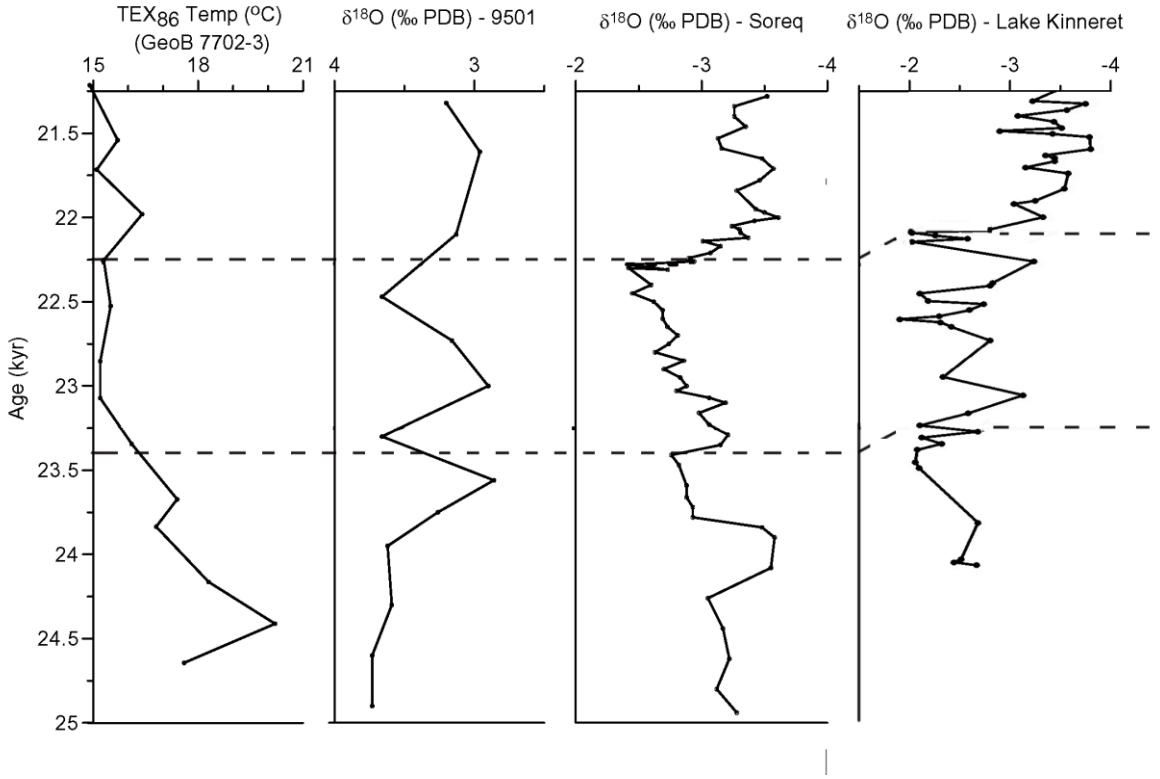

Figure 6.3 A comparison between the $\delta^{18}O$ values of ostracod shells from the OH trench, the $\delta^{18}O$ values of Soreq Cave speleothems (Bar-Matthews et al., 2003), the $\delta^{18}O$ values of foraminifera from the marine record of core 9501 recovered southeast of Cyprus (Almogi-Labin et al., 2009) and the temperature profile of the southeastern Levantine basin, off the Israeli coast based on alkenones and TEX_{86} analyses (Castañeda et al., 2010). The highest $\delta^{18}O$ values occur during the H2 event, ~24 to 22.3 ka BP and they decrease considerably afterwards.

6.3 Hydrological inferences for the Late Glacial Lake Kinneret

After the retreat of Lake Kinneret from its last glacial high stand, the Ohalo area remained an integral part of the lake representing a marginal shallow water environment. To the south, as the lake level declined, a large fluvial plain developed across the entire southernmost part of the present day Lake Kinneret (see Hazan et al., 2005). With the drop in the local base level, the Jordan River cut into the southern Lake Kinneret sediment. Yavniel River possibly drained into the area as well, transporting water and sediments into the fluvial plain. At the bottom of the trench (and the stratigraphically corresponding section in the KIN core) $^{87}Sr/^{86}Sr$ – Sr/Ca ratios of the *C. torosa* valves are more similar to the Tiberias Spa waters (Table 6.2, figure 6.2). The Tiberias Spa discharges water with high salinity (18 mg/L Cl, Stein et al., 1997) that might have dominated Lake Kinneret solutes during its high stand period. During the high stand, it is possible that the lake waters penetrated the mountain aquifers and the waters discharged back into the lake after its level dropped (see a similar scenario for the southern Lake Lisan as discussed by Torfstein et al., 2008). The Tiberias Spa waters lie between the compositions of the Jordan River waters (very low Cl and Sr concentrations; 18.3 and 0.1 mg/L, respectively) and the Dead Sea brine (Cl and Sr concentrations of 220 and 0.3 g/L, respectively) (Stein et al., 1997) indicating an enhanced contribution of the Dead Sea $CaCl_2$ brine to the last glacial Lake Kinneret. This could either reflect the mixing of the glacial Lake Kinneret water with Lake Lisan water during the time of convergence or more likely an enhanced flow of saline springs with solute composition similar to those of Tiberias Spa to the glacial Lake Kinneret. During the last glacial lake convergence, Lake Kinneret acted as a big estuary that pushed freshwater southward to the northward-expanding Lake Lisan.

The exposures of the high stand Lake Kinneret sediment that extends to the Yarmouk sill (Figure 1.1) are composed of primary-carbonates in the form of calcite rather than aragonite found in Lake Lisan deposits (Hazan et al., 2005). Thus, it appears that the Dead Sea-Lake Lisan brine did not "cross" the southern margin of the Kinnarot basin (the Yarmouk River sill, figure 1.1). The scenario of enhanced activity of the saline springs providing the ancient $CaCl_2$ brine to the lake appears more likely. This is also consistent with the significantly lower Mg content (and Mg/Ca ratio) in the Kinneret saline springs relative to their content in Dead Sea brines that do not support aragonite deposition. If Tiberias Spa water represents the last high stand glacial lake (~27-25 ka BP), then the paleo-lake is distinctly different from the modern Lake Kinneret that shows lower $^{87}Sr/^{86}Sr$ and Sr/Ca ratios (~ 0.7076 and ~0.007, respectively, figure 6.2). The modern Lake Kinneret (before 1964 saline water diversion canal construction) appears to be less affected by the saline springs and more affected by the Jordan River (Figure 6.2). Since most of the Sr is supplied by the saline springs, the diminishing effect of the springs appears to be more important to the overall hydrologic budget of modern Lake Kinneret. The enhanced effect of the saline springs with high $^{87}Sr/^{86}Sr$ and Sr/Ca ratios during the high stand period is consistent with the Goldschmidt et al., (1967) model that predicts higher discharge of the saline springs to the lake during times of enhanced precipitation in the Galilee – Golan regions.

Table 6.2 $\delta^{18}O$, Sr/Ca and $^{87}Sr/^{86}Sr$ in freshwater and brines in Lake Kinneret and its water sources

Source	$\delta^{18}O$ (‰)	Sr/Ca (eq.)	$^{87}Sr/^{86}Sr$	References
FRESHWATER				
Lake Kinneret	0.0	0.0076	0.70747	1,2
Jordan River – Arik bridge	-6.9 to -5.9	0.0010	0.70669	1,2
Jordan River – Josef Bridge		0.0004	0.70723	1
Kibbutzim Stream		0.0024	0.70810	3
Rainwater	-7.3		0.70860	4
BRINES				
Dead Sea	+4.4 to +4.9	0.0086	0.70802- 0.70803	1
Tiberias Spa	-3.0	0.0079- 0.0087	0.70783- 0.70785	1, 4, 5
Tabgha springs	-5.7 to -6.2	0.0088- 0.0111	0.70776- 0.70781	3, 4, 5
Fuliya springs	-1.6	0.0037- 0.0055	0.70786- 0.70799	5,6, 7

(1) Stein et al. (1997); (2) Gat (1970); (3) Lev (2006); (4) Gat et al. (1969); (5) Halicz et al., (2003); (6) Bergelson et al. (1999); (7) Klein-Ben David et al. (2005)

During the lake level decline following the high stand, both the activity of the saline springs and the Jordan River inflow weakened. The shallow water environment that possibly occupied the retreating southwestern shore of Lake Kinneret was more dominated by seasonal runoff from the surface cover of the Galilee Mountains. The retreat of Lake Kinneret at ~ 24 cal ka BP coincides with the H2 event in the northern Atlantic. Bartov et al., (2003) and Torfstein et al., (2012) pointed out the coincidence between the H-events in the north Atlantic and catastrophic drops of tens of meters in Lake Lisan level that resulted in lake overturn and deposition of gypsum. Bartov et al., (2003) proposed that the very cold conditions during the Heinrich events affected also the eastern Mediterranean (mainly via atmospheric teleconnection) and switched off the cyclonic engine of vapor and rain production in the central Levant region. The sedimentary section recovered by the OH trench and the KIN2 core provides the sedimentological and geochemical environment of the Lake Kinneret during the H2 time interval. The $^{87}Sr/^{86}Sr$ ratio of ~ 0.70810 of the inflow water that filled the retreating lake is consistent with composition of runoff from the Galilee Highlands that erode the mountain soils exposed on the land surface. The soils (e.g. terra rossa), in turn are composed mainly of eolian desert dust that was blown to the region mainly during the last glacial period (Haliva-Cohen et al., 2012).

6.4 Conclusions

1. This study describes the hydrological-environmental conditions of Lake Kinneret during the time interval of ~ 24 to 21 cal ka BP encompassing the lake retreat from its last glacial MIS2 (~ 27-25 ka BP) high stand of ~ 170 m bsl to its late glacial low stand at ~ 214 m bsl. Field research was conducted in the Ohalo shore that was exposed during a modern lake retreat in 1999.
2. Sedimentary sequences were recovered by trenching and drilling. The chronology of the recovered sections was obtained by radiocarbon dating of organic debris and *Melanopsis* shells and by U-Th dating of aragonite casts yielding an age–height model between 24 and 21 ka cal BP. The lower part of the trench section coincides with the age of the Heinrich event H2 at northern latitudes.
3. Ostracods (*Cyprideis torosa*) and benthic foraminifera (*Ammonia tepida* and *Cribroelphidium* cf. *C. vadescens*) were recovered from the trench. The high numbers of ostracods and *A. tepida* at the base of the trench (~ 23 ka BP) indicate higher salinity than modern Lake Kinneret and seem to be related to the increasing aridity in the region during the H2 event. Upwards in the section ostracodes and foraminifera abundances are lower and variable. The dominance of the somewhat fresher water foraminifer *Cribroelphidium* cf. *C. vadescens*, in the upper part of the section coincides with a significant decrease in $\delta^{18}O$ values of *C. torosa* that apparently indicates an increase in regional runoff.
4. $^{87}Sr/^{86}Sr$ and $\delta^{18}O$ isotope ratios were obtained from ostracod valves and were used for the identification of water sources and reconstruction of hydrological conditions in the watershed. $^{87}Sr/^{86}Sr$ range between ~ 0.70789 and ~0.70815, and $\delta^{18}O$ values range from -2 to -4‰, from the bottom to the top of the trench (~ 24-21 ka cal BP). The $^{87}Sr/^{86}Sr$ ratios lie between the last glacial lake waters with $^{87}Sr/^{86}Sr$ ~0.70785 and regional runoff waters with $^{87}Sr/^{86}Sr$ ~ 0.70815. The glacial lake waters are currently represented by the Tiberias Spa saline solution. The 2‰ decrease in the $\delta^{18}O$ values is consistent with the change in the composition of east Mediterranean waters – the source of the regional precipitation between 24 and 21 ka cal BP indicating that the Ohalo-shore environment was dominated at that period by regional run-off.
5. The H2 cold event at the northern Atlantic was expressed by severe aridity in the watershed of Lake Kinneret - Dead Sea. The drying was accompanied by lake level retreat and formation of a shallow “wet-land” at the Ohalo shore. The retreating lake received waters from occasional runoff with $^{87}Sr/^{86}Sr$ ~ 0.7081 indicating erosion of the dried mountains soils that were developed on the mountain surface during the MIS2 wet glacial.

Chapter 7: Water sources

7.1 General

Lake Kinneret received freshwater and brines from various fresh and saline water sources. The identification of these sources is based on the chemical and Sr-isotope composition of ostracod shells and primary carbonates recovered from the sedimentary cores that were drilled at the bottom of the lake at water depths of 213.0-229.0 m bsl.

7.2 Freshwater and brine contribution to Lake Kinneret

Sr/Ca ratios $^{87}Sr/^{86}Sr$ isotope ratios in ostracod shells (e.g. *C. torosa)* and in primary carbonates recovered from the cores are used in this section to characterize the composition of the waters that filled Lake Kinneret during the late Quaternary (past 40 ka), and the contribution of the different water sources to the lake. These sources are the Jordan River, runoff and saline brines. The origin of the saline water at the vicinity of Lake Kinneret was extensively studied by Goldschmidt et al., (1967), Mazor (1968), Mazor and Mero (1969a, b) and others. Previous studies aimed to divide the saline springs into major groups; each is characterized by different temperature, salinity and elemental ratios. For example, Goldschmidt (1967) found that brines with high Ca/Mg ratios are dominant at the western area of the lake, while brines with low Ca/Mg are prominent in the eastern area. Mazor and Mero (1969a) offered to divide the brines into four groups: Ein-Gev (east), Zemah (south), Tiberias (south-west) and Fuliya-Barbutim-Tabgha (north-west). The most prominent is the Ca-chloride brines at the western springs vs. the Mg-chloride brines at the eastern springs (Mazor and Mero 1969, Starinsky 1974).
In table 7.1 I display chemical parameters that characterize the four groups (Rn1, Rn2, Rn2 and Rn4) according to Starinsky (1974). The explanation to the differences between the four types of brines is the dilution and evaporation of the Ca-chloride brines.
Modern LK shows wide variability in $^{87}Sr/^{86}Sr$ values.The spatial variations in $^{87}Sr/^{86}Sr$ values between the brines and the different contributions of the brines to the lake are probably the reasons for the range of $^{87}Sr/^{86}Sr$ values that were measured in the modern lake, as will be elaborated below.

Most of the samples from the various cores lie on two mixing arrays (figure 7.2): The first, between the Dead Sea brine and the Jordan basaltic water and the second, between regional runoff and the modern lake water. Most of the samples from the deeper part of the lake (KIN2 and SOG3) lie on the first array while samples from the margins lie mostly on the second array (SOG2 and Ohalo).

The modern Lake Kinneret water lie at Sr/Ca values of 0.006 and one higher value of 0.0076. The $^{87}Sr/^{86}Sr$ ratios lie between 0.70747 to 0.70765, different from other freshwater sources in the vicinity (Tables 3.1 and 6.2 and figure 7.1): the Jordan River with low Sr/Ca and $^{87}Sr/^{86}Sr$ values (0.0004-0.0010 and 0.7067-0.7072), water that drains the basaltic lithologies (~0.003-0.005 and 0.70745-0.70750) and runoff with low Sr/Ca and high $^{87}Sr/^{86}Sr$ values (~0.003 and ~0.7082). It is also different from values of the Kinneret brines, with high Sr/Ca and $^{87}Sr/^{86}Sr$ values (e.g. Tiberias Spa 0.0095 and 0.7078). It is most likely that the composition of the modern LK waters is a result of mixing of freshwater (Jordan River and basaltic water) with brines.

The Sr/Ca vs. $^{87}Sr/^{86}Sr$ ratios that reflect the lake water during the high stand last glacial period (MIS2), the interval of H2, the Younger Drays and the later Holocene in the lake (figure 7.2) show variables but significant shifts from the modern lake values.
The high-stand of last glacial period (MIS2) is represented by core KIN2 (below 215.5 m) where primary calcite was clearly identified and OH7 where ostracod shells were recovered. The rationale for this is that it appears that the calcite that was analyzed at the top part of the core is not pure primary calcite that represents the water. I consider it to be composed of a mixture of biogenic, primary and allochthonous calcite that enters the lake from the surrounding mountains with the runoff. I come to this conclusion from looking at the grain size and carbonate content (Figure 3.3) and at the Al_2O_3 vs. Fe_2O_3 diagram (Figure 5.1). I see that (1) the sediments are coarser and richer in carbonate at

the top (from 213.0 to 215.0 m bsl) and at the bottom of the core (from 221.5 to 222.0 m bsl) compared to the middle segment of the core (from 215.0 to 221.5 m bsl), and (2) higher values of Al_2O_3 and Fe_2O_3 at sediments that represent the high level period, implying leaching of carbonate from these sediments. Also, from SEM observations, I note the existence of large numbers of calcareous nano-plankton at the top of the core. Also contributing to this conclusion is the comparison between values from bulk carbonates from KIN2 and values from ostracod shells from Ohalo trench (OH7, figure 3.12): $^{87}Sr/^{86}Sr$ values that were measured on bulk carbonate from KIN2 borehole are similar to values measured on bulk carbonate from the same depth at the Ohalo trench (OH7) and are lower than values measured in ostracods from the same depth at the Ohalo trench.
Both primary calcite from KIN2 and the ostracods from OH7 show similar Sr/Ca and $^{87}Sr/^{86}Sr$ suggesting that the ratio reflect the lake water at that time. Sr/Ca in the water as inferred from bulk carbonate range from 0.0062 to 0.0067 (applying partition coefficient of 0.21, Katz and Nishri, 2013). $^{87}Sr/^{86}Sr$ values in the lake water as inferred from bulk carbonate range from 0.70771 to 0.70780. The majority of the samples from KIN2 borehole resemble saline (brine) water of Tiberias Spa ($^{87}Sr/^{86}Sr$ ~ 0.70785, Sr/Ca ~ 0.0079) values (Figure 7.2). This suggests enhanced input of the saline water during the last glacial high stand period. The saline water could represent a mixture between Dead Sea brine and local sources of salinity such as Fuliya, Tiberias spa and Tabgha springs (Figure 7.1). During the high stand period (~27-24 ka BP) the southern Lake Lisan expanded northward and converged with Lake Kinneret. This could allow increasing influence of the Dead Sea brine on Lake Kinneret water. At the same time enhanced activity of the fresh water aquifers and runoff could raise the hydrological head and intensify the discharge of the local saline springs. This is consistent with the Goldschmidt model that relates the discharge of the saline spring to the fresh water head of the Galilee Mountains (Goldschmidt et al. 1967). The springs' discharge is controlled by precipitation: the more precipitation on the Galilee Mountains the higher is the hydrological head and the discharge of the saline springs (the brines) to the lake (Figure 7.4). The similarity between Sr/Ca and $^{87}Sr/^{86}Sr$ composition of the last glacial and the Tiberias Spa water may indicate that the latter represents the high stand lake solution that currently discharge back to the lake. Previous studies already postulated that saline water was entrapped in the subsurface when the Kinarot Basin was covered by Lake Lisan and discharge into the freshwater lake (e.g., Bergelson et al., 1999, Hurwitz et al., 1999).

The H2 period (~ 23.8-22 ka BP) recovered in Ohalo trench and SOG2 core represent samples from the margins of the lake. This period was accompanied by regional aridity that resulted in lake level drop (Lev et al., 2014 and referenced therein) that is consistent with the massive marls facies (Figures 3.1 and 3.5). Both records show striking similarity. Sr/Ca in *C. torosa* from these sites lie at ~0.003-0.0035 (using partition coefficients Kd[Sr] ~ 0.7 (Lev et al., 2014) and $^{87}Sr/^{86}Sr$ values of 0.7081-0.7078 (Figures 3.9 and 3.10). These values are significantly different from the modern lake values and trending towards the composition of the regional Galilee Highlands runoff that drain the soil surface cover (e.g. Galilee spring values in Spiro et al., 2011). In contrast to the samples from the deeper parts of the lake (e.g. KIN2) it seems that the influence of the brines on the marginal water is small. The $^{87}Sr/^{86}Sr$ ratios of the Galilee Highlands surface cover as inferred from the ostracod values resemble values that are recorded in settled dust in Judea Mountains (Haliva-Cohen et al., 2012). Thus, it appears that settled dust was a major component of the Galilee Highlands surface cover indicating dust transportation to this region during H2 period.

The Younger Dryas (YD) samples presented in core SOG2 (Figure 3.10) appear to lie on the array between the regional runoff and the saline springs. SOG2 samples are shifted towards the mixture between the saline springs and the modern lake water indicating the transition from marginal to somewhat deeper conditions. At that time interval the lake level stood above 226 m bsl (possibly 10 m above, because of the presence of ostraods).

The Holocene is recovered only in core SOG3 showing $^{87}Sr/^{86}Sr$ ratios decreasing from the early the late Holocene. The values in the lake's water decrease from 0.70773 in the early Holocene towards 0.70765 in late Holocene with Sr/Ca ratio ranging between 0.0078 and 0.0067, respectively (Figure 3.11). These values lie between the last glacial waters of KIN2 and modern Lake Kinneret water (Figure 7.2). They are less radiogenic compared with the Tiberias Spa and with KIN2 high stand lake. This could indicate a reduced contribution of the brines (e.g., Tiberias Spa) compared to the high stand period. The modern lake however shows less radiogenic values of $^{87}Sr/^{86}Sr$ extending from 0.70745 to 0.70765 and Sr/Ca around 0.006.

Brackish diatoms were identified by Ehrlich (1985) at SOG2. The brackish diatoms and the high $^{87}Sr/^{86}Sr$ - low Sr/Ca ratio in the water as inferred from ostracods from SOG2 (Figures 3.5, 3.10) imply high salinity that could be mistaken for an enhanced contribution of brines to the lake during low-stand period. SOG3 is located closer to the brines so we would expect signs of higher salinity in SOG3 as well. However, no diatoms were recovered from contemporaneous sediments at SOG3 (Figures 3.7, 3.11). Therefore we conclude that the salinity of the lake at the south part does not imply high contribution of brines throughout the lake but represent the remains of water from the high period. The low salinity and low contribution of the brines during arid periods is also in agreement with the Goldschmidt et al., (1967) model (Figure 7.4).

7.3 Temporal changes in radiocarbon reservoir age

The changes in the relative contributions of the runoff, freshwater and brines to the lake also affect the reservoir age. During H2 low stand water level, reservoir age of Lake Kinneret was ~800 years due to high contribution of runoff. On the other hand, the YD high stand water level period was characterized in reservoir age of ~5,000 years, expressing the high contribution of the brines. Talma et al., (1997) analyzed fresh and saline waters from the Dead Sea drainage area and showed that runoff waters are characterized by high percent of modern carbon values, whereas springs that percolate throughout the Cretaceous carbonate aquifers are characterized by significantly lower values. We can assume that the same mechanism rules in Lake Kinneret; Runoff that rapidly washes the surface contributes water with high concentration of modern carbon, whereas water of the brines went though an interaction with the surrounding rocks. The latter contribute carbon without ^{14}C, resulting in low values of percent modern carbon.

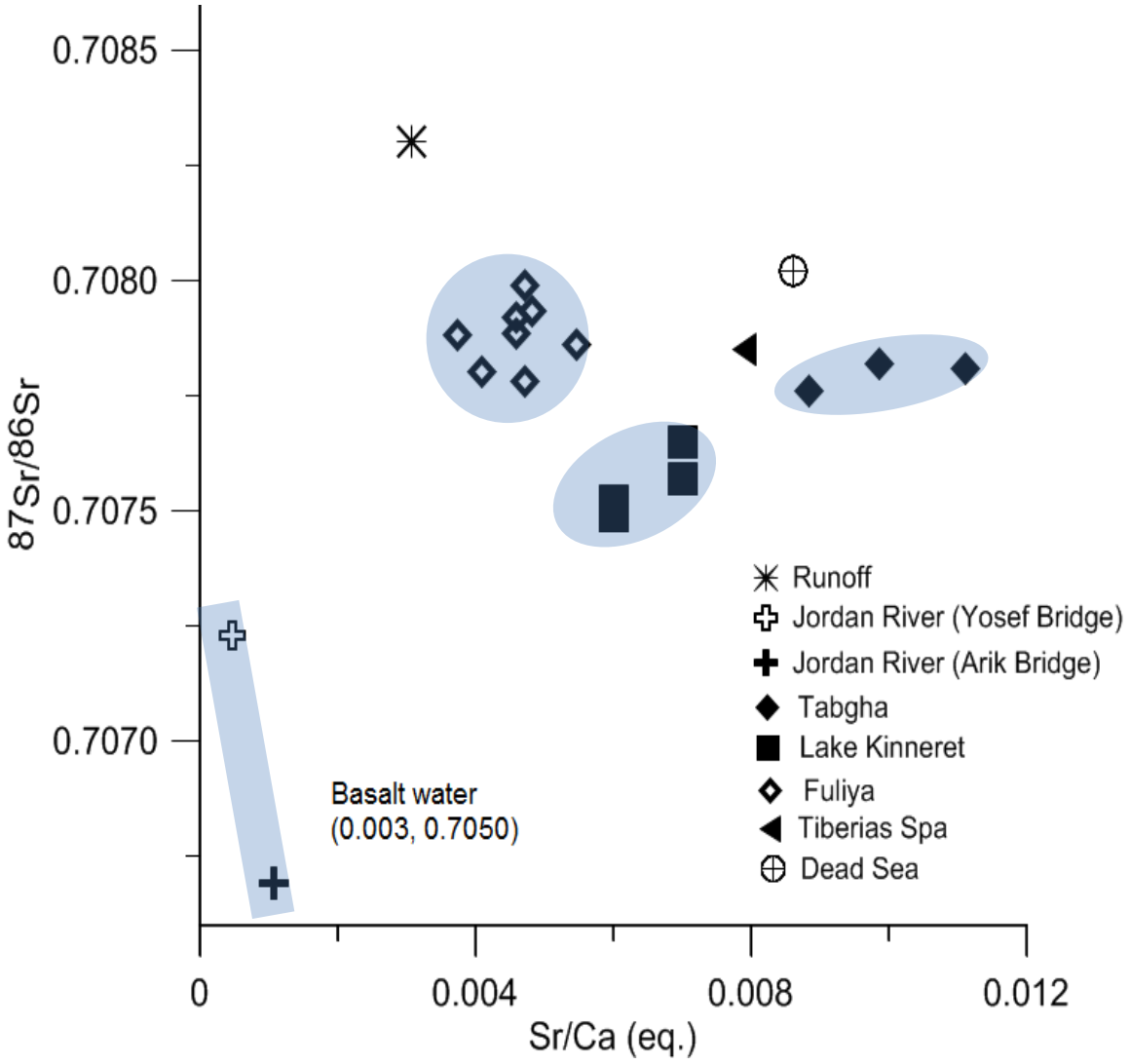

Figure 7.1 Sr/Ca vs. $^{87}Sr/^{86}Sr$ of the different water types. Modern Lake Kinneret is a mixture between Jordan River fresh water with low Sr/Ca and $^{87}Sr/^{86}Sr$ values and brines with high Sr/Ca and $^{87}Sr/^{86}Sr$ values. Jordan River also displays a wide range of $^{87}Sr/^{86}Sr$ values, with higher values that represent carbonate contribution, and low values that represent basalt contribution.

Table 7.1 Chemical parameters in brines with salinity >27,000 mg/L (Starinsky, 1974)

Group	TDS (g/L)	Sr/Ca	^{m}Sr ($x10^{3}$)	Sr (mg/L)	Cl/Br	$^{m}SO_4/^{m}Cl$ ($x10^{-3}$)	$^{m}Ca/^{m}Mg$	$^{m}K/^{m}Cl$	$^{m}Na/^{m}Cl$
Rn1	27-33	---	---	---	75-100	9-18	0.30-0.36	0.018	0.60-0.65
Rn2	28-36	---	---	---	80-100	0.05-0.10	0.33-0.40	0.010-0.013	0.60-0.65
Rn3	29-31	0.0087-0.0088*	0.733-0.753*	64-66*	75-80	15-17	2.1-3.9	0.018	0.55-0.60
Rn4	28-31	---	---	---	135-145	30-50	1.3-2.1	0.017	0.70-0.76

Ratios are molar ratios.
Rn1 are 3 boreholes at the east shore of the lake;
Rn2 are 2 boreholes at the south shore of the lake;
Rn3 are 5 boreholes at the south-west shore of the lake;
Rn4 are 2 boreholes at the north-west shore of the lake.
* values at Tiberias Spa drilling.

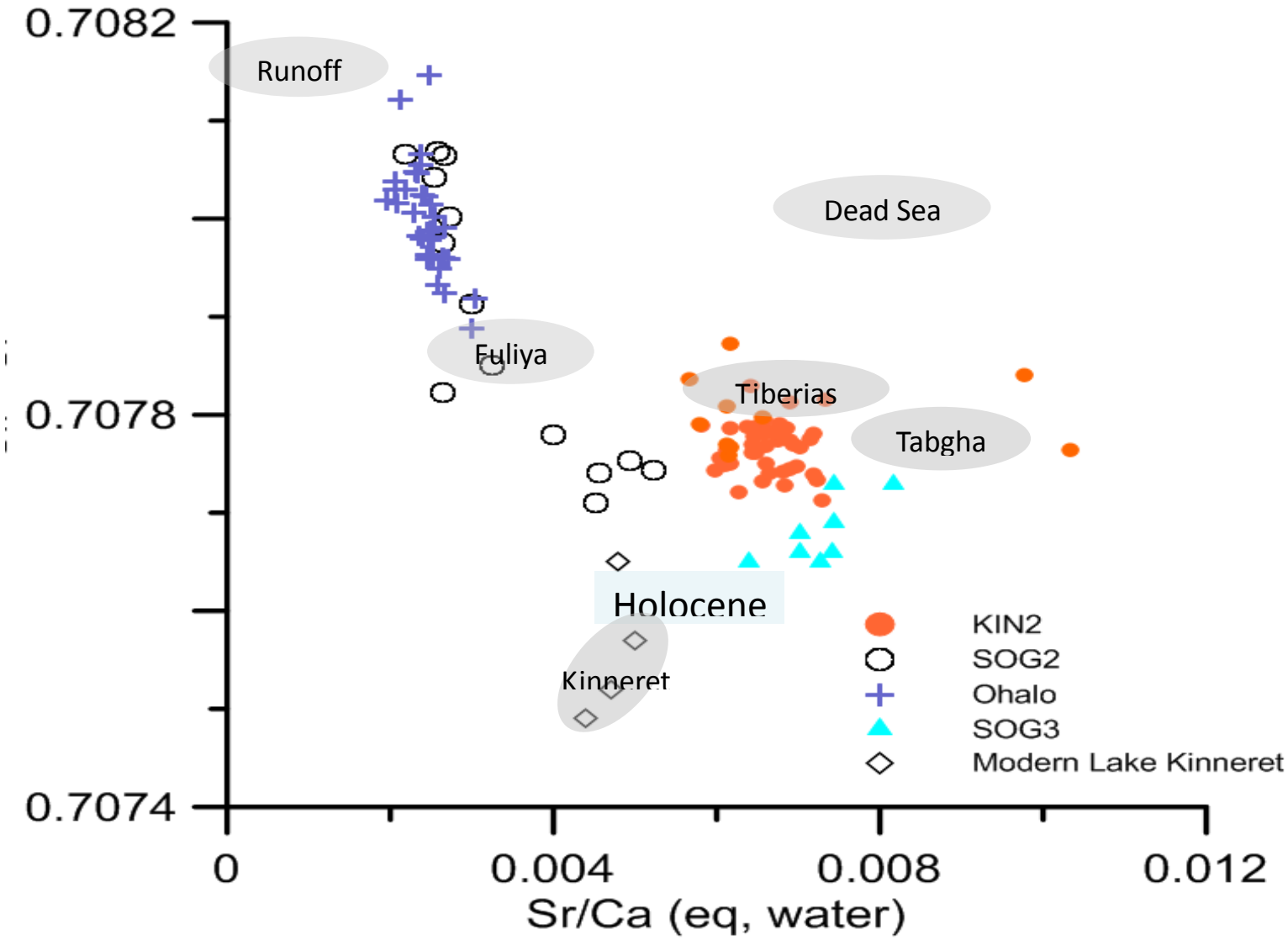

Figure 7.2 Sr/Ca vs. $^{87}Sr/^{86}Sr$ of water. KIN2 values are inferred from bulk carbonates. SOG2, SOG3 and Ohalo trench values are inferred from ostacod shells. For water values see table 6.2. Water values shift from high Sr/Ca and low $^{87}Sr/^{86}Sr$ values during glacial time, to low Sr/Ca and high $^{87}Sr/^{86}Sr$ values during H2. $^{87}Sr/^{86}Sr$ values decrease during YD period and resemble glacial values. These shifts represent changes in water sources.

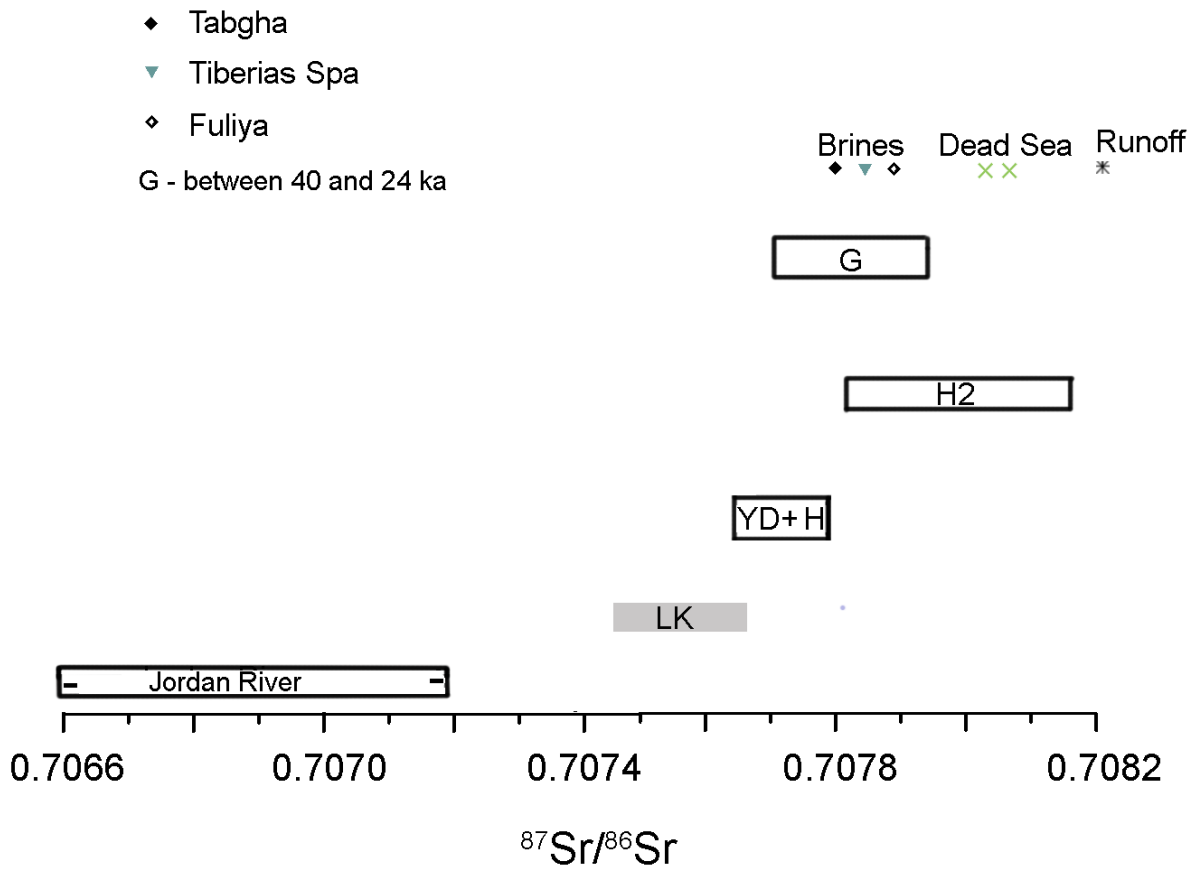

Figure 7.3 $^{87}Sr/^{86}Sr$ values during glacial period, H2, YD and Holocene based on ostracod shells and bulk carbonates. High contribution of brines during glacial period shifts to high contribution of runoff during H2. YD period shows return to glacial period values and Holocene Lake Kinneret shows high contribution of Jordan River.

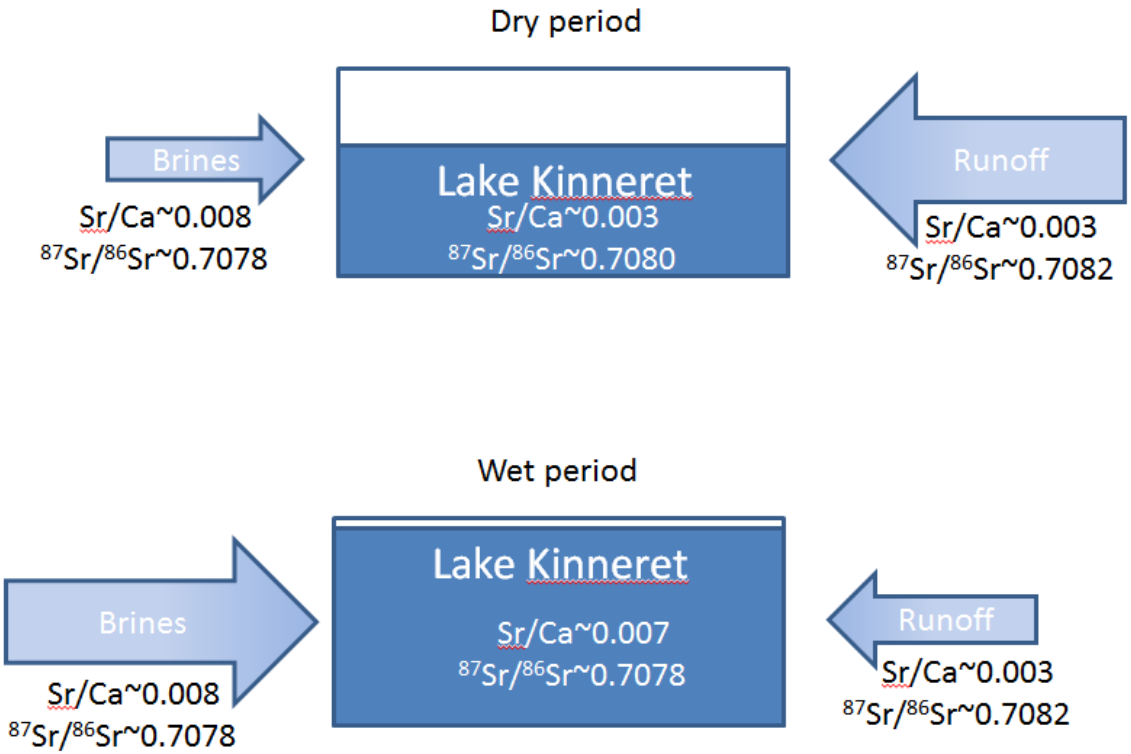

Figure 7.4 Schematic diagram based on the Goldschmidt model, showing high and low water level and main water source of brines and runoff during dry and wet periods. The diagram demonstrates changes in Sr/Ca and $^{87}Sr/^{86}Sr$ isotope ratios as a function of changes in water sources.

7.4 Conclusions

1. Chemistry and isotopes ratios of ostracod shells and primary carbonates are used to infer the change through time in the contribution of water sources (e.g., Jordan River, brines and runoff) to the lake.
2. The water at the south–western part of Lake Kinneret during the high-stand period is represented by KIN2 borehole. Sr/Ca ratios range from 0.0062 to 0.0067 and $^{87}Sr/^{86}Sr$ range from 0.70771 to 0.70800. H2 (post high stand) period at the south part of Lake Kinneret is represented by Ohalo trench and SOG2 borehole. Sr/Ca ratios range from 0.0023 to 0.0036 and $^{87}Sr/^{86}Sr$ range from 0.70791 to 0.70815. Younger Drays period at the north west part of the lake is represented by SOG3 borehole and characterized by Sr/Ca ratios of 0.0079 to 0.0086 and $^{87}Sr/^{86}Sr$ values of 0.70773. Younger Drays period at the south part of the lake is represented by SOG2 borehole and characterized by Sr/Ca ratios of 0.0043 to 0.0056 and $^{87}Sr/^{86}Sr$ values of 0.70771- 0.70778.
3. The late Quaternary lake's waters appear to lie on two mixing arrays: The first, between the Dead Sea brine and the Jordan basaltic water and the second, between regional runoff and the modern lake water. Most of the samples from the deeper part of the lake (KIN2 and SOG3) lie on the first array while samples from the margins lie mostly on the second array (SOG2 and Ohalo).
4. $^{87}Sr/^{86}Sr$ and Sr/Ca ratios of the lake water during the KIN2 interval resemble those of Tiberias Spa (0.70785). It is either that the contribution of the brines during high-stand was significantly high, or that the Tiberias Spa represents the water of the high stand, showing the influence of an unknown end member, characterized by higher $^{87}Sr/^{86}Sr$ values.
5. During glacial period Jordan River contributed less water to the lake, possibly because of the winter conditions that prevailed causing freezing of the soil above Mt. Hermon. The extreme water level rise requires supply of freshwaters from other sources in the watershed of the lake.
6. After lake level drop (H2 event) the water at the vicinity of SOG2 borehole resembles the water at Ohalo area. The water sources during the post high stand period were saline springs and runoff. $^{87}Sr/^{86}Sr$ ratios (~0.708) is higher than most of the brine, indicating that the area was dominated by seasonal floods.
7. The existence of brackish diatoms at SOG2 during H2 is in contrary to the barren of diatoms at SOG3, implying that during low water level the contribution of the brines is minor, and the salinity of the lake had decreased compared to the salinity during the high level period.
8. The low salinity and low contribution of the brines during H2 arid period and the higher contribution of the brines during the wetter YD period implies a relation between high and low water-stands and high and low contribution of the brines to the lake. This is in agreement with the Goldschmidt model.

Chapter 8: Summary

8.1 Overview

This study describes the hydrological-environmental conditions of Lake Kinneret during the time interval from 40 to 2 cal ka BP. Water and surface sediment samples containing living ostracods were collected from four sites around Lake Kinneret (Ginosar, Ma'agan, Shitim and Tabgha). Fossil ostracods, foraminifera and bulk sediments were recovered from four cores and a trench: Ohalo trench and KIN2 borehole at the southwest shore of the lake, SOG2 borehole at the south part of the lake at surface elevation of 224.0 m bsl and SOG3 at the northwest part of the lake at surface elevation of 229.0 m bsl.

The chronology of the recovered sections was obtained by radiocarbon dating of organic debris, ostracods and *Melanopsis* shells and by U-Th dating of aragonite casts. The Ohalo trench covers the period from 27 to 20 ka cal BP and the KIN2 core from ~40 to 21 ka cal BP. The SOG2 borehole covers the time interval from 25 to 12 ka cal BP and SOG3 from 25 to 2 ka cal BP. The Ohalo trench and KIN2 core are sensitive to lake level declines and contain sedimentary hiatuses. Between 27-25 ka cal BP lake level was high and reached ~170 m bsl. At ~ 23.8 ka cal BP (the H2 event) the lake declined to ~ 212 m bsl (from the Ohalo site).

The cores and the trench comprise mainly of alternating massive and laminated layers of primary calcite and detrital calcite, quartz and clays. The primary calcite was deposited from the lake, whereas the detrital material was transported into the lake by rivers, runoff and direct settled dust. Grain size analysis performed on bulk sediments from KIN2, SOG2 and SOG3 show temporal and spatial variations. Climate changes during the Pleistocene and Holocene are characterized by cyclic shifts between cold, warm, humid and dry conditions. These shifts have influence on desert dust transport and they are recorded in the sedimentary sections that were deposited in Lake Kinneret. Grain size in bulk sediments recovered by the trench and boreholes are used as proxy to detritus material source during the transition from high to low level, including the H2 and YD time intervals.

The water that fills Lake Kinneret is comprised of a mixture of Ca-chloride brines and freshwater. The brines are originated in the late Neogene Sedom lagoon and recharge into the lake in response to hydrological conditions that reflects regional climate. Trace element geochemistry and isotope ratios can provide information on the chemistry of paleo-environments. Sr/Ca ratios, $^{87}Sr/^{86}Sr$ isotope ratios and $\delta^{18}O$ values of ostracod shells *(C. torosa)* and primary carbonates are used to identify the sources of waters that filled Lake Kinneret during the late Quaternary (past 40 ka).

The sedimentary and geochemical data is combined to reconstruct in high resolution the limnology history of Lake Kinneret in the last ~40 ka and to examine the response of Lake Kinneret as part of a complex DST lacustrine system (the freshwater body in the north and the terminal, saline water body in the south) to the regional climate.

8.2.1 Last glacial period (~27-25 cal ka BP)

Last glacial period (~27-25 cal ka BP) was a high lake level period. Sr/Ca and $^{87}Sr/^{86}Sr$ ratios of water during high level period are based on primary carbonates from KIN2 borehole and range from 0.0062 to 0.0067 and from 0.70771 to 0.70800 respectively. $^{87}Sr/^{86}Sr$ and Sr/Ca ratios of the lake water during the KIN2 interval resemble those of Tiberias Spa (0.70783 - 0.70785) and imply less contribution of Jordan River. The extreme water level rise reflects a wet period and requires supply of freshwaters from enhanced rains in Lake Kinneret watershed. The low contribution of the Jordan River possibly reflects the winter conditions that prevailed causing freezing of Mt. Hermon.

Grain sizes of sediments from Lake Kinneret from the high stand period are typically 5-8μm, similar to those of the Lisan sediments (8-10μm), indicating a common source of desert dust storms. In contrary to the wet conditions that prevailed at the area of LK during the last

glacial period, extreme arid conditions persisted in the Sahara resulting in enhanced desert dust transport to the region that accumulated in the northern Negev desert of Israel and the Judean and Galilee Mountains.
The Fe_2O_3 vs. Al_2O_3 figure indicates the degree of leaching of the soluble components from the original dust material during pedogenic processes. Washout of the carbonates enriches the residual rock in Al and Fe. Low carbonate content in the sediments from high level period is in agreement with the high Al and Fe in the sediments, showing high contribution of detrital component to the lake. During high level lake dust was transported from distance sources (Sahara desert) and soluble components were leached out from the sediments.

8.2.2 Post glacial – Younger Drays

The H2 cold event at the northern Atlantic was expressed by severe aridity in the watershed of Lake Kinneret - Dead Sea. The drying was accompanied by lake level retreat and formation of a shallow "wet-land" at the Ohalo shore. Sr/Ca and $^{87}Sr/^{86}Sr$ ratios at H2 period are based on ostracods from Ohalo trench and SOG2 borehole. It ranges from 0.0023 to 0.0036 and from 0.70789 to 0.70815 respectively lying between brines and regional runoff waters with $^{87}Sr/^{86}Sr \sim 0.70815$. $\delta^{18}O$ values that were deduced from ostraocds from Ohalo trench range from -2 to -4‰, from the bottom to the top of the trench (~ 24-21 ka cal BP). The 2‰ decrease in the $\delta^{18}O$ values is consistent with the change in the composition of east Mediterranean waters – the source of the regional precipitation, indicating that the Ohalo-shore environment was dominated at that period by regional run-off.

During H2 period the sediments at Lake Kinneret were mostly transported into the lake by easterlies winds that brought desert dust from other source than the Sahara Desert. The Fe_2O_3 vs. Al_2O_3d from sediments from H2 period also indicate that dust was carried into the lake from less distance source resulting in less leaching compared to the glacial period.
The high numbers of the ostracod *Cyprideis torosa* and the foraminifera *Ammonia tepida* at the base of Ohalo trench (~ 23 ka BP) and the existence of brackish diatoms at SOG2 indicate higher salinity during the H2 event than modern Lake Kinneret. However, the barren of diatoms at SOG3 imply that during low water level the contribution of the brines is minor, and the salinity of the lake had decreased compared to the salinity during the high level period.
The YD period is known as a return to glacial conditions, reflected in wetter conditions in the Kinneret watershed and increase in water level. SOG2 samples show different $^{87}Sr/^{86}Sr$ ratios (0.7078 to 0.7081) from the KIN2 samples of the high-stand period (0.7077 to 0.7079). It seems that while during the last glacial period the connection to Lake Lisan is strongly distinguished, during the YD period the contribution of the brines is amplified.

Grain sizes of the sediments that represent the YD are also not identical to the values of the KIN2 samples. Grain size of sediments from YD period implies a moderate traveling distance of dust into the lake.

8.2.3 Holocene

It is noteworthy that the only segment that represent the Holocene period is the top of SOG3 borehole. The lithology of SOG3 at that segment shows laminated and massive marls, reflecting closed fluctuations in lake level.
Grain sizes mode of samples that represent the Holocene are 16, 18 and 24 μm, showing wide distribution. The coarse sediments imply that the distanced Sahara desert could not be the source of dust during Holocene period. The similarity to the dust samples that were collected at Jerusalem (~20-30 μm) indicates a close source of detrital matter.
Sr/Ca ratios in ostracod shells from SOG3 borehole that represent the Holocene ranges from 0.0047 to 0.0055, with a much higher Sr/Ca ratio compared with SOG2. $^{87}Sr/^{86}Sr$ ratios in ostracods range from 0.70765 to 0.70773, showing slightly lower values compared with SOG2. Sr/Ca and $^{87}Sr/^{86}Sr$ values of SOG3 samples probably represent the affect of the saline springs has on the chemistry of the water as the location of the borehole is at the north-western part of the lake, not far from the saline springs.

8.2.4 Reservoir ages

The changes in the relative contributions of the runoff, freshwater and brines to the lake also affect the reservoir age. During H2 low stand water level, reservoir age of Lake Kinneret was ~800 years due to high contribution of runoff. The YD high stand water level period was characterized in reservoir age of ~5,000 years, expressing the high contribution of the brines. Runoff rapidly washes the surface and contributes water with high concentration of modern carbon, whereas water of the brines interacts with the surrounding rocks. The latter contribute carbon without ^{14}C, resulting in low values of percent modern carbon.

8.2.5 The Goldschmidt model

The low salinity and low contribution of the brines during H2 arid period and the higher contribution of the brines during the wetter glacial and YD periods implies a relation between high and low water-stands and high and low contribution of the brines to the lake. This is in agreement with the Goldschmidt model: the discharge of the brines into the basin is controlled by variations in precipitation input in the mountains west of the basin. More precipitation on the western Galilee Mountains results in increased head of the freshwater aquifers in the Galilee Mountains and enhanced discharge of brines into LK.

Bibliography

Almogi-Labin, A., Perelis-Grossovicz, L., and Raab, M. (1992). Living Ammonia from a hypersaline inland pool, Dead Sea Area, Israel. *Journal of Foraminiferal Research* 22, 257-266.

Almogi-Labin, A., Schilman, B. and Flako-Zaritsky, S. (2004). Micro-faunal ecosystem of the Timsah springs: Environmental and stable isotopes characterization. Geological Survey of Israel, pp 46.

Athersuch, J., Horne, D.J. and Whittaker, J.E. (1990). Marine and brackish water ostracods, in: Kermack, M.D., Barnes, R.S.K. (Eds.), Synopses of the British fauna (new series). The Linnean society of London, The Estuarine and brackish water sciences association, pp 360.

Ayalon, A., Bar-Matthews, M., Frumkin, A. and Matthews, A. (2013). Last Glacial warm events on Mount Hermon: the southern extension of the Alpine karst range of the east Mediterranean. *Quaternary Science Reviews* 59, 43-56.

Bar-Matthews, M., Ayalon, A. and Kaufman, A. (1997), Late Quaternary Paleoclimate in the Eastern Mediterranean Region from Stable Isotope Analysis of Speleothems at Soreq Cave, Israel. *Quaternary Research*, 47(2), 155-168.

Bartov, Y., Goldstein, S.L., Stein, M. and Enzel, Y. (2003). Catastrophic arid episodes in the Eastern Mediterranean linked with the North Atlantic Heinrich events. *Geology* 31, 439-442.

Bartov, Y., Stein, M., Enzel, Y., Agnon, A. and Reches, Z. (2002). Lake levels and sequence stratigraphy of Lake Lisan, the Late Pleistocene precursor of the Dead Sea *Quaternary Research* 57, 9-21.

Bartov, Y., Steinitz, G., Eyal, M. and Eyal, Y. (1980). Sinistral movement along the Gulf of Aqaba (Elat)—its age and relation to the opening of the Red Sea. *Nature* 285 220–221.

Baruch, U. (1986). The Late Holocene vegetational history of Lake Kinneret (Sea of Galilee), Israel. *Paleorient* 12, 37-48.

Belmaker, R., Stein, M., Beer, J., Christl, M., Fink, D. and Lazar, B. (2014). Beryllium isotopes as tracers of Lake Lisan (last Glacial Dead Sea) hydrology and the Laschamp geomagnetic excursion. *Earth and Planetary Science Letters* 400, 233-242.

Ben-Avraham, Z., Amit, G., Golan, A. and Begin, Z.B. (1990). The bathymetry of Lake Kinneret and its structural significance. *Israel Journal of Earth Sciences* 39, 77-83.

Ben-Avraham, Z., Ginzburg, A. and Yuval, Z. (1981). Seismic reflection and refraction investigations of Lake Kinneret-central Jordan Valley, Israel. *Tectonophysics* 80, 165-181.

Ben-Avraham, Z., Shaliv, G. and Nur, A. (1986). Acoustic reflectivity and shallow sedimentary structure in the Sea of Galilee, Jordan Valley. *Marine Geology* 70, 175-189.

Ben-Avraham, Z., ten Brink, U., Bell, R. and Reznikov, M. (1996). Gravity field over the Sea of Galilee; evidence for a composite basin along a transform fault. *Journal of Geophysical Research* 101, 533-544.

Benson, L.V., Burdett, J.W., Kashgarian, M., Lund, S.P., Phillips, F.M. and Rye, R.O. (1996). Climatic and Hydrologic Oscillations in the Owens Lake Basin and Adjacent Sierra Nevada, California. *Science*, 274, 746-749.

Bergelson, G., Nativ, R. and Bein, A. (1999). Salinization and dilution history of ground water discharging into the Sea of Galilee, the Dead Sea Transform, Israel. *Applied Geochemistry* 14, 91-118.

Boomer, I. and Godwin, M. (1993). Palaeoenvironmental reconstruction in the Breydon Formation, Holocene of East Anglia. *Journal of Micropalaeontology* 12, 35-46.

Carpenter, S.J., Lohmann, K.C., Holden, P., Walter, L.M., Huston, T.J. and Halliday, A.N. (1991). $\delta^{18}O$ values, and Sr/Mg ratios of Late Devonian abiotic marine calcite: Implications for the composition of ancient seawater. *Geochimica et Cosmochimica Acta* 55, 1991-2010.

Chivas, A.R., De Deckker, P. and Shelley, J.M.G. (1986). Magnesium content of non-marine ostracod shells: a new palaeosalinometer and palaeothermometer. *Palaeogeography, Palaeoclimatology, Palaeoecology* 54, 43-61.

Coplen, T.B., Kendall, C. and Hopple, J. (1983). Comparison of stable isotope reference samples. *Nature* 302, 236-238.

Crouvi, O., Amit, R., Enzel, Y., Porat, N. and Sandler, A. (2008). Sand dunes as a major proximal dust source for late Pleistocene loess in the Negev Desert, Israel. *Quaternary Research* 70, 275-282.

Develle, A.L., Gasse, F., Vidal, L., Williamson, D., Demory, F., Van Campo, E., Ghaleb, B. and Thouveny, N. (2011). A 250 ka sedimentary record from a small karstic lake in the Northern Levant (Yammouneh, Lebanon) *Paleoclimatic implications*. 305, 10-27.

Dubowski, Y., Erez, J. and Stiller, M. (2003). Isotopic paleolimnology of Lake Kinneret. *Limnology and Oceanography* 48, 68-78.

Ehrlich, A. (1985). The eco-biostratigraphic significance of the fossil diatoms of Lake Kinneret. *GSI Current Research* 5, 24-30.

Engstrom, D.R. and Nelson, S.R. (1991). Paleosalinity from trace metals in fossil ostracodes compared with observational records at Devils Lake, North Dakota, USA. *Palaeogeography, Palaeoclimatology, Palaeoecology* 83, 295-312.

Enzel, Y., Agnon, A. and Stein, M. (2006). New Frontiers in Dead Sea Paleoenvironmental Research. The Geological Society of America, p. 253.

Enzel, Y., Amit, R., Dayan, U., Crouvi, O., Kahana, R., Baruch, Z. and Sharon, D. (2008). The climatic and physiographic controls of the eastern Mediterranean over the late Pleistocene climates in the southern Levant and its neighboring deserts. *Global Planetary change*, 60, 165-192.

Flako-Zaritsky, S. (2006). Micro-faunal ecosystem of the Timsah springs. Geological Survey of Israel, pp 85

Flako-Zaritsky, S., Almogi-Labin, A., Schilman, B., Rosenfeld, A. and Benjamini, C. (2011). The environmental setting and microfauna of the oligohaline Timsah pond, Israel: The last remnant of the Kabara swamps. *Marine Micropaleontology* 80, 74-88.

Flexer, A., Yellin-Dror, A., Kronfeld, J., Rosenthal, E., Ben-Avraham, Z. and Arts Davidson, L. (2000). A Neogene salt body as the primary source of salinity in Lake Kinneret. Archiv für Hydrobiologie, *Advances in Limnology* 55, 69-85.

Frenzel, P. and Boomer, I. (2005). The use of ostracods from marginal marine, brackish waters as bioindicators of modern and Quaternary environmental change. *Palaeogeography, Palaeoclimatology, Palaeoecology* 225, 68-92.

Freund, R. (1965). A model of the structural development of Israel and adjacent areas since upper Cretaceous times. *Geological Magazine* 102, 189-205.

Ganor, E., Deutsch, Y. and Foner, H.A. (2000). Mineralogical composition and sources of airborne sSettling particles on Lake Kinneret (the Sea of Galilee), Israel. *Water, Air, & Soil Pollution* 118, 245-262.

Ganor, E. and Foner, H.A. (1996). The mineralogical and chemical properties and the behaviour of aeolian Saharan dust over Israel In. Kluwer Academic Publishers, pp 163-172.

Ganor, E., Foner, H.A., Brenner, S., Neeman, E. and Lavi, N. (1991). The chemical composition of aerosols settling in Israel following dust storms. *Atmospheric Environment*. Part A. General Topics 25, 2665-2670.

Garfunkel, Z. (1981). Internal structure of the Dead Sea leaky transform (rift) in relation to plate kinematics. *Tectonophysics* 80, 81-108.

Gasse, F., Vidal, L., Develle, A.L. and Van Campo, E. (2011). Hydrological variability in the Northern Levant: a 250 multi-proxy record from the Yannouneh (Lebanon) sedimentary sequence. *Climate of the Past* 7, 1261-1284.

Gat, J.R., Mazor, E. and Tzur, Y. (1969). The stable isotope composition of mineral waters in the Jordan Rift Valley, Israel. *Journal of Hydrology* 7, 334-352.

Gibbard, P. and van Kolfschoten, T. (2004) The Pleistocene and Holocene Epochs. In Gradstein, F. M., Ogg, James G., and Smith, A. Gilbert (eds.), A Geologic Time Scale 2004 Cambridge University Press, Cambridge.

Golani, U. (1962). The Geology of Lake Tiberias region and the hydrogeology of the saline springs. Water planning for Israel Ltd. (TAHAL)

Goldschmidt, M.J., Arad, A. and Neev, D. (1967). The mechanism of the saline springs in the Lake Tiberias depression. *Geology Survey of Israel Bulletin* 45, 19.

Goldshmidt, M.J., Arad, A. and Neev, D. (1967). The mechanism of the saline springs in the Lake Tiberias depression. *Geology Survey of Israel Bulletin* 45, 19.

Goldstein, T. (2004). Lake flood craters in the northwestern part of Lake Kinneret - structure, evolution and relation to water flow (Hebrew). M.Sc. Thesis, Tel Aviv University, Tel Aviv

Haase-Schramm, A., Goldstein, S.I. and Stein, M. (2004). U-Th dating of lake Lisan (late Pleistocene Dead Sea) aragonite and implications for glacial east Mediterranean climate change. *Geochimica et Cosmochimica Acta* 68, 985-1005.

Halicz, L., Michelson, H., Merkel, D. and Bein, A. (2003). מערכת הנביעות המלוחות בכנרת, תמונת מצב גיאוכימית - יוני 2002. Geological Survey of Israel, pp 12.

Haliva-Cohen, A., Stein, M., Goldstein, S.L., Sandler, A. and Starinsky, A. (2012). Sources and transport routes of fine detritus material to the Late Quaternary Dead Sea basin. *Quaternary Science Reviews* 50, 55-70.

Hazan, N. (2003). Reconstruction of Kinneret Lake levels in the last 40,000 years. M.Sc Thesis, Hebrew University, Jerusalem

Hazan, N., Stein, M., Agnon, A., Marco, S., Nadel, D., Negendank, J.F.W., Schwab, M.J. and Neev, D. (2005). The Late Quaternary limnological history of Lake Kinneret (Sea of Galilee), Israel. *Quaternary Research* 63, 60-77.

Heimann, A. and Braun, D. (2000). Quaternary stratigraphy of the Kinnarot Basin, Dead Sea Transform, northeastern Israel. *Israel Journal of Earth Sciences* 49, 31-44.

Heimann, A., Steinitz, G., Mor, D. and Shaliv, G. (1996). The Cover Basalt Formation, its age and its regional and tectonic setting: implications from K-Ar and $^{40}Ar/^{39}Ar$ geochronology. *Israel Journal of Earth Sciences* 45, 55-71.

Hu, F.S., Ito, E., Brubaker, L.B. and Anderson, P.M. (1998). Ostracode Geochemical Record of Holocene Climatic Change and Implications for Vegetational Response in the Northwestern Alaska Range. *Quaternary Research* 49, 86-95.

Hurwitz, S., Garfunkel, Z., Ben-Gai, Y., Reznikov, M., Rotstein, Y. and Gvirtzman, H. (2002). The tectonic framework of a complex pull-apart basin; seismic reflection observations in the Sea of Galilee, Dead Sea Transform. *Tectonophysics* 359, 289-306.

Hurwitz, S., Goldman, M., Ezersky, M. and Gvirtzman, H. (1999). Geophysical (TDEM) delineation of a shallow brine beneath a fresh-water lake, the Sea of Galilee. *Water Resources Research* 35, 3631-3638.

Jones, T.R. (1857). A monograph of the Tertiary Entomostraca of England. Palaeontographical Society of London, 68.

Kalderon-Asael, B., Erel Y., Sandler, A. and Dayan, U. (2009). Mineralogical and chemical characterization of suspended atmospheric particles over the east Mediterranean based on synoptic-scale circulation patterns. Atmospheric Environment, 43(25), 3963-3970.

Katz, A. (2003). The geochemical response of Lake Kinneret (the Sea of Galilee) to Drought years. Israel Ministry of Infrastructure.

Katz, A. and Nishri, A. (2013). Calcium, magnesium and strontium cycling in stratified, hardwater lakes: Lake Kinneret (Sea of Galilee), Israel. *Geochimica et Cosmochimica Acta* 105, 372-394.

Kim S., T. and O'Neil J.R. (1997). Equilibrium and nonequilibrium oxygen isotope effects in synthetic carbonates. *Geochemica et Cosmochimica Acta*, 61(16), 3461-3475.

Klein-BenDavid, O., Gvirtzman, H. and Katz, A. (2005). Geochemical identification of fresh water sources in brackish groundwater mixtures; the example of Lake Kinneret (Sea of Galilee), Israel. *Chemical Geology* 214, 45-59.

Kolodny, Y., Katz, A., Starinsky, A., Moise, T. and Simon, E. (1999). Chemical tracing of salinity sources in Lake Kinneret (Sea of Galilee), Israel. *Limnology and Oceanography* 44, 1035-1044.

Lev, L. (2006). *Melanopsis* shells as chronometers and paleo-environmental tracers of Lake Kinneret and its vicinity, Israel. Thesis, Tel Aviv University, Tel Aviv.

Lev, L. (2008). *Melanopsis* shells as chronometers and paleo-environmental tracers of Lake Kinneret and its vicinity, Israel. Geological Survey of Israel, pp 55.

Lev, L., Almogi-Labin, A., Mischke, S., Ito, E., Ben-Avraham, Z. and Stein, M. (2014). Paleohydrology of Lake Kinneret during the Heinrich event H2. *Palaeogeography, Palaeoclimatology, Palaeoecology* 396, 183-193.

Lev, L., Boaretto, B., Heller, J., Marco, S. and Stein, M. (2007). The feasibility of using *Melanopsis* shells as radiocarbon chronometers, Lake Kinneret, Israel. *Radiocarbon* 49, 1003-1015.

Magny, M. (2001). Palaeohydrology changes as reflected by lake level fluctuations in the Swiss Plateau, the Jura Mountains and the northern French Pre-Alps during the Last Glacial-Holocene transition: A regional synthesis. *Global and Planetary change*, 30, 85-101.

Magny, M. and Ruffaldi, P. (1995), Younger Dryas and early Holocene lake level fluctuations in the Jura mountains, France. *Boreas*, 24(2), 155-172.

Marcus, E. and Slager, J. (1985). The sedimentary-magmatic sequence of the Zemah-1 well (Jordan-Dead Sea Rift, Israel) and its emplacement in time and space. Israel *Journal of Earth Sciences* 34, 1-10.

Martens K. and Ortal, R. (1999). Diversity and zoogeography of inland water Ostracoda (Crustacea) in Israel (Levant). *Israel Journal of Zoology*, 45(1), 159-173.

Mazor, E. and Mero, F. (1969a). Geochemical tracing of mineral and fresh water sources in the Lake Tiberias Basin, Israel. *Journal of Hydrology* 7, 276-317.

Mazor, E. and Mero, F. (1969b). The origin of the Tiberias-Noit mineral water association in the Tiberias-Dead Sea Rift Valley, Israel. *Journal of Hydrology* 7, 318-333.

Mazor, I.E. (1968). Genesis of mineral waters in the Tiberias - Dead Sea - Arava Rift Valley, Israel, Int. Geol. Congr., Prague, pp. 56-80.

McCulloch, M.T., De Deckker, K. and Chivas, A.R. (1989). Strontium isotope variations in single ostracod valves from the Gulf of Carpentaria, Australia: a palaeoenvironmental indicator. *Geochimica et Cosmochimica Acta* 53, 1703-1710.

McCulloch, M.T. and De Deckker, P. (1989). Sr-isotope constraints on the Mediterranean environment at the end of the Messinian salinity crisis. *Nature* 342, 62-65.

Mero, F. and Mandel, S. (1963). The hydrological mechanism of the saline springs of the western shore of Lake Kinneret (in Hebrew). TAHAL-Water Planning for Israel Ltd, pp 10.

Mero, F. and Zaltzman, U. (1967). Some geohydrological observations on the saline springs of Lake Kinneret (in Hebrew). TAHAL-Water Planning for Israel Ltd, pp 10.

Migowski, C., Stein, M., Prasad, S., Negendank, J.F.W. and Agnon, A. (2006). Holocene climate variability and cultural evolution in the Near East from the Dead Sea sedimentary record. *Quaternary Research* 66, 421-431.

Mischke, S., Almogi-Labin, A., Ortal, R., Rosenfeld, A., Schwab, M. and Boomer, I. (2010). Quantitative reconstruction of lake conductivity in the Quaternary of the Near East (Israel) using ostracods. *Journal of Paleolimnology* 43, 667-688.

Mischke, S. and Wunnemann, B. (2006). The Holocene salinity history of Bosten Lake (Xinjiang, China) inferred from ostracod species assemblages and shell chemistry: Possible palaeoclimatic implications. *Quaternary International* 154-155.

Nadel, D., Belitzky, S., Boaretto, E., Carmi, I., Heinemeier, J., Werker, E. and Marco, S. (2001). New dates from submerged late Pleistocene sediments in the southern Sea of Galilee, Israel. *Radiocarbon* 43, 1167-1178.

Neev, D. and Emery, E.O. (1967). The Dead Sea. Geological Survey Israel Bulletin 41, 1-147.

Neev, D. and Emery, K.O. (1995a). The Destruction of Sodom, Gomorrah, and Jericho In: Geological, C., and Archaeological Background(Ed). Oxford University Press, New York pp 192.

Neev, D. and Emery, K.O. (1995b). The destruction of Sodom, Gomorrah, and Jericho: geological, climatological and archaeological background In: Neev, D., Emery, K.O. (Ed). Oxford University Press, New York pp 175.

Niemi, T.M., Ben-Avraham, Z. and Gat, Y. (1997). The Dead Sea—The Lake and Its Setting. Oxford University Press, New York, p. 286.

Oviatt C.G. (1997). Lake Bonneville fluctuations and global climate change, *Geology*, 25(2), 155-158.

Rashid, H., Saint-Ange, F., Barber, D.C., Smith, M.E. and Devalia, N. (2012). Fine scale sediment structure and geochemical signature between eastern and western North Atlantic during Heinrich events 1 and 2. *Quaternary Science Reviews* 46, 136-150.

Rasmussen, S.O., Andersen, K.K., Svensson, A.M., Steffensen, J.P., Vinther, B.M., Clausen, H.B., Siggaard-Andersen, M.L., Johnsen, S.J., Larsen, L.B., Dahl-Jensen, D., Bigler, M., Röthlisberger, R., Fischer, H., Goto-Azuma, K., Hansson, M.E. and Ruth, U. (2006). A new Greenland ice core chronology for the last glacial termination. *Journal of Geophysical Research: Atmospheres* 111, D06102.

Reznikov, M., Ben-Avraham, Z., Garfunkel, Z., Gvirtzman, H. and Rotstein, Y. (2004). Structural and stratigraphic framework of the Lake Kinneret. *Israel Journal of Earth Sciences* 53, 131-149.

Rimmer, A., Hurwitz, S. and Gvirtzman, H. (1999). Spatial and temporal characteristics of saline springs: Sea of Galilee, Israel. *Ground Water* 37, 663-673.

Rosenfeld, A., Nathan, Y., Feibel, C.S., Schilman, B., Halicz, L., Goren-Inbar, N. and Siman-Tov, R. (2004). Palaeoenvironment of the Acheulian Gesher Benot Ya'aqov Pleistocene lacustrine strata, Northern Israel-lithology, ostracod assemblages and ostracod shell geochemistry. *Journal of African Earth Sciences* 38, 169-181.

Serruya, C. (1977). Rates of sedimentation and resuspension in Lake Kinneret, in: Golterman, H.L. (Ed.), Interactions Between Sediments and Fresh Water. Junk B.V., Netherlands, pp. 48-56.

Sivan, D., Greenbaum, N., Cohen-Seffer, R., Sisma-Ventura, G. and Almogi-Labin, A. (2011). The origin and disappearance of the late Pleistocene-early Holocene short-lived coastal wetlands along the Carmel coast, Israel. *Quaternary Research* 76, 83-92.

Spiro, B., Ashkenazi, S., Starinsky, A. and Katz, A. (2011), Strontium isotopes in Melanopsis sp. as indicators of variation in hydrology and climate in the Upper Jordan Valley during the Early-Middle Pleistocene. *Journal of Human Evolution* 60, 407-416.

Starinsky, A. (1974). Relationship between Ca-chloride brines and sedimentary rocks in Israel (in Hebrew). Ph.D. Thesis, The Hebrew University of Jerusalem, Jerusalem.

Stein, M. (2001). The sedimentary and geochemical record of Neogene-Quaternary water bodies in the Dead Sea Basin - inferences for the regional paleoclimatic history. *Journal of Paleolimnology* 26, 271-282.

Stein, M. (2014a). The Evolution of Neogene-Quaternary Water-Bodies in the Dead Sea Rift Valley In: Modern Approaches in Solid Earth Sciences. Springer Netherlands, pp 279-316.

Stein, M. (2014b). Late Quaternary Limnological History of Lake Kinneret, in: Zohary, T., Sukenik, A., Berman, T., Nishri, A. (Eds.), Lake Kinneret. Springer, Jerusalem.

Stein, M., Starinsky, A., Katz, S., Goldstein, S.L., Machlus, M. and Schramm, A. (1997). Strontium isotopic, chemical and sedimentological evidence for the evolution of Lake Lisan and the Dead Sea. *Geochimica et Cosmochimica Acta* 61, 3975-3992.

Stiller, M. (1974). Rate of transport and sedimentation in Lake Kinneret. Ph.D Thesis, Weizmann Institute of Science, Rehovot.

Stiller, M. and Kaufman, A. (1985). Paleoclimatic trends revealed by the isotopic composition of carbonates in Lake Kinneret. *Zeitschrift fur Gletscherkunde und Glazialgeologie* 21, 79-87.

Talma, A.S., Vogel, J.C. and Stiller, M. (1997). The radiocarbon content of the Dead Sea, in: Neimi, T.L., Ben Avraham Z. and Gat, J.R. (Eds.), The Dead Sea: The lake and its setting. Oxford University Press, Oxford, pp. 171-183.

Tchernov, E. (1975). The Molluscs of the Sea of Galilee. *Malacologia* 15, 147-184.

Thompson, R., Turner, G.M., Stiller, M. and Kaufman, A. (1985). Near east Paleomagnetic secular variation recorded in sediments from the Sea of Galilee (Lake Kinneret). *Quaternary Research* 23, 176-188.

Torfstein, A., Goldstein, S.L., Kagan, E.J. and Stein, M. (2013). Integrated multi-site U-Th chronology of the last glacial Lake Lisan. *Geochimica et Cosmochimica Acta* 104, 210-231.

Torfstein, A., Goldstein, S.L., Stein, M. and Enzel, Y. (2012). Abrupt changes in Levant precipitation during the last glacial from Dead Sea lake levels, European Geosciences Unior General Assembly, Vienna, Austria.

Waldman, N., Torfstein, A. and Stein, M. (2010). Northward intrusions of low and mid latitude storms across the Saharo-Arabian belt during past interglacials. *Geology*, 38, 567-570.

Walker, M., Johnsen, S., Rasmussen, S. O., Popp, T., Steffensen, J.P., Gibbard, P., Hoek, W., Lowe, J., Andrews, J., Cwynar, L. C., Hughen, K., Kershaw, P., Kromer, B., Litt, T., Lowe, D.J., Nakagawa, T., Newnham, R. and Schwander, J. (2009). Formal definition and dating of the GSSP (Global Stratotype Section and Point) for the base of the Holocene using the Greenland NGRIP ice core, and selected auxiliary records. *Journal of Quaternary Sciences*. 24, 3–17.

Wansard, G., De Deckker, P. and Julia, R. (1998). Variability in ostracod partition coefficients D(Sr) and D(Mg) : Implications for lacustrine palaeoenvironmental reconstructions. *Chemical Geology* 146, 39-54.

Xia, J., Engstrom, D.R. and Ito, E. (1997). Geochemistry of ostracode calcite: Part 2. The effects of water chemistry and seasonal temperature variation on Candona rawsoni. *Geochimica et Cosmochimica* Acta 61, 383-391.

Yaalon, D.H. and Dan, J., (1974). Accumulation and distribution of loess-derived deposits in the semi-desert and desert fringe areas of Israel. *Zeitschrift für Geomorphologie N.F*. 20, 91-105.

Zak, I. (1967). Geology of Mount Sedom (in Hebrew). Ph.D. Thesis, The Hebrew University of Jerusalem, Jerusalem

Appendix A

Table 1. XRD results of bulk sediments from Ohalo trench

	Depth interval (cm)	Absolute depth (m bsl)	Facies	quartz	calcite	dolomite	k-felds.	plagioc.	phyllosil.	aragonite
OH-1	25	211.8	mm	++	+++	+		++	++	
OH-1	29	211.8	mm	++	+++	+		++	++	
OH-2	55	212.1	mm	++	+++	+		+	+	+
OH-2	73	212.2	mm	+	+++	+	+	+	++	+
OH-2	75	212.3	mm	++	++++	+	+	+	++	+
OH-2	77	212.3	mm	++	+++	+	+	++	++	+
OH-2	79	212.3	mm	++	++++	+	++	+	++	+
OH-2	81	212.3	mm	++	+++	+	++	++	++	+
OH-2	83	212.3	mm	++	+++	+	++	+	++	+
OH-2	85	212.4	mm	++	++++	+	++	++	++	+
OH-2	87	212.4	mm	++	++++	++	++	+	++	+
OH-2	89	212.4	mm	++	++++	+	+	+	++	+
OH-2	91	212.4	mm	++	+++	+	+	++	++	+
OH-2	93	212.4	mm	++	+++	+	+	++	++	+
OH-2	95	212.5	mm	++	++++	+	++	++	++	+
OH-2	99	212.5	mm	+	+++	+		+	++	++
OH-2	109	212.6	mm	+	+++	+	+	++	++	
OH-3	147	213.0	mm	+	++++	+		+	+	+
OH-3	183	213.3	mm	++	+++	+		++	++	++
OH-3	199	213.5	mm	++	+++	+		++	++	
OH-3	216	213.7	mm	++	+++	+		++	++	+
OH-5	288	214.4	lm	++	+++	+	+	+	+++	

+	less than 5%
++	5-25%
+++	25-50%
++++	more than 50%
mm	massive marls
lm	laminated marls

Table 2. Color index, carbonate content and percent of fine sediments from Ohalo trench

	Depth in the core (cm)	Absolute depth (m bsl)	L*	a*	b*	%carbonate	%<63μm
OH-1	1	211.5	48	2	12.8	20	88
OH-1	3	211.5	48	2.3	13.6	30	87
OH-1	5	211.6	50	2.3	14.3	11	84
OH-1	7	211.6	49	2.5	14.6	35	76
OH-1	9	211.6	51	2.5	14.9	47	63
OH-1	11	211.6	51	2.2	13.9	40	78
OH-1	13	211.6	54	1.8	13.1	34	87
OH-1	15	211.7	56	0.5	11.1	26	95
OH-1	17	211.7	55	0.8	11.1	24	97
OH-1	19	211.7	57	0.5	10.7	27	90
OH-1	21	211.7	57	0.4	10.2	18	95
OH-1	23	211.7	58	0.5	10.7	21	90
OH-1	25	211.8	54	1.7	12.5	35	81
OH-1	27	211.8	54	1.8	12.5	48	95
OH-1	29	211.8	52	1.4	11.2	38	89
OH-1	31	211.8	48	1.3	10	37	88
OH-1	32	211.8	52	1.4	11.4	40	93
OH-1	34	211.8	47	1.2	9.9	39	92
OH-1	36	211.9	51	1.2	11.2	43	88
OH-1	38	211.9	56	1.4	13	44	80
OH-1	40	211.9	56	1.5	13.4	46	86
OH-1	41	211.9	51	1.2	11.3	53	79
OH-1	45	212	47	1.1	9.4	50	60
OH-2	41	211.9	45	0.9	9.2	48	53
OH-2	43	211.9	49	1	10.2	47	56
OH-2	45	212	50	0.9	10.2	48	58
OH-2	47	212	54	1.2	11.9	47	74
OH-2	49	212	54	1.2	11.9	49	78
OH-2	51	212	49	1	10.6	50	54
OH-2	53	212	49	1.3	10.7	54	41
OH-2	55	212.1	50	1.2	10.9	57	41
OH-2	57	212.1	51	1.2	11.4	55	66
OH-2	59	212.1	52	1.2	11.8	50	87

OH-2	61	212.1	55	1.5	13.4	54	81
OH-2	63	212.1	54	2.1	14.4	59	72
OH-2	65	212.2	54	3.1	16.9	53	72
OH-2	67	212.2	53	3.4	16.5	50	73
OH-2	69	212.2	56	2	14.3	52	79
OH-2	71	212.2	56	1.6	13.2	48	81
OH-2	73	212.2	56	1.6	13.4	51	70
OH-2	75	212.3	56	1.6	13.5	53	65
OH-2	77	212.3	56	1.8	13.9	52	62
OH-2	79	212.3	55	1.8	13.9	52	63
OH-2	81	212.3	54	1.9	13.9	53	60
OH-2	83	212.3	54	1.9	13.8	57	55
OH-2	85	212.4	55	1.8	13.6	58	51
OH-2	87	212.4	56	1.9	13.6	59	60
OH-2	89	212.4	56	2	14.1	54	71
OH-2	91	212.4	55	1.9	13.7	58	82
OH-2	93	212.4	56	2.1	14.1	51	70
OH-2	95	212.5	57	2.3	15.1	44	86
OH-2	97	212.5	58	2.7	15.9	66	64
OH-2	99	212.5	59	2.5	15.9	73	43
OH-2	102	212.5	58	2.1	14.5	41	96
OH-2	105	212.6	56	1.6	13.3	34	99
OH-2	107	212.6	57	1.8	13.7	40	93
OH-2	109	212.6	60	1.7	13.8	46	98
OH-2	111	212.6	59	1.8	13.7	43	98
OH-2	113	212.6	57	1.6	13.6	44	99
OH-2	115	212.7	55	1.6	13.1	34	96
OH-2	118	212.7	61	2	14.4	57	94
OH-2	120	212.7	62	1.8	14.5	57	99
OH-2	122	212.7	61	1.9	14.6	52	96
OH-2	124	212.7	59	1.7	14.6	47	73
OH-2	126	212.8	59	1.5	14	40	98
OH-2	128	212.8	59	2.1	15.5	55	77
OH-2	130	212.8	59	2.4	16.4	47	61
OH-2	132	212.8	58	1.9	14.9	46	75
OH-2	134	212.8	56	1.5	13.7	41	89

OH-3	111	212.6	59	1.9	14.8	42	
OH-3	113	212.6	59	1.9	14.4	51	
OH-3	115	212.7	59	2	14.3	59	88
OH-3	117	212.7	59	2.1	14.4	56	
OH-3	119	212.7	54	1.4	11.4	54	
OH-3	121	212.7	50	1.3	10.3	44	86
OH-3	123	212.7	55	1.5	12.3	48	
OH-3	125	212.8	57	2	13.7	51	
OH-3	127	212.8	56	2.2	14.2	56	66
OH-3	130	212.8	56	2.1	14.4	58	
OH-3	133	212.8	57	2.1	14.6	57	65
OH-3	136	212.9	57	2.1	14.2	57	
OH-3	139	212.9	58	1.8	13.7	45	72
OH-3	141	212.9	57	2	13.8	45	
OH-3	143	212.9	58	2	13.8	52	83
OH-3	145	213	59	2	14.1	53	
OH-3	147	213	59	2	14.4	71	62
OH-3	149	213	56	2.1	14.4	37	
OH-3	151	213	57	2	13.9	44	77
OH-3	153	213	57	1.9	14	47	
OH-3	155	213.1	57	2.1	13.9	46	93
OH-3	157	213.1	57	2.2	14	43	
OH-3	159	213.1	61	2.2	14.2	55	100
OH-3	161	213.1	60	1.8	14.1	43	
OH-3	163	213.1	61	1.7	14.6	44	96
OH-3	166	213.2	63	1.9	14.8	50	
OH-3	166	213.2	59	1.6	14.3	57	79
OH-3	171	213.2	52	3.5	15.3	35	
OH-3	173	213.2	57	1.6	15	37	90
OH-3	175	213.3	60	2.5	16.2	44	
OH-3	177	213.3	61	2.4	15.9	68	71
OH-3	179	213.3	60	2.2	15.2	54	
OH-3	181	213.3	61	1.8	14.5	45	98
OH-3	183	213.3	60	1.8	14	61	
OH-3	185	213.4	64	1.5	13.3	53	100
OH-3	187	213.4	65	1.6	13.5	54	
OH-3	188	213.4	62	2.3	14.2	49	93
OH-3	190	213.4	59	2.3	13.6	32	
OH-3	192	213.4	57	2	13	37	96
OH-3	194	213.4	58	2	13.3	46	

OH-3	196	213.5	59	2.1	13.8	39	
OH-3	197	213.5	59	1.9	13.6	52	
OH-3	199	213.5	58	2.1	13.7	40	97
OH-3	201	213.5	57	2	13.1	43	
OH-3	203	213.5	52	2.2	12.5	36	96
OH-3	205	213.6	57	2.4	14.5	55	
OH-4	201	213.5	55	1.9	13.9	52	85
OH-4	203	213.5	55	2	14	48	90
OH-4	205	213.6	55	2	13.9	60	84
OH-4	207	213.6	57	2	13.9	59	89
OH-4	208	213.6	58	1.9	13.8	55	93
OH-4	210	213.6	57	1.8	13	54	95
OH-4	212	213.6	54	1.2	10.8	52	98
OH-4	214	213.6	58	1.7	13.1	58	96
OH-4	216	213.7	60	1.7	13.5	56	97
OH-4	218	213.7	59	1.8	13.7	47	99
OH-4	220	213.7	59	1.7	14	40	100
OH-4	222	213.7	60	1.9	14.4	46	99
OH-4	224	213.7	60	1.8	14.6	49	98
OH-4	226	213.8	61	2	15.1	46	99
OH-4	228	213.8	59	2	14.6	43	99
OH-4	230	213.8	61	1.9	14.8	55	96
OH-4	232	213.8	62	1.8	14.5	58	96
OH-4	234	213.8	62	1.7	14.3	59	94
OH-4	236	213.9	64	1.7	14.7	68	89
OH-4	238	213.9	63	1.8	14.6	68	91
OH-4	240	213.9	61	1.8	13.8	67	91
OH-4	242	213.9	62	1.7	14.3	63	96
OH-4	244	213.9	60	1.8	14.3	62	97
OH-4	246	214	59	1.8	14.1	56	95
OH-4	248	214	59	1.8	14	55	97
OH-4	250	214	60	1.9	14.2	55	96
OH-4	252	214	61	1.8	13.5	57	98
OH-4	254	214	61	1.9	13.7	57	96
OH-4	256	214.1	62	1.7	13.6	60	94
OH-4	258	214.1	62	1.7	13.7	67	92
OH-4	260	214.1	61	1.3	13	50	94
OH-4	262	214.1	63	1.4	13.5	59	94
OH-4	264	214.1	61	1.4	13.2	64	91
OH-4	266	214.2	60	1.4	13.2	60	91

OH-4	268	214.2	60	1.6	13.8	60	95
OH-4	270	214.2	60	1.6	13.7	49	93
OH-4	272	214.2	62	1.6	14	52	96
OH-4	274	214.2	63	1.5	13.8	56	95
OH-4	276	214.3	62	1.6	14	54	95
OH-4	278	214.3	61	1.6	13.5	49	94
OH-4	280	214.3	60	1.5	13.6	45	93
OH-4	282	214.3	59	1.5	13.5	52	95
OH-4	284	214.3	59	1.5	13.9	44	99
OH-4	286	214.4	60	1.6	14.3	41	100
OH-4	288	214.4	60	1.6	14.4	36	99
OH-4	290	214.4	61	1.5	14.2	33	98
OH-4	292	214.4	61	1.6	14	41	99
OH-4	294	214.4	61	1.4	13.7	30	99
OH-4	296	214.5	57	1.4	13.5	33	100
OH-4	299	214.5	59	1.3	13.6	36	100
OH-5	301	214.5	55	1.9	13.9	52	99
OH-5	303	214.5	55	2	14	48	98
OH-5	305	214.6	55	2	13.9	60	97
OH-5	307	214.6	57	2	13.9	59	91
OH-5	308	214.6	58	1.9	13.8	55	94
OH-5	310	214.6	57	1.8	13	54	97
OH-5	312	214.6	54	1.2	10.8	52	99
OH-5	314	214.6	58	1.7	13.1	58	99
OH-5	316	214.7	60	1.7	13.5	56	94
OH-5	318	214.7	59	1.8	13.7	47	87
OH-5	320	214.7	59	1.7	14	40	94
OH-5	322	214.7	60	1.9	14.4	46	96
OH-5	324	214.7	60	1.8	14.6	49	99
OH-5	326	214.8	61	2	15.1	46	98
OH-5	328	214.8	59	2	14.6	43	95
OH-5	330	214.8	61	1.9	14.8	55	99
OH-5	332	214.8	62	1.8	14.5	58	99
OH-5	334	214.8	62	1.7	14.3	59	98
OH-5	336	214.9	64	1.7	14.7	68	100
OH-5	338	214.9	63	1.8	14.6	68	100
OH-5	340	214.9	61	1.8	13.8	67	97
OH-5	342	214.9	62	1.7	14.3	63	97
OH-5	344	214.9	60	1.8	14.3	62	97
OH-5	346	215	59	1.8	14.1	56	93

OH-5	348	215	59	1.8	14	55	99
OH-5	350	215	60	1.9	14.2	55	95
OH-5	352	215	61	1.8	13.5	57	98
OH-5	354	215	61	1.9	13.7	57	96
OH-5	356	215.1	62	1.7	13.6	60	97
OH-5	358	215.1	62	1.7	13.7	67	97
OH-5	360	215.1	61	1.3	13	50	97
OH-5	362	215.1	63	1.4	13.5	59	97
OH-5	364	215.1	61	1.4	13.2	64	95
OH-5	366	215.2	60	1.4	13.2	60	93
OH-5	368	215.2	60	1.6	13.8	60	78
OH-5	370	215.2	60	1.6	13.7	49	81
OH-5	372	215.2	62	1.6	14	52	84
OH-5	374	215.2	63	1.5	13.8	56	93
OH-5	376	215.3	62	1.6	14	54	89
OH-5	378	215.3	61	1.6	13.5	49	85
OH-5	380	215.3	60	1.5	13.6	45	88
OH-5	382	215.3	59	1.5	13.5	52	
OH-5	384	215.3	59	1.5	13.9	44	
OH-5	386	215.4	60	1.6	14.3	41	
OH-5	388	215.4	60	1.6	14.4	36	
OH-5	390	215.4	61	1.5	14.2	33	
OH-5	392	215.4	61	1.6	14	41	
OH-5	394	215.4	61	1.4	13.7	30	
OH-5	396	215.5	57	1.4	13.5	33	
OH-5	399	215.5	59	1.3	13.6	36	
OH-7	491	216.4	60	1.3	13.5	36	96
OH-7	493	216.4	59	1.3	13.6	55	97
OH-7	495	216.5	57	1.5	13.8	68	98
OH-7	497	216.5	59	1.4	13.3	42	98
OH-7	499	216.5	59	1.4	13.3	31	98
OH-7	501	216.5	57	1.5	13.7	29	99
OH-7	503	216.5	57	1.3	13.1	48	98
OH-7	505	216.6	58	1.6	12.8	33	97
OH-7	507	216.6	59	1.6	13.1	56	91
OH-7	509	216.6	58	1.8	12.9	32	94
OH-7	511	216.6	58	1.8	13.1	42	97
OH-7	513	216.6	58	1.8	13.3	48	99
OH-7	515	216.7	59	1.8	13.3	38	99
OH-7	517	216.7	57	1.4	12	32	94

OH-7	519	216.7	58	1.4	11.9	41	87
OH-7	521	216.7	58	1.6	12.4	50	94
OH-7	523	216.7	59	1.7	13	43	96
OH-7	525	216.8	57	1.7	13	52	99
OH-7	527	216.8	57	1.9	12.9	50	98
OH-7	529	216.8	57	1.9	13.3	47	95
OH-7	531	216.8	59	1.8	13.4	35	99
OH-7	533	216.8	58	1.8	13.4	57	99
OH-7	535	216.9	58	1.7	13.4	33	98
OH-7	537	216.9	57	1.7	13.4	35	100
OH-7	539	216.9	58	1.6	13.4	53	100
OH-7	541	216.9	59	1.8	13.6	48	97
OH-7	543	216.9	61	1.6	13.6	50	97
OH-7	545	217	59	1.3	12.9	47	97
OH-7	547	217	59	1.4	13	48	93
OH-7	549	217	58	1.2	13.5	57	99
OH-7	551	217	57	1.3	13.3	73	95
OH-7	553	217	58	1.4	13.7	48	98
OH-7	554	217	56	1.4	13.6	50	96
OH-7	556	217.1	56	1.1	12.9	60	97
OH-7	558	217.1	57	1.3	13.7	42	97
OH-7	560	217.1	55	1.2	13	33	97
OH-7	562	217.1	56	1.2	13.3	47	97
OH-7	564	217.1	57	1.1	13.2	49	95
OH-7	566	217.2	55	1.2	12.6	40	93
OH-7	568	217.2	58	1.3	13.4	32	78
OH-7	570	217.2	57	1.6	12.9	23	81
OH-7	572	217.2	57	1.4	12.8	48	84
OH-7	573	217.2	58	1	12.6	20	93
OH-7	575	217.3	58	1.1	12.3	50	89
OH-7	577	217.3	57	1.4	12.7	30	85
OH-7	579	217.3	57	1.3	13		88

Sediment color changes can yield high resolution paleoclimatic information. L* characterizes the lightness (approximately equivalent to gray scale reflectance) scaled from 0 (black) to 100 (white), a* measures the color shift from red (+60) to green (-60) and b* measures the color shift from yellow (+60) to blue (-60).

Table 3. Bulk sediments chemistry of Ohalo trench

	Depth interval (cm)	Absolute depth (m bsl)	SiO_2	Al_2O_3	Fe_2O_3	TiO_2	CaO	MgO	P_2O_5	SO_3	K_2O
OH-1	25	211.8	30	6	4.8	0.87	25	2.2	0.4	4.1	0.9
OH-1	29	211.8	26	5.4	3.8	0.79	21	1.8	0.3	3.2	0.9
OH-2	55	212.1	18	3.7	3.5	0.57	33	1.6	0.5	2.9	0.7
OH-2	73	212.2	25	5	3.2	0.75	30	2	0.5	1.7	0.8
OH-2	75	212.3	23	5.3	3.3	0.74	32.9	1.7	0.6	1.5	0.8
OH-2	77	212.3	24	5.4	4.1	0.8	32.9	1.8	0.6	1.3	0.8
OH-2	79	212.3	26	5.6	3.5	0.82	32	1.8	0.6	1.8	0.8
OH-2	81	212.3	23	5	3.6	0.72	33.7	1.7	0.5	1.8	0.7
OH-2	83	212.3	23	5	3	0.7	34.4	1.7	0.6	1.5	0.7
OH-2	85	212.4	21	4.5	3.5	0.64	35.5	1.6	0.5	1.9	0.6
OH-2	87	212.4	22	4.9	3.6	0.66	34.9	1.6	0.6	1.6	0.7
OH-2	89	212.4	22	4.9	3.5	0.66	34.8	1.6	0.6	1.6	0.7
OH-2	91	212.4	20	4.5	3.3	0.59	35.8	1.5	0.5	1.4	0.6
OH-2	93	212.4	23	5.7	3.8	0.72	32.5	1.7	0.5	1.1	0.8
OH-2	95	212.5	26	7	4.7	0.87	29.3	2	0.5	1.7	0.9
OH-2	97	212.5	16	3.9	2.7	0.48	39.1	1.2	0.3	0.9	0.5
OH-2	99	212.5	11	2.4	1.5	0.32	41	1	0.2	0.8	0.4
OH-2	102	212.5	32	7.1	4.5	0.77	27.1	1.9	0.6	0.9	1.3
OH-2	104	212.5	36	8.5	5.9	0.91	22.6	2.1	0.6	1	1.5
OH-2	107	212.6	32	7.4	6.7	0.89	26.1	2	0.5	1.5	1.2
OH-2	109	212.6	27	6	3.4	0.69	28	2	0.6	0.8	1
OH-2	111	212.6	30	6.9	3.7	0.78	28.3	1.8	0.7	1.1	1.1
OH-2	113	212.6	28	6.7	4.2	0.77	28.6	1.7	0.6	1	1.1
OH-2	115	212.7	35	8.7	5.9	0.99	22.5	2.1	0.6	1	1.5
OH-2	118	212.7	22	4.9	2.7	0.49	34.7	1.5	0.6	0.8	0.8
OH-2	120	212.7	22	4.9	2.5	0.43	34.7	1.5	0.7	0.8	0.9
OH-3	147	213.0	13	2.4	1.5	0.37	35	1.1	0.2	0.4	0.3
OH-3	183	213.3	22	4.4	2.5	0.59	35	1.6	0.3	0.5	0.7
OH-3	199	213.5	31	6.8	4.1	0.88	26	2.2	0.4	0.9	1.2
OH-3	216	213.7	25	5.5	3.3	0.69	31	2	0.5	0.4	0.8
OH-5	288	214.4	32	7.3	4.2	0.78	24	2.3	0.5	0.3	1.2

Table 4. Mineralogy of sediments from KIN2 based on XRD

Sample	Segment	Depth interval	Absolute depth	Facies	quartz	calcite	dolomite	k-felds.	plagioc.	phyllosil.	gypsum	aragonite
2248	1	0-3	213.00	mm	++	+++	+	++	++	++		
2249	1	20-23	213.20	mm	++	+++	+	+	+++	+++		
2250	1	40-43	213.40	mm	++	+++	+		++	++	+	
2251	1	60-63	213.60	mm	++	++++	+		++			
2252	1	80-83	213.80	mm	+++	++++	+	++	+	+		
2253	1	94-96.5	213.85	mm								
2254	2	0-3	213.94	mm	++	++++	+		++	++	+	
2255	2	20-23	214.00	mm								
2256	2	40-43	214.20	mm	++	+++	+		++	++		
2257	2	60-63	214.40	mm	++	+++	+		++	++		+
2258	2	80-83	214.60	mm	++	++++	+		+	++		+
2259	2	94-97	214.74	mm	++	++++	+		+	+	+	
2260	3A	0-3	214.77	mm	++	+++	+		+	+++	+	
2261	3A	20-23	215.00	lm	++	+++	+		+	+++		
2262	3A	40-43	215.20	mm	++	++++	+		+	++		
2263	3A	60-63	215.40	mm	++	+++	+	+	+	+++	+	+
2264	3A	80-83	215.60	mm	++	+++	+		++	+++	+	+
2265	3A	86-89	215.66	mm	++	+++	+	+	+	+++		
2266	3B	0-3	215.69	mm	++	++++	+		++	++	+	
2267	3B	20-23	215.90	mm	++	+++	+	++		+++	++	
2268	3B	40-43	216.10	lm	++	+++	+	+	++	+++	+	
2269	3B	60-63	216.30	lm	++	++++	+		+	+		
2270	3B	80-83	216.50	lm	++	+++	+		+	+++	+	
2271	3B	100-103	216.55	lm	++	++++	+		+	+++	+	+
2272	4A	0-3	216.70	lm	++	++++	+		+	++	+	+
2273	4A	20-23	216.75	lm	++	+++			+	+++	+	
2274	4A	40-43	216.95	lm	++	+++			++	+++	+	+
2275	4A	60-63	217.15	lm	++	+++		+	+	+++	+	+
2276	4A	71-74	217.25	mm	++	++++			+	+++	+	
2277	4B	0-3	217.30	mm	++	++++			+	+++	+	+
2278	4B	20-23	217.50	lm								

2279	4B	40-43	217.70	lm	++	+++	+	+	+	+++	+	
2280	4B	60-63	217.90	lm	++	+++		+	++	+++		
2281	4B	80-83	218.10	lm	++	++++			+	+++		
2282	4B	100-103	218.30	lm	++	+++	+		+	+++		
2283	5A	0-3	218.35	lm								
2284	5A	20-23	218.55	lm	++	+++	+		+	+++	+	
2285	5A	40-43	218.75	mm	++	+++			+	+++	++	
2286	5A	60-63	218.95	mm								
2287	5A	67-70	219.00	mm								
2288	5B	0-3	219.05	lm								
2289	5B	20-23	219.25	mm								
2290	5B	40-43	219.45	lm	++	+	+		++	+++	+	
2291	5B	60-63	219.65	lm	++	+++	+	+		+++	+	+
2292	5B	80-83	219.85	lm	++	+++	+		+	+++	+	
2293	5B	95-98	220.00	lm	++	+++	+		++	+++		
2294	6A	0-3	220.05	lm	++	+++	++	++	++	++		+
2295	6A	20-23	220.25	mm								
2296	6A	40-43	220.45	lm								
2297	6A	60-63	220.65	lm	++	+++	+		+	+++		
2298	6A	80-83	220.85	lm	++	+++	+		+	++++	+	
2299	6A	92-95	220.95	lm	++	+++			++	++		
2300	6B	0-3	221.00	lm	++	++++	+	++		++		+
2301	6B	20-23	221.20	mm	++	++++	+	+++				
2302	6B	35-38	221.35	mm	++	+++	+		+	+++		

+	less than 5%
++	5-25%
+++	25-50%
++++	more than 50%
mm	massive marls
lm	laminated marls

Table 5. Color index, carbonate content, mode value of grain size and percent of fine sediments (smaller than 63 μm) in bulk sediments from KIN2 borehole.

Sample	Segment	Depth interval	Absolute depth	L*	a*	b*	%carbonate	Calculated %carbonate*	Grain size mode (μm)	%<63μm
2248	1	0-3	213.00	52.3	3.3	14.8	58	40	23	92
2249	1	20-23	213.20	53.5	2.3	13.5	54	38		91
2250	1	40-43	213.40	55.0	2.5	14.2	65	44		89
2251	1	60-63	213.60	50.5	2.2	13.5	61	42	45	54
2252	1	80-83	213.80	51.1	2.7	14.2	58	40		66
2253	1	94-96.5	213.85	51.6	2.8	14.5	55	38		62
2254	2	0-3	213.94	48.7	2.5	13.1	62	43	31	71
2255	2	20-23	214.00	52.2	2.7	13.8	60	41		86
2256	2	40-43	214.20	52.4	2.4	13.6	64	43		73
2257	2	60-63	214.40	59.7	2.3	10.1	70	47	9.4	74
2258	2	80-83	214.60	59.0	1.7	14.1	74	49	6.1	87
2259	2	94-97	214.74	51.2	2.1	12.9	48	34		98
2260	3A	0-3	214.77	57.1	1.0	9.6	45	33	9.4	98
2261	3A	20-23	215.00	51.0	1.8	12.3	53	37		100
2262	3A	40-43	215.20	54.0	2.2	12.4	71	48		99
2263	3A	60-63	215.40	54.5	2.1	14.0	32	25	23	94
2264	3A	80-83	215.60	48.0	2.7	14.1	28	23		97
2265	3A	86-89	215.66	54.4	2.0	13.5	44	32		90
2266	3B	0-3	215.69	55.7	1.6	12.7	41	30	7.6	91
2267	3B	20-23	215.90	52.9	2.0	13.9	31	25		97
2268	3B	40-43	216.10	53.3	2.2	15.1	38	29		98
2269	3B	60-63	216.30	59.0	1.8	13.9	51	36	7.7	93
2270	3B	80-83	216.50	50.2	2.1	13.4	20	18		98
2271	3B	100-103	216.55	55.8	1.7	12.1	71	47		97
2272	4A	0-3	216.70	55.7	1.6	13.1	59	41	7.4	93
2273	4A	20-23	216.75	58.6	0.9	12.6	57	40		97
2274	4A	40-43	216.95	59.6	3.0	14.7	50	36		94
2275	4A	60-63	217.15	56.2	2.5	13.0	41	30	8.2	99
2276	4A	71-74	217.25	60.7	2.4	13.0	44	32		98
2277	4B	0-3	217.30	61.2	2.8	13.8	67	45		100
2278	4B	20-23	217.50	42.5	4.3	15.1	34	26	6.2	97
2279	4B	40-43	217.70	55.2	1.9	11.6	41	30		98
2280	4B	60-63	217.90	48.3	2.3	12.9	42	31		97
2281	4B	80-83	218.10	59.3	1.9	9.9	55	38	7.1	99
2282	4B	100-103	218.30	58.7	2.1	12.5	45	33		99
2283	5A	0-3	218.35	60.0	2.3	13.8	34	26		96
2284	5A	20-23	218.55	48.5	1.5	11.6	26	21	6.1	95
2285	5A	40-43	218.75	51.5	3.0	15.3	47	34		95
2286	5A	60-63	218.95	54.0	2.7	14.7	53	37		93
2287	5A	67-70	219.00	56.8	2.3	11.4	56	39	5.7	96
2288	5B	0-3	219.05	55.0	2.6	14.0	44	32		94
2289	5B	20-23	219.25	58.3	2.3	11.8	63	43		98
2290	5B	40-43	219.45	59.0	2.4	11.9	53	37	5.6	99
2291	5B	60-63	219.65	61.3	2.3	11.5	39	29		99
2292	5B	80-83	219.85	52.0	0.9	13.6	29	23		96
2293	5B	95-98	220.00	59.7	0.3	9.1	31	24	5.6	97
2294	6A	0-3	220.05	45.5	2.8	14.2	45	33		95

2295	6A	20-23	220.25	56.0	2.6	13.3	55	38		98
2296	6A	40-43	220.45	61.4	2.6	13.9	44	32	5.7	97
2297	6A	60-63	220.65	50.3	2.1	14.0	58	40		99
2298	6A	80-83	220.85	67.3	0.1	12.3	30	24		95
2299	6A	92-95	220.95	53.6	1.7	13.6	79	52	5.2	58
2300	6B	0-3	221.00	59.6	1.7	11.6	71	47		81
2301	6B	20-23	221.20	64.1	1.4	13.4	42	31		90
2302	6B	35-38	221.35	62.6	1.2	13.6	41	31	23	97

Sediment color changes can yield high resolution paleoclimatic information. L* characterizes the lightness (approximately equivalent to gray scale reflectance) scaled from 0 (black) to 100 (white), a* measures the color shift from red (+60) to green (-60) and b* measures the color shift from yellow (+60) to blue (-60).

* Calculated carbonate content based on measured CaO in bulk sediments and calibration according to: calculated carbonate = measured carbonate * 1.73 – 11.3

Table 6. Chemistry of bulk sediments from KIN2

Sample	Segment	Depth interval	Absolute depth	SiO_2	Al_2O_3	Fe_2O_3	TiO_2	CaO	MgO	P_2O_5	SO_3	K_2O
		(cm)	(m bsl)	mg/L	mg/L	mg/L	mg/L	mg/L	mg/L	mg/L	mg/L	mg/L
2248	1	0-3	213.00	28	6.1	3.7	0.76	29.2	1.8	0.6	2.4	0.8
2249	1	20-23	213.20	30	6.1	4.0	0.77	27.7	1.7	0.6	3.5	0.9
2259	2	94-97	214.74	30	6.8	4.5	0.7	26.8	1.9	0.7	2.3	1.1
2260	3A	0-3	214.77	36	8.1	5.3	0.89	21.8	2.3	0.6	2.6	1.3
2261	3A	20-23	215.00	32	7.6	4.5	0.77	25.3	2.1	0.6	1.3	1.3
2270	3B	80-83	216.50	40	9.6	6.1	0.96	16.7	2.5	0.6	4.8	1.4
2271	3B	100-103	216.55	22	5.3	3.8	0.54	31.8	2.1	0.7	4.0	0.8
2272	4A	0-3	216.70	24	5.4	4.3	0.63	31.3	1.8	0.6	2.9	0.7
2281	4B	80-83	218.10	28	7.9	9.1	0.73	26.4	2.0	0.8	1.0	1.3
2282	4B	100-103	218.30	35	8.7	4.3	1.01	22.3	2.1	0.6	0.9	1.4
2292	5B	80-83	219.85	34	8.6	7.1	0.85	20.2	2.3	0.7	6.2	1.3
2293	5B	95-98	220.00	33	8.1	4.7	0.81	23.1	2.1	0.7	2.5	1.2
2294	6A	0-3	220.05	31	7.0	6.4	0.79	23.0	1.9	0.7	4.7	1.0
2301	6B	20-23	221.20	32	7.4	4.2	0.84	26.3	2.1	0.6	0.81	1.1
2302	6B	35-38	221.35	32	7.4	4.2	0.84	26.3	2.1	0.6	2.2	1.1

Table 7. Mineralogy of sediments from SOG2 based on XRD

Depth in the core (cm)	Absolute depth (m bsl)	Facies	quartz	calcite	dolomite	Phyllosil.	k-felds	Plagioc.	aragonite	gypsum
280	226.80	mm	++	++++				++		++
280	226.80	mm	++	+++	+	++		+	+	+
339	227.39	mm	++	+++	+	++		++		
442	228.42	mm	++	++	+	++	++	++		
565	229.65	mm	++	++	+	++		+		+
581	229.81	mm	++	++++				++	+	++
623	230.23	mm	+	++++						++
665	230.65	mm	++	++	+	++	++	++		
800	232.00	mm	++	++	++	+++	++	+		
866	232.66	mm	++	+++	+	++	+	+		
910	233.10	mm	++	++++	+		+	++		+
992	233.92	mm	++	+++	+	+++				

+	less than 5%
++	5-25%
+++	25-50%
++++	more than 50%
mm	massive marls
lm	laminated marls

Table 8. Color index, carbonate content and percent of fine sediments (smaller than 63 μm) in bulk sediments from SOG2

Depth in the core (cm)	Absolute depth (m bsl)	L*	a*	b*	%carbonate	Grain size mode (μm)	%<63μm
204	226.04	54.51	1.45	11.16	61.5	42.9	27.2
209	226.09	58.97	1.97	11.23	61.6		51.0
218	226.18	58.73	1.80	10.57	68.6	15.5	96.4
235	226.35	52.95	1.64	10.87	33.5		99.0
242	226.42	51.70	1.52	10.99	40.4		98.2
280	226.80	58.88	2.44	12.99	55.6	13.4	94.9
304	227.04	67.03	2.08	11.70	45.6		98.7
314	227.14	53.97	1.22	11.47	62.0	10.8	99.2
323	227.23	58.15	3.25	14.64	56.8		98.8
339	227.39	56.81	2.04	12.21	69.6		76.7
371	227.71	54.98	0.78	113.37	56.9		95.8
381	227.81	56.02	1.84	10.89	46.4		96.7
389	227.89	58.82	2.30	11.45	24.7		92.1
400	228.00	54.72	2.03	11.55	27.0	12.1	96.8
409	228.09	56.50	1.09	12.82	23.8		98.2
422	228.22	50.99	2.50	10.62	22.9		97.9
442	228.42	47.18	3.59	17.23	41.7		94.6
486	228.86	51.32	3.47	16.85	32.1	9.07	93.4
500	229.00	52.88	2.15	12.06	33.2	8.59	98.6
513	229.13	52.43	3.20	13.09	30.1	8.14	97.5
527	229.27	54.55	2.54	12.53	33.1		96.8
537	229.37	52.79	2.73	13.71	28.0		98.9
556	229.56	52.02	2.82	14.54	33.7	10.9	97.6
565	229.65	51.95	2.86	10.66	34.2		96.7
581	229.81	44.42	2.83	11.39	27.7	12.3	94.6
623	230.23	48.16	2.94	17.30	46.1	19.2	93.4
633	230.33	42.93	3.64	15.17	38.4		98.2
644	230.44	56.61	2.85	13.39	39.3		99.7
654	230.54	51.01	4.35	18.35	52.0		98.5
665	230.65	53.72	3.92	16.94	40.8	19.2	95.2
676	230.76	51.40	5.12	18.45	32.0		96.0
687	230.87	54.72	2.51	13.24	38.2		97.9
722	231.22	54.37	3.61	14.76	40.9	9.55	96.3
743	231.43	55.96	2.75	14.34	52.1		98.8
751	231.51	48.21	4.38	17.08	41.4		94.4

769	231.69	46.94	3.29	15.41	40.4	9.95	98.0
780	231.80	42.45	3.04	14.86	37.1		93.3
792	231.92	52.64	3.16	13.91	35.7		97.5
800	232.00	48.40	2.32	12.09	24.1	8.25	96.0
822	232.22	41.77	4.07	16.94	25.4		95.6
836	232.36	52.75	5.09	19.36	31.4		97.9
850	232.50	51.11	2.48	12.03	29.7	4.15	96.8
866	232.66	51.04	1.97	12.15	37.8		92.5
882	232.82	50.93	3.72	16.92	27.6		96.7
900	233.00	45.00	3.98	14.19	31.3		96.1
910	233.10	50.24	3.28	15.55	35.8		90.6
922	233.22	54.83	3.41	13.44	35.0		95.4
933	233.33	54.20	4.12	13.94	31.7	11.4	91.6
950	233.50	55.07	4.32	15.83	34.1		93.8
961	233.61	48.19	3.10	15.61	35.2		92.3
973	233.73	59.23	2.76	12.24	39.1		98.3
981	233.81	59.58	2.16	12.67	27.4		96.4
992	233.92	47.84	2.25	9.83	31.0	21.1	92.0

Sediment color changes can yield high resolution paleoclimatic information. L* characterizes the lightness (approximately equivalent to gray scale reflectance) scaled from 0 (black) to 100 (white), a* measures the color shift from red (+60) to green (-60) and b* measures the color shift from yellow (+60) to blue (-60).

Table 9. Mineralogy of sediments from SOG3 based on XRD

Depth in the core (cm)	Absolute depth (m bsl)	Facies	calcite	quartz	Plagioc.	Phyllosil.	k-felds.	gypsum	dolomite	aragonite
222	231.22	mm	++	++	+++	++	+		++	
262	231.62	mm	++	+++	++	+++	++		++	
364	232.64	mm	++	++	+	+++	+		+	+
534	232.54	mm	++	++		+++		+	+	
673	235.73	mm	++++	+	+			++		
673	235.73	mm	+++	++		+++		+	+	
693	235.93	mm	++++	++						
773	236.73	mm	+++	+++		++	++		+	
818	237.18	mm	++++	++		+++			++	

+	less than 5%
++	5-25%
+++	25-50%
++++	more than 50%
mm	massive marls
lm	laminated marls

Table 10. Color inder, carbonate content, mode value of grain size and percent of fine sediments (smaller than 63 μm) in bulk sediments from SOG3

Depth in the core (cm)	Absolute depth (m bsl)	L*	a*	b*	%carbonate	Grain size mode (μm)	%<63μm
121	230.21	58.23	5.39	19.61	69.5	16.3	97.3
134	230.34	48.83	6.88	19.93	20.6		92.9
143	230.43	52.76	3.26	14.70	16.4		90.3
154	230.54	51.24	5.33	17.54	44.4	18.3	95.0
166	230.66	46.40	8.70	21.76	38.8		99.2
174	230.74	47.92	4.73	15.38	51.5	24.5	91.6
184	230.84	47.57	5.22	15.63	35.1		96.3
194	230.94	50.87	4.01	15.06	50.5		95.8
222	231.22	50.53	3.99	15.31	18.3	14.8	88.7
233	231.33	40.69	7.06	19.21	20.3		98.3
243	231.43	43.40	7.82	20.36	33.0		87.6
252	231.52	42.53	6.65	18.32	29.3		99.0
262	231.62	40.87	5.80	16.76	11.3		99.1
272	231.72	36.41	4.63	13.20	35.0	15.0	97.0
282	231.82	46.68	7.26	20.37	25.5		99.1
292	231.92	51.89	4.06	13.88	44.0		89.7
323	232.23	42.17	8.80	18.71	14.6		98.9
333	232.33	47.51	3.60	10.82	15.5	21.6	97.9
344	232.44	42.83	8.08	19.93	23.3		98.8
354	232.54	39.27	8.34	18.28	10.7		99.9
364	232.64	40.90	6.87	18.03	18.8	13.4	92.4
374	232.74	47.61	4.38	13.08	32.3		97.4
384	232.84	38.73	3.64	10.08	19.5		94.5
393	232.93	46.16	8.86	20.29	32.7		91.6
423	233.23	33.51	5.32	13.40	16.8		99.0
433	233.33	40.92	5.69	13.99	24.4		94.1
443	233.43	47.27	6.92	20.00	33.9	11.5	97.6
452	233.52	49.92	4.22	13.45	24.5		97.3
463	233.63	41.33	6.59	16.02	17.6		90.8
473	233.73	49.80	2.77	12.91	8.3		82.9
482	233.82	48.30	1.37	11.43	28.3	14.0	97.4
492	233.92	53.15	0.38	7.64	26.2		97.2
516	234.16	46.87	3.51	13.01	21.9		91.8
523	234.23	46.34	6.86	17.62	23.4		88.8
534	234.34	43.29	5.88	17.02	26.0	17.6	94.0

544	234.44	40.02	6.43	16.77	27.2		95.5
554	234.54	41.34	6.16	16.49	17.5		94.1
563	234.63	45.45	4.18	14.21	18.9		98.0
573	234.73	49.13	4.62	13.48	17.5		94.4
583	234.83	46.54	0.73	7.45	13.5		91.4
593	234.93	42.03	1.46	9.96	17.1	14.6	94.6
646	235.46	46.35	3.36	13.50	31.8		94.4
653	235.53	48.96	3.87	14.41	39.9		83.6
663	235.63	48.84	1.99	10.61	47.7	4.17	88.8
673	235.73	51.87	1.53	10.91	65.6		87.2
683	235.83	54.33	1.04	9.92	78.5		87.2
693	235.93	60.15	3.39	15.06	70.5	3.36	83.0
760	236.6	52.49	1.90	11.69	63.6	4.25	88.9
773	236.73	55.97	3.76	15.77	67.2		79.3
782	236.82	51.98	4.11	18.00	60.8	3.88	77.0
792	236.92	50.58	4.55	18.68	50.3		81.3
818	237.18	59.20	1.62	7.53	66.5		85.4
828	237.28	48.93	4.16	14.47	68.5		79.4
838	237.38	46.69	6.81	17.99	55.6		75.9
843	237.43	52.24	3.56	14.69	59.5		74.3

Sediment color changes can yield high resolution paleoclimatic information. L* characterizes the lightness (approximately equivalent to gray scale reflectance) scaled from 0 (black) to 100 (white), a* measures the color shift from red (+60) to green (-60) and b* measures the color shift from yellow (+60) to blue (-60).

Table 11. Sr/Ca, Mg/Ca, $\delta^{18}O$, $\delta^{13}C$ and $^{87}Sr/^{86}Sr$ in ostracods from Ohalo trench (OH)

	Depth in the core (cm)	Absolute depth (m bsl)	Mg/Ca (eq)	Sr/Ca(eq)	$\delta^{13}C$	$\delta^{18}O$	$^{87}Sr/^{86}Sr$
OH-1	9	211.6	0.0096	0.0020			
OH-1	25	211.8	0.0205	0.0020	-7.78	-3.97*	0.70802
OH-1	25	211.8	0.0140	0.0020			
OH-1	25	211.8	0.0134	0.0020			
OH-1	25	211.8	0.0192	0.0020			
OH-1	25	211.8	0.0133	0.0020			
OH-1	29	211.8	0.0157	0.0025			
OH-1	31	211.8	0.0159	0.0021			
OH-1	34	211.8	0.0122	0.0018			
OH-1	36	211.9	0.0173	0.0023			
OH-2	41	211.9	0.0169	0.0026	-7.08	-3.33*	
OH-2	43	211.9	0.0193	0.0022	-7.04	-3.93*	
OH-2	47	212.0	0.0229	0.0025	-6.43	-3.72*	
OH-2	49	212.0	0.0179	0.0028			
OH-2	51	212.0	0.0148	0.0022	-6.91	-3.17*	
OH-2	51	212.0	0.0172	0.0024			
OH-2	55	212.1	0.0222	0.0020	-6.96	-3.58*	0.70799
OH-2	59	212.1	0.0175	0.0023	-6.84	-3.66*	0.70801
OH-2	61	212.1	0.0153	0.0025			
OH-2	61	212.1	0.0157	0.0025			
OH-2	61	212.1	0.0154	0.0025			
OH-2	61	212.1	0.0138	0.0023	-7.14	-2.96*	0.70801
OH-2	63	212.1	0.0171	0.0025	-7.77	-3.56*	0.70796
OH-2	65	212.2	0.0160	0.0024	-7.64	-3.98*	0.70799
OH-2	65	212.2	0.0164	0.0026			
OH-2	65	212.2	0.0139	0.0022			
OH-2	65	212.2	0.0144	0.0025			
OH-2	65	212.2	0.0142	0.0025			
OH-2	65	212.2	0.0124	0.0025			
OH-2	67	212.2	0.0126	0.0025			
OH-2	71	212.2	0.0136	0.0024			
OH-2	73	212.2	0.0165	0.0026	-7.44	-3.99*	
OH-2	77	212.3	0.0170	0.0024	-7.56	-3.48*	
OH-2	79	212.3	0.0151	0.0023	-7.27	-3.58*	
OH-2	81	212.3	0.0162	0.0023	-7.27	-3.58*	
OH-2	85	212.4	0.0250	0.0022	-7.44	-3.26*	
OH-2	89	212.4	0.0196	0.0024	-7.12	-3.74*	

OH-2	95	212.5	0.0154	0.0028			
OH-2	99	212.5	0.0241	0.0027	-7.24	-3.69*	
OH-2	102	212.5	0.0121	0.0028			
OH-2	107	212.6	0.0169	0.0025	-7.83	-3.36*	
OH-2	109	212.6	0.0153	0.0025	-7.36	-3.12*	0.70815
OH-2	113	212.6	0.0155	0.0025			0.70798
OH-2	115	212.7	0.0156	0.0024			0.70807
OH-2	118	212.7	0.0159	0.0022	-6.72	-3.45*	0.70803
OH-2	122	212.7	0.0154	0.0023			0.70798
OH-2	122	212.7	0.0145	0.0024			
OH-2	126	212.8	0.0160	0.0023	-7.26	-2.84	
OH-2	128	212.8	0.0148	0.0023	-6.72	-1.97	0.70798
OH-2	130	212.8	0.0114	0.0023	-7.64	-2.24	
OH-2	132	212.8	0.0143	0.0024	-7.75	-2.60	0.70802
OH-2	134	212.8	0.0117	0.0023	-6.77	-1.97	
OH-3	127	212.8	0.0144	0.0026			
OH-3	130	212.8	0.0163	0.0025			
OH-3	136	212.9	0.0151	0.0025			
OH-3	136	212.9	0.0176	0.0024			
OH-3	139	212.9	0.0135	0.0024			
OH-3	143	212.9	0.0143	0.0028			
OH-3	145	213.0	0.0168	0.0024			
OH-3	147	213.0	0.0165	0.0025	-8.08	-3.35	0.70798
OH-3	151	213.0	0.0165	0.0023			
OH-3	155	213.1	0.0148	0.0023			
OH-3	157	213.1	0.0211	0.0024			
OH-3	159	213.1	0.0159	0.0023			
OH-3	161	213.1	0.0125	0.0023	-7.55	-2.88	
OH-3	163	213.1	0.0132	0.0024	-7.93	-2.85	0.70805
OH-3	168	213.2	0.0135	0.0021	-7.81	-2.06	
OH-3	173	213.2	0.0107	0.0021	-8.54	-2.16	
OH-3	175	213.3	0.0161	0.0023	-7.90	-2.78	0.70805
OH-3	179	213.3	0.0126	0.0023	-6.72	-2.62	
OH-3	183	213.3	0.0146	0.0024	-7.07	-2.28	0.70796
OH-3	183	213.3	0.0176	0.0025			
OH-3	183	213.3	0.0156	0.0025			
OH-3	183	213.3	0.0183	0.0023			
OH-3	183	213.3	0.0175	0.0028			
OH-3	183	213.3	0.0145	0.0028			
OH-3	185	213.4	0.0137	0.0024	-6.83	-1.83	
OH-3	187	213.4	0.0129	0.0024	-7.13	-2.29	

OH-3	190	213.4	0.0189	0.0023	-7.24	-2.41	0.70805
OH-3	194	213.4	0.0125	0.0025			
OH-3	196	213.5	0.0155	0.0024			
OH-3	199	213.5	0.0146	0.0025	-8.00	-2.85	
OH-3	201	213.5	0.0131	0.0026			0.70795
OH-3	203	213.5	0.0113	0.0026			
OH-3	205	213.6	0.0148	0.0027			
OH-3	219	213.7	0.0129	0.0030			
OH-4	224	213.7	0.0220	0.0024	-9.04	-2.32	0.70798
OH-4	236	213.9	0.0234	0.0023	-7.48	-3.23	0.70792
OH-4	238	213.9	0.0154	0.0025			0.70800
OH-4	244	213.9	0.0193	0.0023	-8.06	-2.6	0.70795
OH-4	248	214.0	0.0163	0.0025			0.70792
OH-4	256	214.1	0.0178	0.0021	-8.35	-2.6	0.70800
OH-4	258	214.1	0.0154	0.0022			0.70812
OH-4	260	214.1	0.0184	0.0021	-7.62	-2.72	
OH-4	264	214.1	0.0163	0.0023	-7.67	-2.08	0.70794
OH-4	267	214.2	0.0159	0.0022	-7.19	-2.31	0.70795
OH-4	270	214.2	0.0156	0.0025	-7.31	-2.03	0.70796
OH-4	272	214.2	0.0159	0.0022			0.70797
OH-4	276	214.3	0.0118	0.0024			0.70802
OH-4	280	214.3	0.0098	0.0021	-9.23	-2.01	0.70802
OH-4	284	214.3	0.0133	0.0021	-8.36	-2.05	0.70803
OH-5	292	214.4	0.0075	0.0021			0.70804
OH-5	307	214.6	0.0125	0.0027			0.70792
OH-5	319	214.7	0.0129	0.0030	-7.80	-2.72	0.70789
OH-5	321	214.7	0.0144	0.0026			0.70793
OH-5	323	214.7	0.0158	0.0030			0.70792
OH-5	335	214.9	0.0147	0.0026			
OH-5	343	214.9	0.0147	0.0027	-8.05	-2.53	0.70796
OH-5	345	215.0	0.0164	0.0027	-8.08	-2.45	0.70796
OH-5	346	215.0	0.0149	0.0021			
OH-5	347	215.0	0.0149	0.0021	-7.65	-2.70	0.70799
KIN2	2257	213.8	0.0142	0.0022			0.70801
KIN2	2258	214.0	0.0164	0.0023			0.70805

The unmarked samples were measured at the Geological Survey of Israel

Table 12. Sr/Ca, Mg/Ca, $\delta^{13}C$, $\delta^{18}O$ and $^{87}Sr/^{86}Sr$ in ostracods from SOG2

Depth in the core (cm)	Absolute depth (m bsl)	Mg/Ca (eq)	Sr/Ca (eq)	$\delta^{13}C$	$\delta^{18}O$	$^{87}Sr/^{86}Sr$
204	226.04	0.0087	0.0039	-6.74	-1.66	0.70774
204	226.04	0.0113	0.0037	-6.56	-2.50	0.70775
204	226.04	0.0118	0.0030			0.70778
209	226.09	0.0081	0.0033			0.70771
209	226.09	0.0069	0.0034			0.70774
218	226.18	0.0127	0.0020	-9.08	-2.60	0.70798
280	226.80	0.0116	0.0018	-8.94	-1.77	
290	226.90	0.0198	0.0017			
304	227.04	0.0170	0.0016			0.70807
339	227.39			-7.79	-2.82	
381	227.81	0.0128	0.0020	-8.67	-1.98	0.70806
389	227.89	0.0132	0.0020	-7.43	-2.11	
473	228.73	0.0124	0.0020	-10.33	-1.92	0.70800
513	229.13	0.0166	0.0020			
556	229.56	0.0173	0.0019	-10.92	-1.82	
565	229.65	0.0105	0.0019			0.70804
581	229.81	0.0115	0.0019	-11.35	-3.52	0.70807
623	230.23	0.0148	0.0020			0.70782
792	231.92			-11.11	-2.79	
910	233.10	0.0136	0.0024	-9.60	-3.93	0.70785
922	233.22	0.0117	0.0022			0.70791
950	233.50	0.0152	0.0025			
961	233.61	0.0146	0.0022			

Table 13. Sr/Ca, Mg/Ca, $\delta^{13}C$, $\delta^{18}O$ and $^{87}Sr/^{86}Sr$ in ostracods from SOG3

Depth in the core (cm)	Absolute depth (m bsl)	Mg/Ca (eq)	Sr/Ca (eq)	$^{87}Sr/^{86}Sr$
121	230.21	0.0075	0.0052	0.70768
154	230.54	0.0084	0.0052	0.70766
174	230.74	0.0094	0.0047	0.70765
184	230.84	0.0084	0.0055	0.70766
194	230.94	0.0070	0.0054	0.70765
222	231.22	0.0073	0.0053	
292	231.92	0.0066	0.0055	0.70769
443	233.43	0.013	0.0058	
452	233.52	0.0080	0.0055	0.70773
653	235.53	0.010	0.0044	

Table 14. Sr/Ca, Mg/Ca, $\delta^{13}C$, $\delta^{18}O$ and $^{87}Sr/^{86}Sr$ in bulk carbonate from OH7

Depth in the core (cm)	Absolute depth (m bsl)	Mg/Ca (eq)	Sr/Ca (eq)	$\delta^{13}C$	$\delta^{18}O$	$^{87}Sr/^{86}Sr$
411	215.61	0.053	0.00126	–1.06	–3.86	0.70779
421	215.71	0.093	0.00121	–2.10	–3.29	0.70767
429	215.79	0.074	0.00122	–2.04	–3.82	0.70774
434	215.84	0.046	0.00121	–0.80	–3.60	0.70792
444	215.94	0.037	0.00123	–1.32	–3.48	0.70776
450	216.00	0.057	0.00124	–1.77	–3.30	0.70773
460	216.10	0.045	0.00130	–2.51	–3.89	0.70775
466	216.16	0.036	0.00126	–1.46	–3.17	0.70775
472	216.22	0.026	0.00128	–1.41	–3.07	0.70775
480	216.30	0.033	0.00131	–0.62	–3.49	0.70776
486	216.35	0.058	0.00130	–1.60	–3.78	0.70775

Table 15. Sr/Ca, Mg/Ca, $\delta^{13}C$, $\delta^{18}O$ and $^{87}Sr/^{86}Sr$ in bulk carbonate from KIN2

Sample	Segment	Depth interval	Absolute depth	Mg/Ca	Sr/Ca	$\delta^{13}C$	$\delta^{18}O$	$^{87}Sr/^{86}Sr$
		(cm)	(m bsl)	(eq)	(eq)			
2248	1	0-3	213.00	0.033	0.0013	-2.4	-5.67	0.70787
2249	1	20-23	213.20	0.031	0.0014			0.70780
2250	1	40-43	213.40	0.039	0.0013			0.70776
2251	1	60-63	213.60	0.031	0.0012	-1.8	-5.22	0.70784
2252	1	80-83	213.80	0.029	0.0013			0.70777
2253	1	94-96.5	213.85	0.029	0.0013			0.70779
2254	2	0-3	213.94	0.032	0.0012	-1.84	-4.67	0.70781
2255	2	20-23	214.00	0.028	0.0013			0.70777
2256	2	40-43	214.20	0.024	0.0021			0.70784
2257	2	60-63	214.40	0.026	0.0022	-1.14	-3.23	0.70776
2258	2	80-83	214.60	0.046	0.0013	-1.79	-4.93	0.70776
2259	2	94-97	214.74	0.039	0.0014			0.70779
2260	3A	0-3	214.77	0.043	0.0015	-1.26	-3.79	0.70773
2261	3A	20-23	215.00	0.044	0.0015			0.70777
2262	3A	40-43	215.20	0.047	0.0013			0.70779
2263	3A	60-63	215.40	0.036	0.0012	-0.17	-2.9	0.70779
2264	3A	80-83	215.60	0.086	0.0013			0.70774
2265	3A	86-89	215.66	0.064	0.0014			0.70778
2266	3B	0-3	215.69	0.031	0.0013	-2.06	-4.91	0.70775
2267	3B	20-23	215.90	0.072	0.0014			0.70779
2268	3B	40-43	216.10	0.044	0.0014			0.70779
2269	3B	60-63	216.30	0.057	0.0014	-2.29	-5.14	0.70773
2270	3B	80-83	216.50	0.049	0.0013			0.70783
2271	3B	100-103	216.55	0.047	0.0014			0.70779
2272	4A	0-3	216.70	0.023	0.0013	-1.68	-4.22	0.70774
2273	4A	20-23	216.75	0.053	0.0014			0.70777
2274	4A	40-43	216.95	0.042	0.0014			0.70796
2275	4A	60-63	217.15	0.049	0.0013	-1.88	-4.93	0.70776
2276	4A	71-74	217.25	0.035	0.0015			0.70782
2277	4B	0-3	217.30	0.036	0.0015			0.70778
2278	4B	20-23	217.50	0.071	0.0013	-2.14	-4.58	0.70775
2279	4B	40-43	217.70	0.047	0.0014			0.70775
2280	4B	60-63	217.90	0.042	0.0014			0.70776
2281	4B	80-83	218.10	0.029	0.0013	-1.65	-3.44	0.70772
2282	4B	100-103	218.30	0.037	0.0014			0.70776
2283	5A	0-3	218.35	0.042	0.0015			0.70777
2284	5A	20-23	218.55	0.042	0.0014	-2.25	-4.44	0.70777
2285	5A	40-43	218.75	0.035	0.0014			0.70777
2286	5A	60-63	218.95	0.042	0.0014			0.70778
2287	5A	67-70	219.00	0.046	0.0014	-2.39	-4.15	0.70778
2288	5B	0-3	219.05	0.049	0.0014			0.70781
2289	5B	20-23	219.25	0.046	0.0014			0.70774
2290	5B	40-43	219.45	0.051	0.0014	-2.08	-5.03	0.70778
2291	5B	60-63	219.65	0.05	0.0014			0.70774

2292	5B	80-83	219.85	0.057	0.0015			0.70775
2293	5B	95-98	220.00	0.068	0.0014	-1.77	-5.35	0.70777
2294	6A	0-3	220.05	0.088	0.0014			0.70773
2295	6A	20-23	220.25	0.047	0.0015			0.70778
2296	6A	40-43	220.45	0.047	0.0014	-1.53	-4.61	0.70789
2297	6A	60-63	220.65	0.058	0.0015			0.70771
2298	6A	80-83	220.85	0.036	0.0015			0.70774
2299	6A	92-95	220.95	0.077	0.0014	-2.58	-5.51	0.70779
2300	6B	0-3	221.00	0.129	0.0015			0.70772
2301	6B	20-23	221.20	0.028	0.002			0.70786
2302	6B	35-38	221.35	0.025	0.0016	-4.73	-8.44	0.70780
2303	6B	50-53	221.50	0.031	0.0014			0.70775
2304	6B	70-73	221.70	0.037	0.0014			0.70773

תקופת הגלציאל בין 27 ל- 25 אלפי שנים לפני היום היתה תקופה רטובה באיזור אגם הכינרת. מפלס האגם היה גבוה (~170 מטרים מתחת לפני הים) והאגם היה מחובר לאגם הליסן בדרום. בהתבסס על כימיה ויחסים איזוטופים של קרבונטים ניתן להסיק כי תרומת המעיינות לאגם היתה גבוהה בתקופת המפלס הגבוה. בניגוד לתנאים באיזור הכינרת, תנאי יובש קיצוניים שררו באיזור מדבר סהרה. בהתבסס על גודל גרגר נראה בסבירות גבוהה כי המרכיב הדטריטי הגיע ממרחק רב, ככל הנראה מהסהרה אל אגם הכינרת.

הנפילה במפלס האגם בין השנים 24 ו- 20 אלף שנים לפני היום קשורה לעליה ביובש באיזור, במהלך ולאחר אירוע היינריך (H2), שהיה אירוע קור בצפון האטלנטי. ירידה של 2‰ בערכי $\delta^{18}O$ בסוף האירוע נמצאת בהתאמה לשינוי בהרכב המים במזרח הים התיכון – מקור המשקעים בתקופה. הדבר מצביע על כך שמקורות המים באיזור החוף באוהלו היו מושפעים בעיקר מהנגר העילי. במהלך התקופה שלאחר המפלס הגבוה, נראה כי תנאים יבשים שררו באיזור, שמקורם ברמה ברומטרית ושקע מעל הים האדום. אלה הם הגורמים לרוחות מזרחיות המביאות אבק לכינרת ממדבריות ערב. בחינה של Fe_2O_3 כנגד Al_2O_3 מצביעה גם היא על כך שהאבק הוסע מרחק קצר יותר וכתוצאה מכך נגרם פחות סינון של חומר קרבונטי מהאבק. מספרים גבוהים של אוסטרקודים, בעיקר *Cyprideis torosa* ופורמיניפרים מסוג *Ammonia tepida* בבסיס התעלה באוהלו (23 אלפי שנים לפני היום) מצביעים על עליה במליחות במהלך אירוע היינריך 2 לעומת הכינרת הרצנטית. הסדימנטים הצעירים ביותר באוהלו הם מגיל ~20 אלפי שנים לפני היום, כלומר חלה הפסקה בהצטברות סדימנטים, ככל הנראה בשל שיווי משקל בין אספקת סדימנטים לבין הסרתם.

אירוע Younger Drays היה מאופין בחזרה לתנאים גלציאלים, והדבר בא לידי ביטוי באגם בעליה במפלס המים. יחסים איזוטופים של סטרונציום מצביעים על ירידה בנגר העילי ביחס לאירוע היינריך 2 ותרומה גדולה יותר של המעיינות, בדומה לתקופת המפלס הגבוה. תנאי האקלים בתקופה זו היו קיצוניים פחות מאשר בתקופת המפלס הגבוה. בהתאמה, מקור החומר הדטריטי לאגם היה אבק מדברי ממרחקים קצרים יותר.

מחקר זה מחזק את הקשר שבין התקופות היבשות והרטובות, מפלס מי האגם ותרומת המעיינות כמקור מים עיקרי בתקופות גשומות. ממצאים אלה נמצאים בהתאמה למודל גולדשמידט, לפיו המעיינות נדחפים על ידי מי התהום כך שמשקעים רבים יותר גורמים לעליה בתרומת התמלחות לאגם.

תקציר

עבודה זו מנסה לשפוך אור על ההסטוריה הלימנולוגית של אגם הכינרת במהלך ארבעים אלף השנים האחרונות. תקופת זמן זו כוללת את הגלציאל האחרון, אירוע היינריך (H2) ו Younger Drays וכן חלק מההולוקן. תקופות זמן שונות אלה מאופיינות בתנאי אקלים אזוריים מוגדרים שמשתקפים בסמנים לימנולוגים והידרולוגים. השינויים העיקריים שנבחנו ונדונים בעבודה זו הם שינויים במפלס המים, מקורות המים לאגם ומקורות האבק לאגם: מי אגם הכינרת מורכבים מתמלחות קלציום –כלוריידיות ומים מתוקים. מקורן של התמלחות בלגונת סדום מהניאוגן המאוחר, והן נכנסות לאגם בתגובה לתנאים ההידרולוגים שמשקפים את האקלים האיזורי. לשינויים אקלימיים במהלך הפליסטוקן וההולוקן יש השפעה על מעבר אבק מדברי, והם נקלטים ונשמרים בחתכים הסדימנטרים שהושקעו באגם הכינרת.

הליתולוגיה, המינרלוגיה וגודל הגרגר של הסדימנטים, כמו גם הכימיה (Sr/Ca) והיחסים האיזוטופים ($^{87}Sr/^{86}Sr$ ו- $\delta^{18}O$) של קסוות האוסטרקודים מהווים את הכלי העיקרי בו השתמשתי בעבודה זו. בנוסף, נעשה שימוש במאספי מיקרופאונה גירניים (אוסטרקודים ופורמיניפרים). התוצאות עברו השוואה לאגם הליסן וים המלח מתקופות זמן מקבילות, ושינויים באגם הכינרת נבחנו כחלק ממערכת איזורית מחד, ומערכת מיימית בתוך היבשה, מאידך.

דוגמאות מים וסדימנטים מפני השטח שהכילו אוסטרקודים חיים נאספו בארבעה אתרים מסביב לאגם הכינרת (גינוסר, מעגן, שיטים, טבחה). אוסטרקודים מאובנים, פורמיניפרים וסדימנטים נדגמו מארבעה קידוחים ותעלה: התעלה וקידוח KIN2 באוהלו אשר בחוף הדרום מערבי של הכינרת, קידוח SOG2 בדרום האגם, בנקודה בה גובה פני הקרקעית 224.0 מטרים מתחת לפני הים, וקידוח SOG3 בצפון מערב האגם, בנקודה בה גובה פני הקרקעית 229.0 מטרים מתחת לפני הים.

הקידוחים והתעלה מורכבים בעיקר מחילופים של שכבות למינריות ושכבות עבות של קלציט אוטיגני ודטריטי, קוורץ וחרסיות. הקלציט האותיגני הושקע ממי האגם, בעוד שהחומר הדטריטי הוסע אל האגם על ידי נחלים, נגר עילי ואבק ששקע ישירות על האגם.

חומר אורגני (ענפים, עצים) וקונכיות אוסטרקודים ומלנופסידים תוארכו בפחמן-14 וקנים ארגוניטים תוארכו באורניום-תוריום על מנת להכין מודל גיל-גובה עבור התעלה באוהלו ושלושת הקידוחים הנוספים. התעלה מכסה את התקופה שבין 27 ל 20 אלף שנים לפני היום. קידוח KIN2 הצמוד מכסה את התקופה שבין 40 ל- 21 אלף שנים לפני היום. קידוח SOG2 כולל את פרק הזמן שבין 25 ו- 12 אלף שנים לפני היום, וקידוח SOG3 כולל את פרק הזמן בין 25 ואלפיים שנים לפני היום.

המכון הגיאולוגי
משרד התשתיות הלאומיות
האנרגיה והמים

פליאוהידרולוגיה ופליאו לימנולוגיה של אגם הכינרת ברביעון העליון מתוך סדימנטים אגמיים וקונכיות קרבונטיות

לילך לב

עבודה זו הוגשה כחיבור לקבלת תואר "דוקטור לפילוסופיה" באוניברסיטת תל אביב

העבודה נעשתה בהדרכתם של:

פרופ' צבי בן אברהם, המכון למדעי כדור הארץ, אוניברסיטת תל אביב.
פרופ' מרדכי שטיין, המכון הגיאולוגי, ירושלים.
ד"ר אהובה אלמוגי – לבין, המכון הגיאולוגי, ירושלים.

דוח מס' GSI/14/2016 ירושלים, תמוז תשע"ו, יולי 2016